POWER FACTOR IMPROVEMENT BY THYRISTOR CONTROL IN TRACTION AND INDUSTRIAL POWER SUPPLY SYSTEMS

A Thesis Submitted
in Partial Fulfilment of the Requirements
for the Degree of
MASTER OF TECHNOLOGY

By
BINOY K. PATEL

to the
DEPARTMENT OF ELECTRICAL ENGINEERING
INDIAN INSTITUTE OF TECHNOLOGY, KANPUR
DECEMBER 1979

T O

MY PARENTS

.

EE-1979-M-PAT-POW

CERTIFICATE

It is certified that this work entitled
"Power Factor Improvement by Thyristor Control in
Traction and Industrial Power Supply Systems" by
Binoy Krishna Patel has been carried out under my
supervision and that this work has not been sub-
mitted elsewhere for a degree.

(Dr. S.R. Doradla)
Assistant Professor,
Department of Electrical Engineering,
Indian Institute of Technology,
Kanpur.

26.12.79

ACKNOWLEDGEMENT

CONTENTS

LIST OF TABLES

LIST OF FIGURES

Figure No.	Title	Page

NOMENCLATURE

a_n , b_n : Fourier coefficients

c_n : peak value of nth harmonic

C : capacitance

DSP : displacement factor

E : load EMF , volts

f : supply frequency , Hz

i_S : instantaneous value of supply current , amp

i_L : instantaneous value of load current , amp

i_{LN} : instantaneous value of normalised load current , amp

i_C : instantaneous value of capacitor current , amp

i_{TCR} : instantaneous value of TCR current , amp

I : rms value of current , amp

I_{SRMS} : rms value of source current , amp

I_{nRMS} : rms value of nth harmonic component in the source current , amp

I_L : rms value of load current , amp

I_C : rms value of capacitor current , amp

I_{TCR} : rms value of TCR current , amp

I_{TCRF} : rms value of fundamental component in TCR current , amp

L : inductance

m   : normalised value of load EMF

R   : resistance

t   : time , sec.

Z   : impedance

α , $\emptyset$: triggering angles

β : extinction angle

γ : time instant at which instantaneous ac supply voltage equals load EMF

θ : power factor angle

ψ_n : phase angle of nth harmonic

ω : angular frequency of ac supply voltage , rad/sec.

ABSTRACT

This thesis is concerned with the study of
improvement of power factor in (1) ac-fed traction systems
(2) industrial power supply systems.

A comparative study of the external performance
characteristics of the following converter circuit configu-
rations is made assuming continuous and constant load
current : Fully controlled converter with optional free-
wheeling, Fully controlled converter, Forced commutated
converter with symmetrical single pulse-width control.
The performance characteristics of the fully controlled
converter with optional freewheel are also verified experi-
mentally. Furthermore, the different possible modes of
operation are recognised with various load circuit para-
meters under rectification and inversion operations.
These modes are identifed on the operating diagrams of the
converter. A graphical procedure for estimating the mini-
mum inductance for continuous current operation is presented.

Different methods of reactive power compensation
are briefly reviewed. The thyristor phase-controlled rea-
ctor for dynamic VAR compensation in industrial power

systems is explained in detail. A single-phase thyristor controlled reactive power compensator is built and experimental results are obtained with the compensator under steady state and transient operating conditions.

CHAPTER I

INTRODUCTION

1.1 INTRODUCTION

Power factor is an important performance quantity in ac power system. It is defined as the ratio of active power input to the apparent power input from the ac supply. Thus, large reactive power requirement causes the system to operate at low power factor. Almost all major loads connected to the power supply system consume large amount of lagging reactive power. Induction motors which constitute nearly about seventy percent of industrial load operate at lagging power factor. Induction and arc furnaces widely used in metallurgical industries (mainly steel plants) draw large amount of reactive power. The domestic consumers also consume considerable amount of lagging current due to extensive use of arc and fluorescent lamps and also pump drives used for irrigation purposes. With the advent of high power semiconductor switches, the static thyristor power converters are fast replacing conventional M - G sets for the control of dc drives. Phase angle control [1 - 3] is commonly used in these ac to dc thyristor power converters to obtain vari-

able dc output. The power factor on the ac side deteriorates considerably with large phase angle delays at light load conditions. The thyristor converters have gained much popularity specially in electric traction system, paper and textile mills, and in rolling mills in steel industries. With an increasing number of such drives operating on an ac supply, there is ever increasing demand for reactive power from the supply system.

All these above requirements add up to a very large lagging reactive power demand from the power supply system thus causing the system to operate at considerably low power factor. Supply power factor is vital for an economical design and efficient, reliable and quality operation of the system. There are many disadvantages [4] if the supply power factor is poor. Some of them are as follows :

(1) It causes large I^2R loss in the system, i.e., in the generators and transmission lines because of the large current. This causes unnecessary heating of the system components.

(2) It causes the source generators to operate at decreased power factor thus increasing the kVA loading on the source generators and circuits to cause an over-

loaded condition and prevents capacity for additional load growth.

(3) By increasing kVA load on the generators, it prevents any possibility of additional kW loading which may be placed on the generators if prime-mover capacity is available.

(4) It causes poor voltage regulation at the load. Particularly in HVAC systems with long transmission lines, the resultant over-voltages due to load rejection affect insulation co-ordination.

(5) It decreases voltage level at the load thus lowering the power transfer capability.

(6) The cross-sectional area of bus bars and the contacts of the switchgears have to be increased since they have to be designed for the maximum current which would correspond to the minimum power factor for the same kW to be transferred in the ac supply system.

(7) Low power factor results in an overall increased investment in system facilities per kW of load supplied.

Hence, the utility authorities as well as the consumers have always given due attention to devise means to improve the power factor for reliable and economic operation of the system.

1.2   OUTLINE OF THESIS

1.2.1 Improvement of power factor in ac traction power supply system

The problem of reactive power has always been given much attention in the field of single-phase ac traction where thyristor converters are used for the control of the dc traction motors. The railway power systems are weaker having low short-circuit capacity than industrial power systems [5]. Furthermore, it is highly uneconomical to compensate reactive power externally because the traction system is fed by sub-stations located at short intervals. It is also not desirable to compensate reactive power by capacitor banks housed in the locomotive from the standpoint of space and weight. Besides, a fixed bank of capacitors may not be able to achieve perfect compensation as the load is fluctuating. It is advantageous to achieve improvement in power factor by modification of the converter circuit rather than by external compensation. Broadly two classes of converters have emerged [1 , 2] using line commutation and forced commutation. The converters employing forced commutation are complex while those employing line commutation are relatively simple. Half-controlled converters are generally employed in ac traction since they provide better supply power factor

compared to fully controlled converters [3] . However, the half-controlled bridge circuit provides only uni-directional output voltage. It cannot provide at its output terminals dc voltage of negative polarity which is essential for regeneration. This is a serious limi-tation, especially in traction applications where regen-eration of load energy to the supply line might result in substantial economy. W. Farrer and D.". Andrew [6] developed a novel control strategy for the full bridge-thyristor converter circuit which has given characteristics identical in form to those of a half-controlled thyristor bridge without sacrificing regenerative capability. In chapter II, the input and output characteristics assuming constant load current are obtained for (i) conventional fully controlled converter, (ii) fully controlled converter with facility for freewheeling control [6] , and (iii) for-ced commutated converter with single symmetrical pulse-width modulation control [8] and compared among these three control schemes. Experimental results with large inductance in the load circuit are obtained to corroborate the theoretical results. Details of the control circuit are also given.

The operating diagrams [1 , 13] showing different modes of operation with actual load circuit

parameters for a fully controlled converter circuit with
freewheel facility are discussed thoroughly in chapter III.
Continuous current operation of the converter is desirable
[14] . Estimation of minimum inductance to be connected
in the load circuit to achieve continuous current operation
of the fully controlled converter with optional freewheel-
ing is also carried out in chapter III.

1.2.2 Improvement of power factor in utility systems

The problem of power factor improvement in ac
loads is very wellknown since the inception of ac trans-
mission and distribution. This is, in fact, attempted at
various stages in the power system network : domestic
consumers, bulk power consumers, industrial power systems
and HVAC network. The domestic consumer derives maximum
benefit if he operates his equipments at maximum power
factor. The bulk consumers are also usually charged
tariffs for the kVA installed in addition to the actual kW
consumed. This would mean that there is a considerable
saving if the power factor of the bulk load is improved.
In the case of large industrial power systems, where the
loads are normally concentrated in one plant and served
from one network terminal, the reactive power demand of
large, and fluctuating industrial loads is either reduced
or cancelled resulting in improved power factor at the

supply network feeding the industrial load. In the HVAC network, the magnitude of the voltage at a bus is very much dependent on the balance of reactive power at the bus. The objective in this case is, therefore, not to view in terms of power factor improvement since the loads are not localised, but to regulate the voltage at the bus in the event of planned and unplanned disturbances of both loads and generation.

Chapter IV of this thesis clearly enumerates chronologically different methods of power factor improvement in industrial power systems. The relative merits and demerits of the different types of external compensators are also outlined. The different reactive power compensators used for the improvement of power factor are,

(1) Fixed capacitors

(2) Switched capacitors

(3) Synchronous condensers

(4) Static reactor compensators

In case of static reactor compensators, the different methods of realizing a variable inductor are outlined.

In chapter V , description of a practical static reactive compensator using a fixed capacitor and a

thyristor phase-controlled reactor (inductor) used to continuously improve the power factor of single-phase loads is given. The control circuit details are explained and experimental results showing steady-state and transient behaviour of the system are thoroughly discussed. Some modifications required in the control circuit to improve its response are clearly mentioned.

In chapter VI , overall conclusions are drawn and guidelines for further research work are mentioned.

CHAPTER II

CONVERTER CIRCUITS FOR POWER FACTOR
IMPROVEMENT IN TRACTION POWER SUPPLY

2.1. INTRODUCTION

Solid-state thyristor control of dc drives is
playing an important role in the variable speed drive system
and also in traction systems. The replacement of MG sets,
g-arc converters and other conventional controllers used in
earlier installations of traction systems by thyristor power
controllers is a logical process of evolution. Solid-state
thyristorised drives have numerous outstanding advantages,
such as, minimal maintainance, less bulk and weight, higher
efficiency, faster time response and so on.

The phase-angle-control is commonly used in the
solid-state control of dc drives fed from an ac supply.
This is a simple control scheme, but the supply power factor
deteriorates considerably with larger phase-angle delays.
Besides, harmonics in the ac supply line and ripple in the
output voltage is generated. Forced commutation is used to
improve supply power factor [7,8] . In fact, this techni-
e was successfully used in West Germany railway traction
system and many other parts of the world to minimise reactive
power drawn by single-phase ac-fed traction motor drives [5] .

This method is also used to minimise supply harmonics and reduce any particular undesirable harmonic and its multiples [9]. Inspite of the complexity of forced commutation which involves more power semiconductor switches and additional commutating elements, this principle is used and in fact operationally tested in traction systems to improve power factor [5]. The ripple voltage at the dc terminals can be minimised by increasing the number of phases of the ac supply which is the normal practice in the industrial field. However, in traction systems this is not possible since the traction motor drives are supplied from single-phase ac supply system. As a result, the railway power systems are weaker having low short-circuit capacity than industrial supply systems. Therefore, the problem of reactive power has always been given more attention in the field of traction than with stationary controlled drives in industrial field [5].

The reactive power drawn from ac supply system can be minimised by external compensation. External compensation involves installation of power factor correction devices which take leading reactive current to compensate for the lagging current drawn by the thyristor-controlled dc traction drives. A bank of capacitors connected across the input terminals of a thyristor converter can serve as a power factor correction device to some extent. Because of a large

current and low frequency, large-sized capacitors are required. The external compensation is therefore not desirable from the standpoints of space and weight in traction locomotives. Furthermore, it is not economical to instal power factor correcting apparatus at the substation since a large number of substations feed traction power supplies. However, the power factor correction devices find widespread application in industrial power systems.

In traction systems, improvement in supply power factor can only be achieved by disconnecting the supply line from the load circuit and providing an alternate path for the load current to freewheel for some part of the period of the supply frequency. In forced commutated circuits, this can be arranged at any instant in the cycle. In line-commutated full bridge converter circuit, it is not possible to provide an alternate path for the load current with conventional triggering pulses as used in phase-angle control. With a free-wheeling diode connected across the full-bridge circuit, alternate path for the load current can be provided after the supply voltage reverses. Half-controlled bridge circuits provide inherent free-wheeling path for the load current when the ac supply voltage is disconnected from the load circuit by phase-angle control. There is a significant reduction in reactive power consumption in half-controlled thyristor bridge circuits when compared to that in full-

bridge circuit. However, the half-controlled bridge circuit provides only unidirectional output voltage and hence cannot sustain a negative voltage which is essential for regeneration. This is a serious limitation, especially in traction applications where regeneration of load energy to the supply line might result in substantial improvement in energy consumption. W. Farrer and D.F. Andrew [6] developed a novel control strategy for the full-bridge thyristor converter circuit which has given characteristics identical in form to those of a half-controlled thyristor bridge without sacrificing regenerative capability. The principles of this control technique are discussed in detail in the reference [6] .

In this chapter of the Thesis, the detailed study of input and output characteristics of full-bridge converter circuit with novel control strategy developed by W. Farrer and D.F. Andrew has been carried out. The performance characteristics such as power factor, fundamental power factor, harmonic factor and ripple voltage have been obtained assuming constant load current for (i) conventional fully controlled converter, (ii) fully controlled converter with facility for free-wheeling control as developed by W. Farrer and D.F. Andrew; (iii) forced commutated converter with single symmetrical pulse-width modulation control. The

performances are compared among the three control schemes
and the merits and demerits of each of the schemes are
outlined. A simple open-loop control circuit has been built
to verify waveforms of fully-controlled converter with free-
wheel·ıg control. To corroborate the theoretical results,
experimental results for thyristor converter with optional
free-wheel are obtained with a large inductance in the load
circuit.

2.2. PRINCIPLES OF OPERATION

2.2.1. Fully controlled converter circuit configuration

Fig. 2.1 shows single-phase fully controlled
converter circuit. In traction systems, the load usually
consists of dc motors. Inductors are also inserted in the
load circuit to reduce ripple in the armature current.
With a fairly large inductance in the load circuit, the
load current may be assumed to be continuous and constant.
The operation of the converter circuit is well documented
in literature [1 , 3] . However for the sake of complete-
ness, a brief explanation of the circuit operation is des-
cribed. Thyristors T_1 , T_2 and T_3 , T_4 are turned-on at
some delay angle, α in the positive and negative half
cycles of the supply frequency respectively. When T_1 and
T_2 are turned-on together in positive half cycle, current
flows from source through T_1 to load and back to source
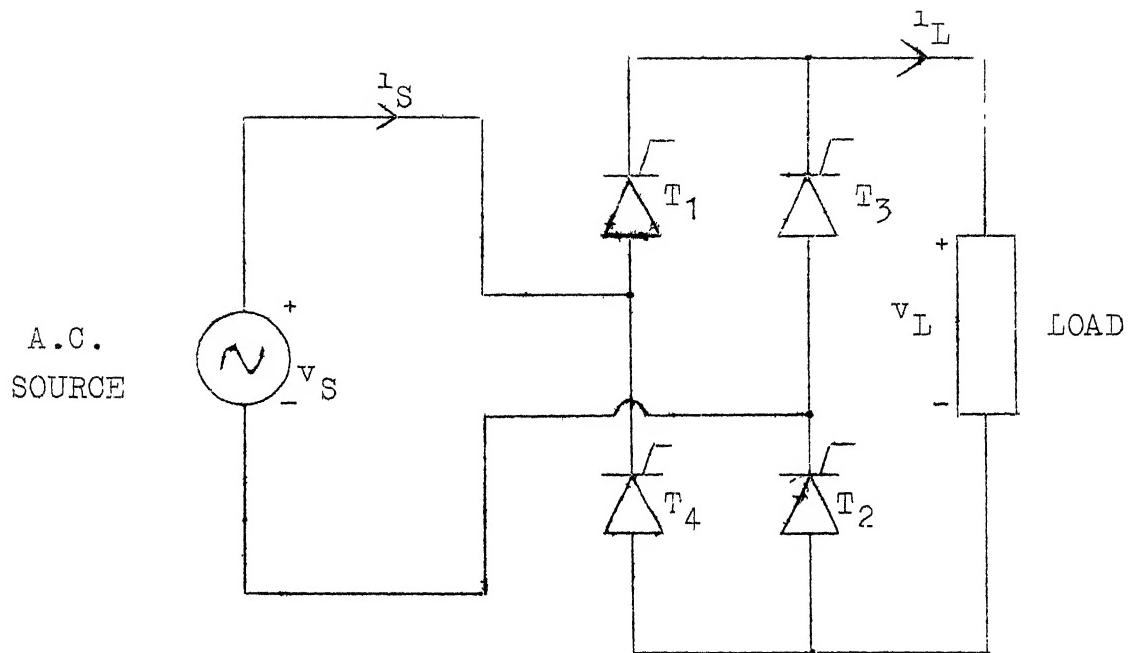
Fig. 2.1 Basic single phase fully controlled
converter for DC drives.
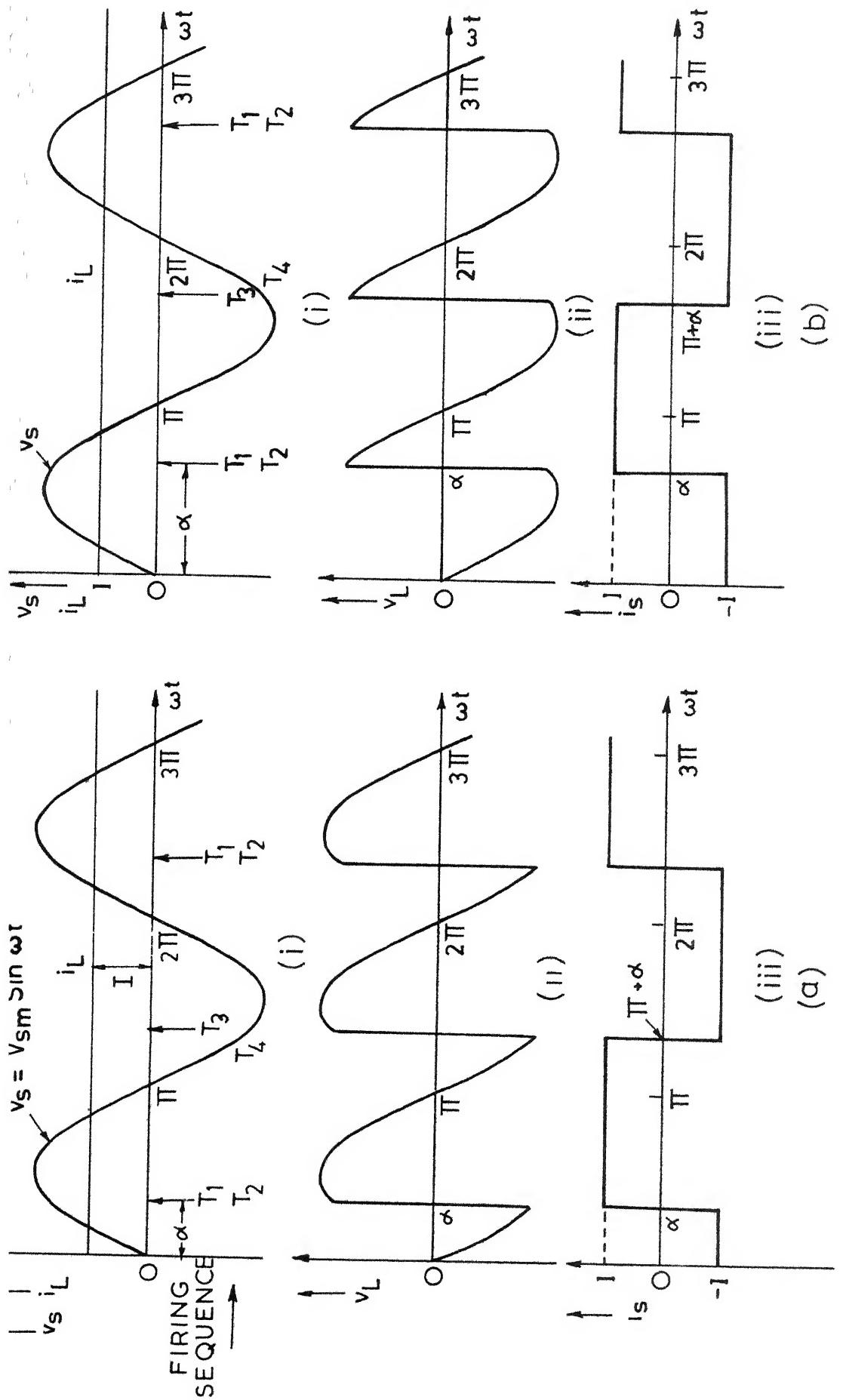
FIG 2.2 VOLTAGE AND CURRENT WAVEFORMS FOR CONVENTIONAL FULL CONTROL
(a) RECTIFICATION MODE   (b) INVERSION MODE

(i) SOURCE VOLTAGE AND LOAD CURRENT   (ii) LOAD VOLTAGE AND LOAD CURRENT   (iii) SOURCE CURRENT

through T_2 . By turning T_3 and T_4 on after one half period
in the negative half cycle, a negative voltage appears
across T_1 and T_2 , reverse biases them and turns them off
by line commutation. The current now flows from source
through T_3 to load and back to source via T_4 and thus gets
reversed in the ac supply. Depending upon the value of
α , the mean output voltage may be positive or negative.
With positive mean output voltage, the converter operates
as a rectifier with power flow from ac source to the load.
On the other hand, the converter operates as a line commu-
tated inverter with power flow from load to ac source
when the mean output voltage is negative. The voltage and
current waveforms of Fig. 2.1 are shown in Fig. 2.2 for
rectification and inversion modes. The changeover from
rectification to inversion takes place at $\alpha = 90°$ theo-
retically. It is clear from the waveforms that the load
is always connected to the source.

2.2.2. Fully controlled converter with optional free-wheeling

In the fully controlled converter circuit,
source current whether positive or negative always flows
unidirectionally in the load. Obviously, this results in
low power factor especially at large delay angles. If T_1
and T_3 or T_3 and T_4 are replaced by power semiconductor

diodes or if a power semiconductor diode is connected across the output terminals, the source can be disconnected from the load circuit and an alternate free-wheeling path can be provided for the load current for some part of the period of the supply frequency. The converter circuit would then become the familiar half-controlled circuit [3] . Since no mean negative voltage can be developed across the output terminals of a half-controlled converter circuit , it is not possible to operate the converter circuit in the inversion mode. However, in traction locomotives, there may be significant energy saving if load energy is regenerated to the ac source. With a slight modification in the conventional triggering of the fully controlled converter circuit, it is possible to incorporate free-wheeling and inversion modes. In this triggering scheme, one phase shifter controls the triggering angle or angle of connection, α of the main thyristor pairs T_1 , T_2 and T_3 , T_4 as described in section 2.2.1 in the conventional manner. Also it involves another phase shifter which controls the free-wheeling interval. This additional phase shifter controls the triggering angle or angle of disconnection, $\emptyset$ of the series-aiding thyristor pairs T_1 , T_4 and T_2 , T_3 . Thyristors T_1 and T_2 are **fired** at some delay angle , α in the positive half cycle of the supply voltage and

current flows from source through T_1 to load and back to
source via T_2 . T_1 and T_2 continue to conduct upto the
instant $\emptyset$ in the next half cycle when T_3 is fired and
gate pulse to T_2 is maintained. T_1 gets commutated by
line commutation and the current is transferred to T_3 .
Thus, the source is disconnected from the load and the
load current free-wheels through T_2 and T_3. The free-
wheeling of the load current continues upto $\propto$ in the
negative half cycle when T_4 is fired and the gate pulse
to T_3 is maintained. As T_4 turns-on, T_2 gets commutated
by the negative line voltage appearing across it and the
source again gets connected to the load. The current now
flows from the source through T_3 , load, T_4 and back to
the source. Thus, the source current gets reversed when
compared to the earlier half cycle. The current continues
to flow upto $\emptyset$ in the next positive half cycle when T_1 is
fired and the gate pulse to T_4 is maintained. T_3 gets
commutated the moment T_1 turns on. The load current free-
wheels through T_1 and T_4 . Again at $\propto$ in the positive
half, T_2 is fired and the gate pulse to T_1 is maintained.
The source is now connected to load and the above mention-
ed events repeat. The firing sequence along with voltage
and current waveforms are shown in Fig. 2.3.(a). In order
to realize the benefit of maximum power factor in the
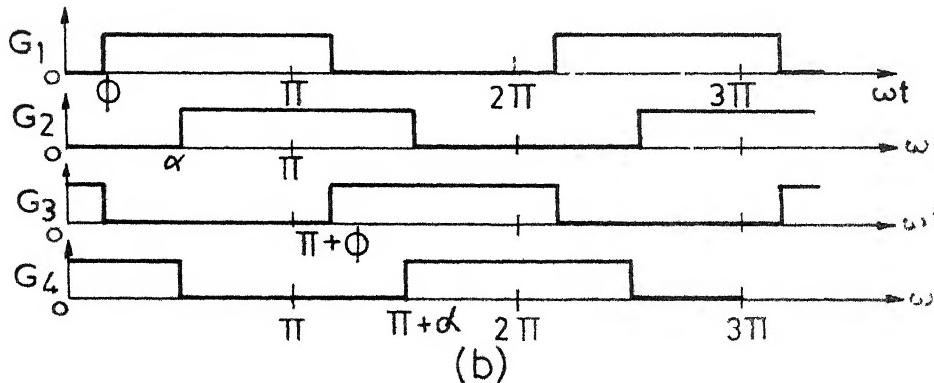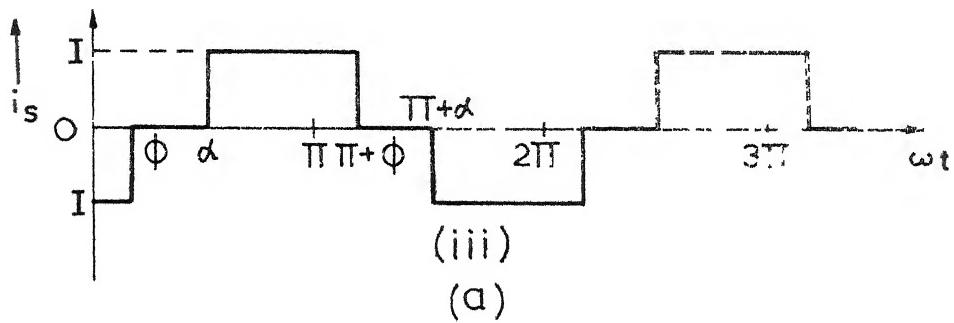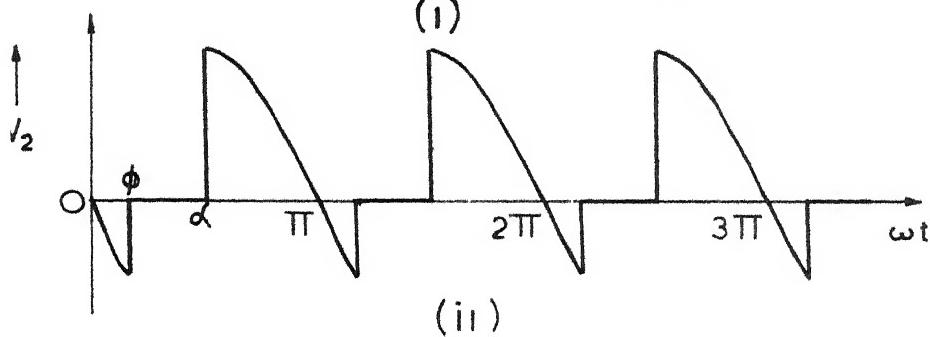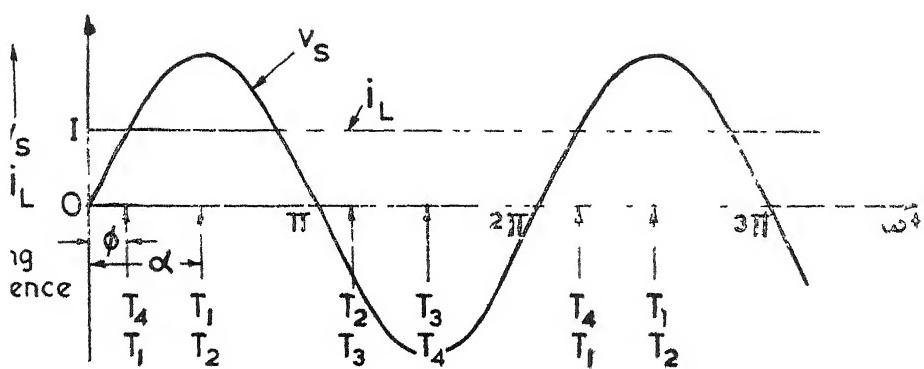
a) CURRENT AND VOLTAGE WAVEFORMS FOR OPTIONAL
FREE WHEEL CONTROL WITH VARIABLE α & φ

b) FIRING PULSES
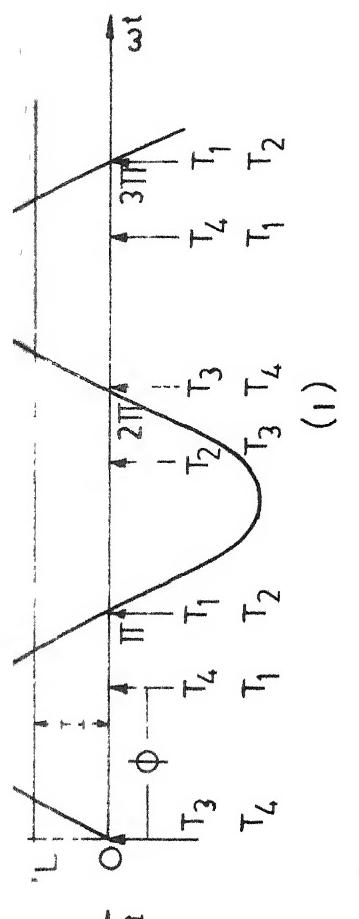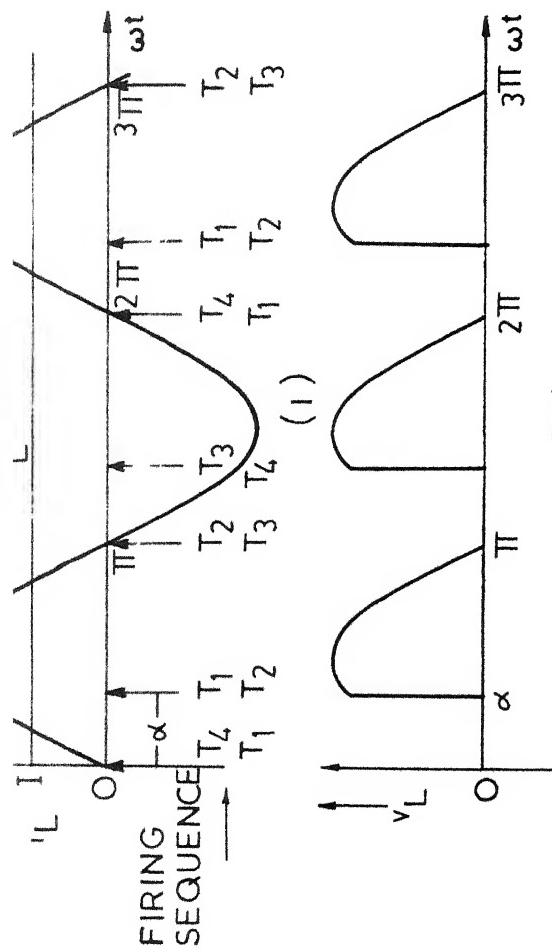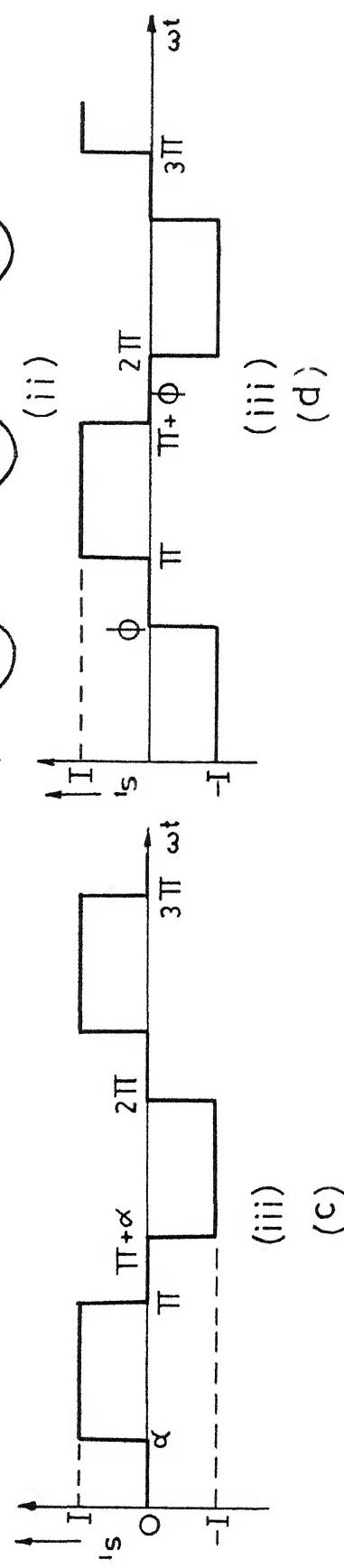
FIG 2.3 WAVEFORMS FOR OPTIONAL FREE WHEEL CONTROL (c) FOR RECTIFICATION MODE WITH $\phi = 0°$ (d) FOR INVERSION MODE WITH $\alpha = \pi$

rectification mode, the triggering angle, $\emptyset$ is held constant at zero and the triggering angle, α is varied from zero to π to vary the mean output voltage from positive maximum to minimum. The firing sequence along with current and voltage waveforms for a particular firing angle, α is shown in Fig. 2.3.(c). Similarly, in the inversion mode negative mean output voltage is varied from minimum to maximum by fixing α at π and varying $\emptyset$ from zero to π for maximum power factor. The voltage and current waveforms alongwith the firing sequence for a particular triggering angle, $\emptyset$ is shown in Fig. 2.3.(d). Although this triggering strategy results in maximum power factor, there are other performances such as output voltage ripple and input harmonic content which may not be minimum. Therefore, the fully controlled converter circuit with optional free-wheeling is analysed for different combinations of triggering angles α and $\emptyset$.

2.2.3. Forced commutated converter circuit

Fig. 2.4. shows single-phase forced commutated converter circuit. The dotted box essentially consists of a thyristor with its commutation circuitry. In the positive half cycle, when terminal A is positive with respect to terminal B, thyristors T_1 and T_2 are turned on at α connecting the source to the load. If the source is to be disconnected from the load, T_1 is turned
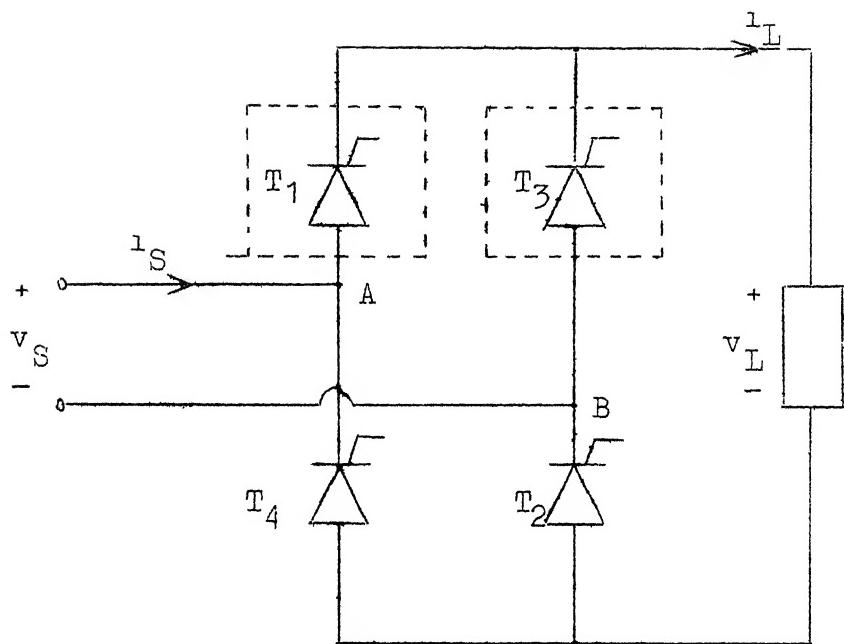
Fig. 2.4   Single phase forced-commutated converter
            circuit.

off at $(\pi - \alpha)$ by forced commutation and T_2 is gated
on simultaneously so as to provide free-wheeling path for
the load current. It is therefore not necessary to wait
for the reversal of supply voltage for free-wheeling act-
ion. In the negative half cycle, T_3 and T_4 are turned on
at $(\pi + \alpha)$ for connecting the source to the load.
The free-wheeling action is provided by turning T_1 and T_4
on at $(2\pi - \alpha)$. This single symmetrical pulse-width
modulation [8] provides maximum power factor in the forced
commutation scheme. The waveforms of voltage and current
along with firing sequence for the symmetrical single
pulse width modulation for both rectification and inver-
sion modes are shown in Fig. 2.5. Maximum to minimum
positive mean dc output can be controlled by varying α
from zero to $\pi/2$.

2.3. INPUT AND OUTPUT PERFORMANCES OF CONVERTER CIRCUITS CONNECTED TO TRACTION POWER SUPPLIES

Assuming constant load current, the main operat-
ing characteristics of interest are (i) fundamental power
factor , (ii) total power factor of the input current from
the ac source , (iii) input harmonic factor , and (iv) ripple
voltage at the dc terminals.

(i) The fundamental power factor is defined
as the power factor of the fundamental component in the
source current.

FIG 2.5 VOLTAGE AND CURRENT WAVEFORMS FOR SYMMETRICAL SINGLE PULSE WIDTH
(a)RECTIFICATION MODE   (b)INVERSION MODE
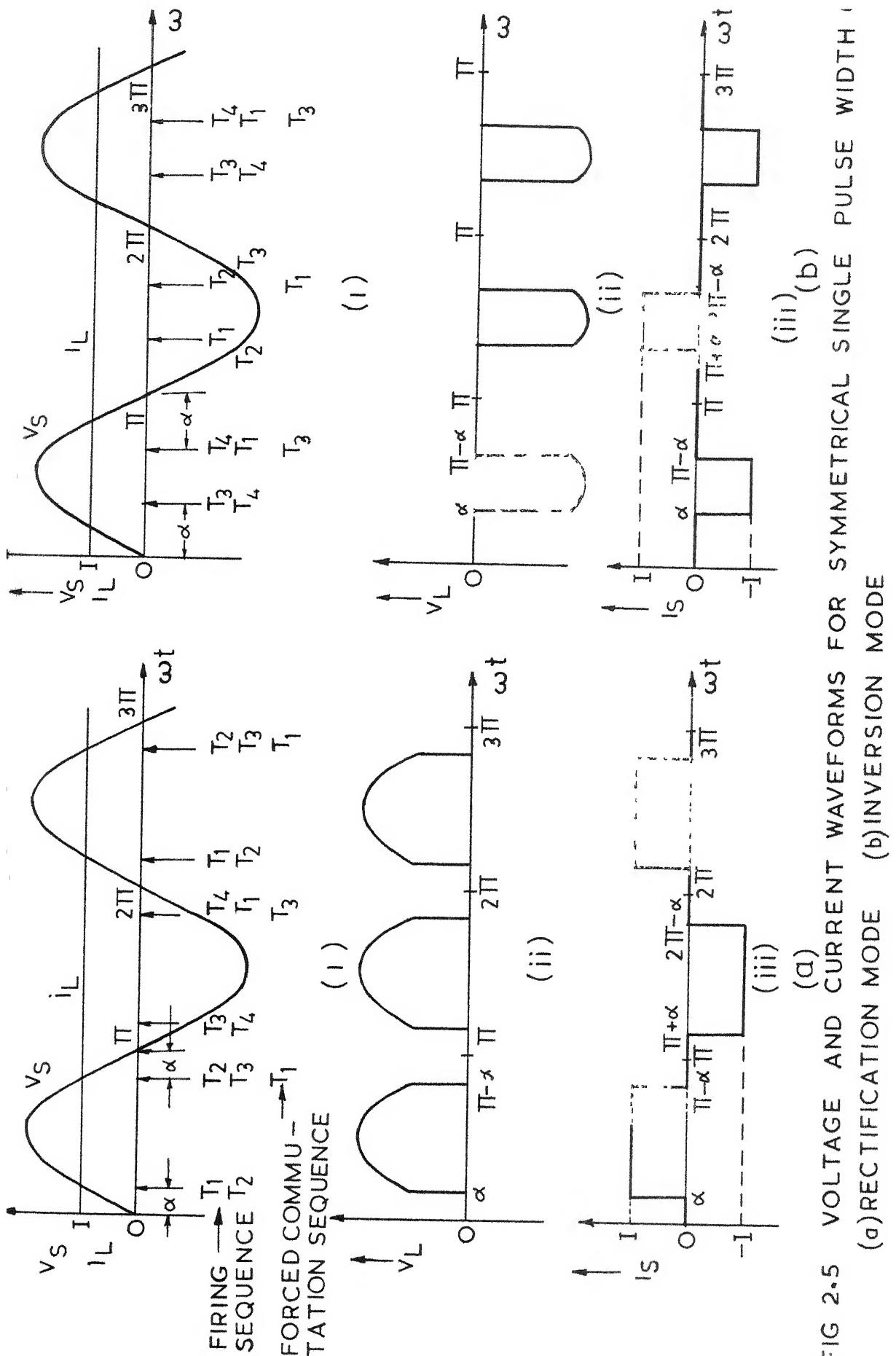
(ıı) The total power factor is defined as the ratio of active power input to the apparent volt-ampere input. Assuming sinusoidal ac source ,

Total Power Factor $= (I_{1RMS} / I_{SRMS}).\cos \psi_1$

where I_{1RMS} = RMS value of the fundamental component in the source current

I_{SRMS} = RMS value of the source current

$\cos \psi_1$ = Fundamental power factor

The ratio I_{1RMS} / I_{SRMS} is termed as the distortion factor and $\cos \psi_1$ as the displacement factor (DSP) [3] .

(ııı) The input harmonic factor is a measure of harmonic distortion in the ac supply.

Input Harmonic Factor $= \dfrac{\text{Input Harmonic content}}{\text{RMS value of fundamental component of the source current}}$

$= (I_{SRMS}^2 - I_{1RMS}^2)^{\frac{1}{2}} / I_{1RMS}$

(ıv) The ripple voltage at the dc terminals is expressed in terms of peak-to-peak (p-p) voltage ripple factor which is the per-unit value of the p-p output voltage ripple with base chosen as the maximum possible p-p output voltage ripple which is obtained in case of conventional scheme with $\alpha = 90°$. The maximum possible p-p output voltage ripple is obviously $2V_{Sm}$ where

V_{Sm} is the peak value of the source voltage. This,

P-p Voltage Ripple Factor = p-p output voltage ripple/$2V_{Sm}$

In what follows, the expressions for the average value of the output voltage (V_{LAV}), RMS value of the source current (I_{SRMS}), the RMS value of the fundamental component of the source current (I_{1RMS}) and displacement factor (cos ψ_1 or DSP) are derived for the different converter circuit configurations mentioned in section 2.2. in order to compute the input and output performances.

2.3.1. Conventional fully controlled bridge

Referring to Fig. 2.2., the following expressions can be easily obtained.

$$V_{LAV} = (2V_{Sm}/\pi).\cos\alpha$$

where V_{Sm} is the peak of supply voltage.

$$I_{SRMS} = I$$

$$I_{1RMS} = 2\sqrt{2}\,I\,/\,\pi$$

$$\psi_1 = \alpha$$

Fundamental power factor (DSP) = $\cos\psi_1 = \cos\alpha$

Total power factor = $(2\sqrt{2}/\pi).\cos\alpha$

$$\text{Input harmonic factor} = \frac{(I_{SRMS}^2 - I_{1RMS}^2)^{1/2}}{I_{1RMS}} = (\pi^2/8 - 1)^{1/2}$$

P - p voltage ripple factor = $0.5 (1 + \sin \alpha)$

2.3.2. Fully controlled bridge with optional free-wheel control

The expressions for this case are easily obtained referring to Fig. 2.3.(a). They are given below.

$$V_{LAV} = \left(V_{Sm} / \pi\right)(\cos \emptyset + \cos \alpha)$$

$$I_{SRMS} = I \left[\frac{\pi + \emptyset - \alpha}{\pi}\right]^{1/2}$$

$$I_{1RMS} = (2I / \pi) \left[1 + \cos(\alpha - \emptyset)\right]^{1/2}$$

$$\psi_1 = (\alpha + \emptyset)/2$$

$$\text{Total power factor} = 2 \cos\left(\frac{\alpha + \emptyset}{2}\right) \left[\frac{1 + \cos(\alpha - \emptyset)}{\pi(\pi + \emptyset - \alpha)}\right]^{1/2}$$

Input harmonic factor $= (I^2_{SRMS} - I^2_{1RMS})^{1/2} / I_{1RMS}$

$$= \left[\frac{1}{2} \left\{\frac{\pi(\pi + \emptyset - \alpha)}{1 + \cos(\alpha - \emptyset)}\right\}^{1/2} - 1\right]^{1/2}$$

The p-p (peak-to-peak) output voltage ripple will have different expressions depending on the values of α and $\emptyset$. Thus, we obtain,

P - p voltage ripple factor = 0.5 (1 + sin∅)   ,

$$\text{for } 0 \leqslant \emptyset \leqslant \pi/2$$

$$\text{and } 0 \leqslant \alpha \leqslant \pi/2$$

$$= 0.5 \,(\sin \alpha + \sin\emptyset) \quad ,$$

$$\text{for } 0 \leqslant \emptyset \leqslant \pi/2$$

$$\text{and } \pi/2 < \alpha \leqslant \pi$$

$$= 0.5 \,(\sin \alpha + 1) \quad ,$$

$$\text{for } \pi/2 < \emptyset \leqslant \pi$$

$$\text{and } \pi/2 < \alpha \leqslant \pi$$

If rectification mode only is desired, the triggering angle ∅ is fixed at zero and α is varied from zero to π to control mean output voltage from maximum to zero. The expressions for this particular case are obtained by substituting ∅ = 0 in the above general expressions for optional fly-wheel. Thus, we get,

$$V_{LAV} = (V_{Sm} / \pi) \,(1 + \cos \alpha)$$

$$I_{SRMS} = I \left[\frac{\pi - \alpha}{\pi} \right]^{1/2}$$

$$I_{1RMS} = (2I/\pi) \,(1 + \cos\alpha)^{1/2}$$

Fundamental power factor = cos (α /2)

$$\text{Total power factor} = 2 \cos (\alpha /2) \left[\frac{1 + \cos \alpha}{\pi (\pi - \alpha)} \right]^{1/2}$$

$$\text{Input harmonic factor} = \left[\frac{1}{2} \left\{ \frac{\pi(\pi-\alpha)}{1+\cos\alpha} \right\}^{1/2} - 1 \right]^{1/2}$$

P - p voltage ripple factor = 0.5 , for $0 \leqslant \alpha \leqslant \pi/2$

$\qquad\qquad\qquad\qquad$ = 0.5 sin α , for $\pi/2 < \alpha \leqslant \pi$.

$\qquad$ Similarly, if inversion mode is desired, the triggering angle, α is fixed at π and ϕ is controlled from zero to π for variable output voltage. The expressions for this case are obtained by substituting $\alpha = \pi$ in the general expressions for optional freewheel. Thus, we get

$$V_{LAV} = (V_{Sm}/\pi)(\cos\phi - 1)$$

$$I_{SRMS} = I(\phi/\pi)^{1/2}$$

$$I_{1RMS} = (2I/\pi)(1 - \cos\phi)^{1/2}$$

Fundamental power factor = $-\sin(\phi/2)$

$$\text{Total power factor} = -2\sin(\phi/2)\left[\frac{1-\cos\phi}{\pi\cdot\phi} \right]^{1/2}$$

$$\text{Input harmonic factor} = \left[\frac{1}{2}\left(\frac{\pi\cdot\phi}{1-\cos\phi} \right)^{1/2} - 1 \right]^{1/2}$$

P - p voltage ripple factor = 0.5 sin ϕ , for $0 \leqslant \phi \leqslant \pi/2$

$\qquad\qquad\qquad\qquad$ = 0.5 , for $\pi/2 < \phi \leqslant \pi$.

2.3.3. Symmetrical single pulse-width modulation control scheme

Referring to Fig. 2.5.(a) , for rectification operation, the different expressions are obtained as follows:

$$V_{LAV} = \left(2V_{Sm} / \pi\right) \cos \alpha$$

$$I_{SRMS} = I \left(\frac{\pi - 2\alpha}{\pi}\right)^{1/2}$$

$$I_{1RMS} = (2\sqrt{2} I / \pi) \cos \alpha$$

$$\psi_1 = 0$$

Fundamental power factor = $\cos \psi_1 = 1$

Total power factor = $2\sqrt{2} \cos \alpha / \left[\pi(\pi - 2\alpha)\right]^{1/2}$

Input harmonic factor = $\left[\dfrac{\pi(\pi - 2\alpha)}{3\cos^2 \alpha} - 1\right]^{1/2}$

P - p voltage ripple factor = 0.5

Similarly, the expressions for inversion mode are obtained referring to Fig. 2.5.(b) . For this mode, the expressions are the same as those obtained for rectification mode. However, because of power flow from the output to ac source, the expressions for average load voltage, fundamental power factor and total power factor

become negative.

2.4 CONTROL CIRCUIT FOR THYRISTOR CONVERTER WITH OPTIONAL FREE-WHEEL

The main block diagram of the firing circuit is shown in Fig. 2.6 which produces triggering pulses to thyristors in the sequence shown in Fig. 2.3 (b) . The supply sinusoid is fed as the input to the synchronised ramp generator at the output of which a ramp is produced in each half cycle of the supply sine wave. At the α-control comparator the ramp is compared with $V_{ref(\alpha)}$ to get rectangular pulses in each half cycle. The position of the rising edge of the rectangular pulse that fixes triggering angle, α can be controlled from zero to π by the variation of $V_{ref(\alpha)}$. Similarly $\emptyset$ can be varied from zero to π by controlling $V_{ref(\emptyset)}$ at the other comparator. These rectangular pulses are then stretched to 180° by pulse stretchers. The pulse-stretcher output in the $\emptyset$ control channel is the gate pulse for T_1 and its complement is the gate pulse for T_3 as seen from Fig. 2.3 (a) that G_3 and G_1 are complementary. Similarly, the pulse stretcher output in the α-control channel and its complement are the gate pulses for G_2 and G_4 respectively. Of course, these gate pulses go through high frequency modulation, pulse amplification and pulse transformer stages before being finally applied the gate of the thyristors.
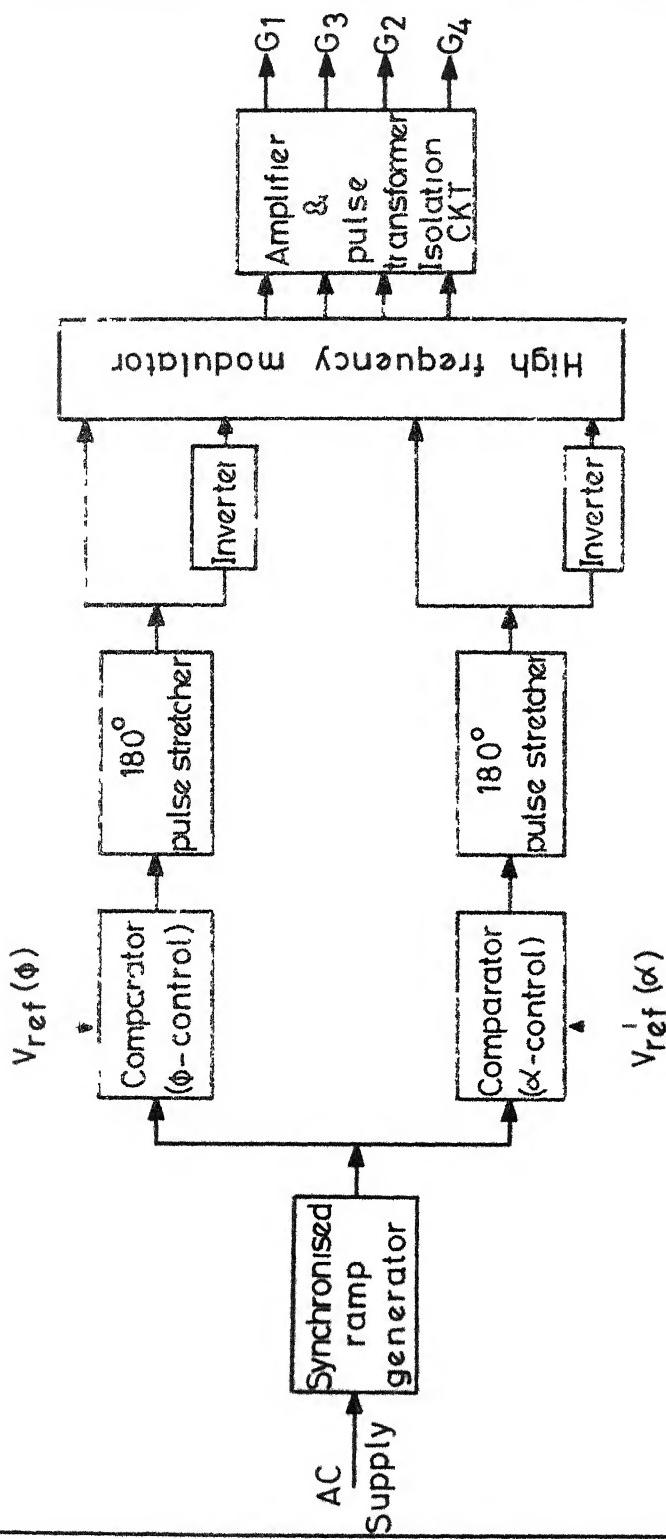
Fig. 2.6   Block   diagram   of   the   firing   circuit .

The pulse transformers provide isolation between power circuit and the firing circuit. The associated circuits for different blocks are described illustrating pertinent waveforms.

Synchronised ramp generator: The circuit is shown in Fig. 2.7.(a) . The 230V supply is first stepped down to 9V and fed to the non-inverting input of an opamp operating in the open-loop mode to get a square wave output synchronised to the supply sine wave. The 5.1V zener diode connected across the output makes it TTL compatible. The waveform at the point marked Ⓐ is shown in Fig. 2.8 . This is fed to a dual monostable. One of the monostables is triggered by the rising edge and the other by the falling edge of the square wave. The external components R and C are so chosen that the monostable output pulse-width is just enough to completely discharge the $0.2\mu F$ charging capacitor in the ramp generator. R and C have been chosen as 47k and $0.01\mu F$ respectively. The outputs of the dual monostable are ANDed using NAND gates and fed to the input of the ramp generator. The ramp generator is realized using discrete components. It gives fairly linear ramp output because of the charging of the capacitor by constant current source. The amplitude of the ramp is adjusted to +5V by the 4.7k potentiometer. Further linearization of the ramp is achieved using an opamp as shown in Fig. 2.7.(a).
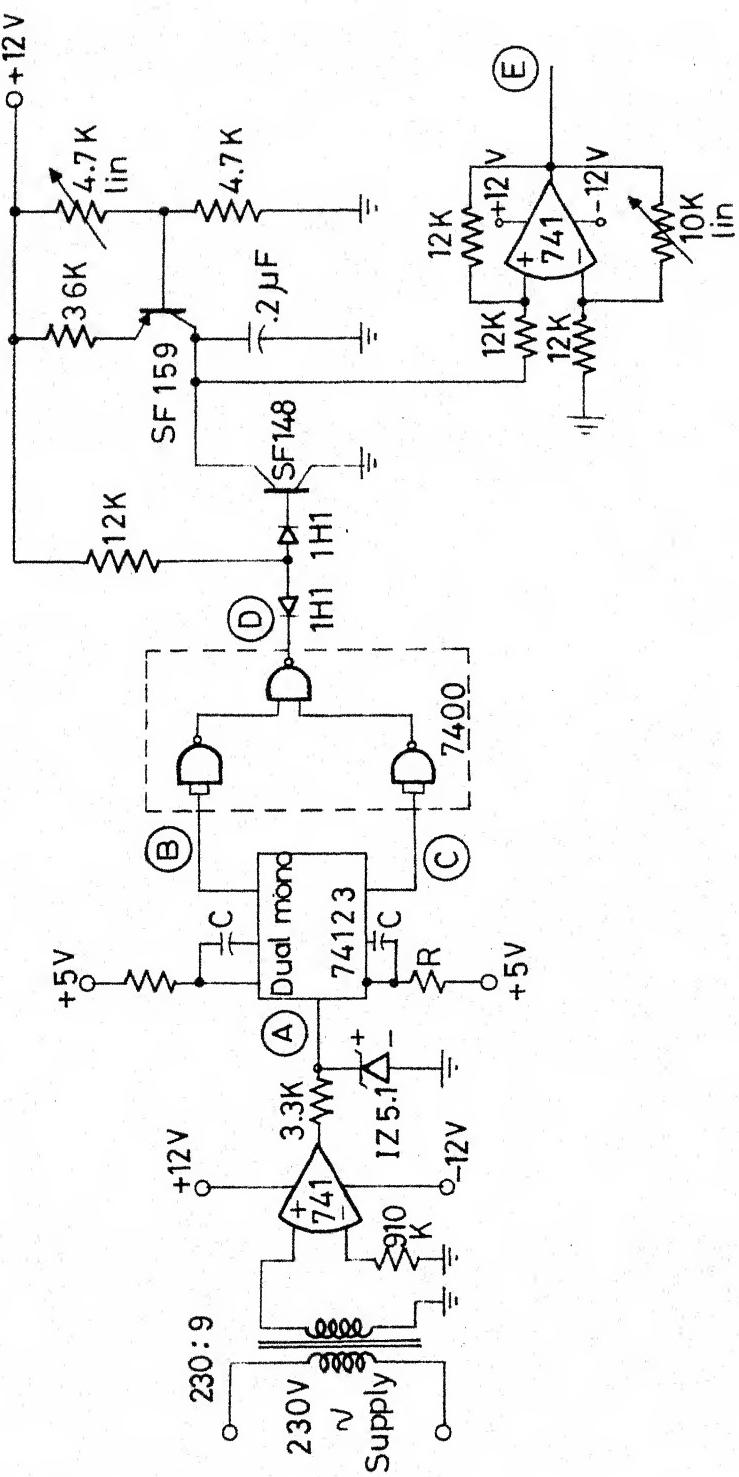
Fig. 2.7 (a)   Circuit diagram for syn. ramp generator.
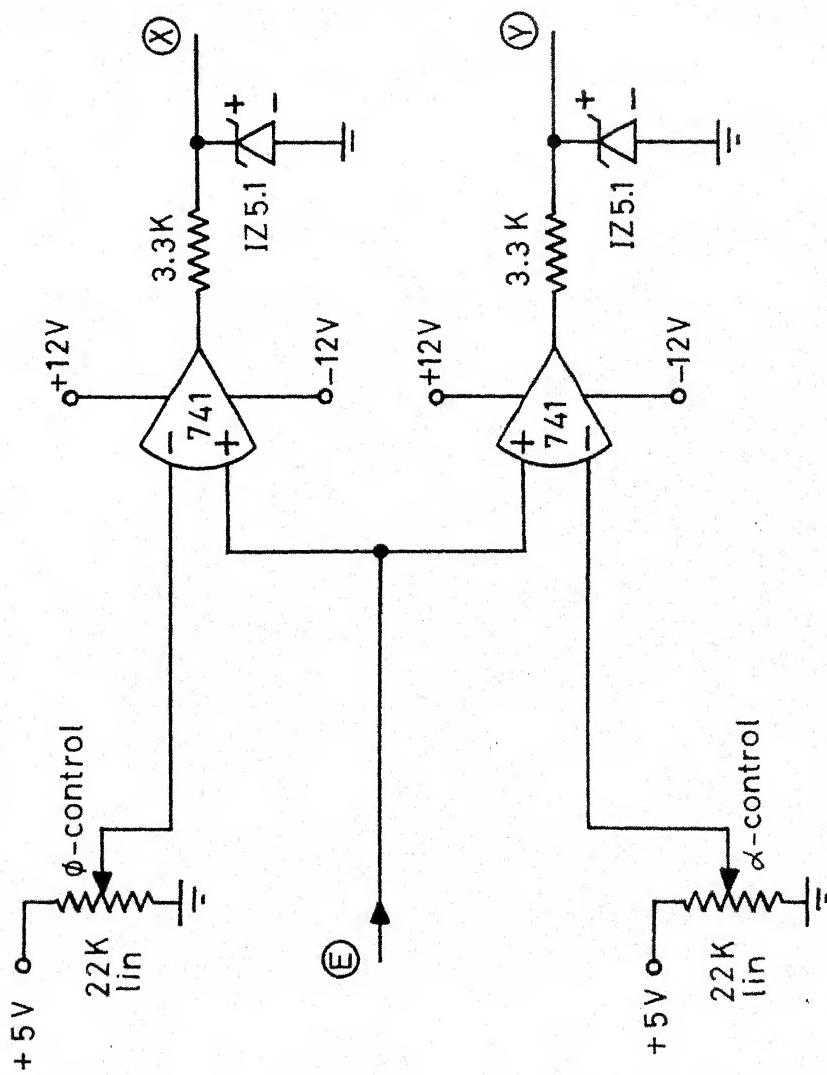
Fig. 2.7 (b) Circuit diagram for comparators.
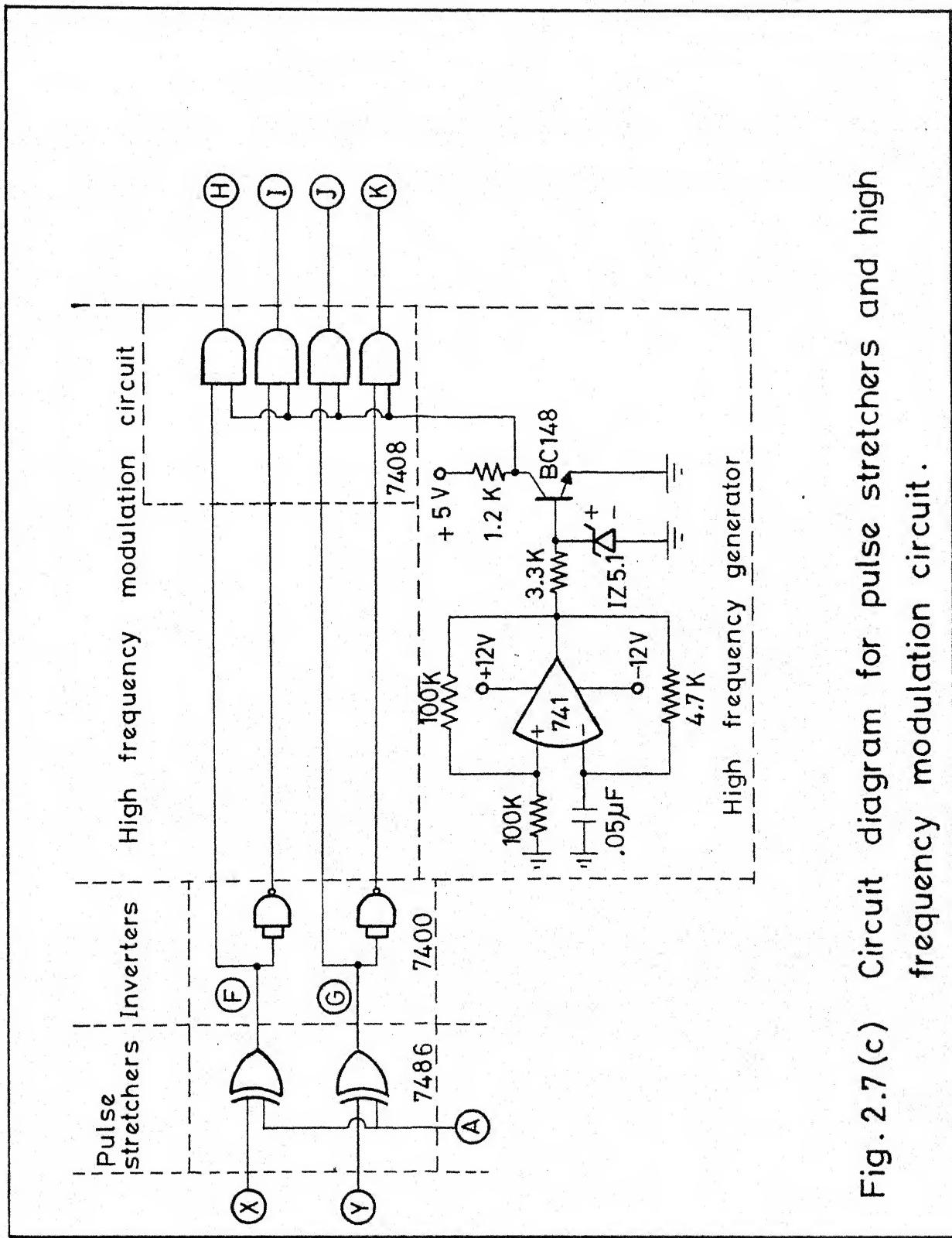
Fig. 2.7(c) Circuit diagram for pulse stretchers and high frequency modulation circuit.
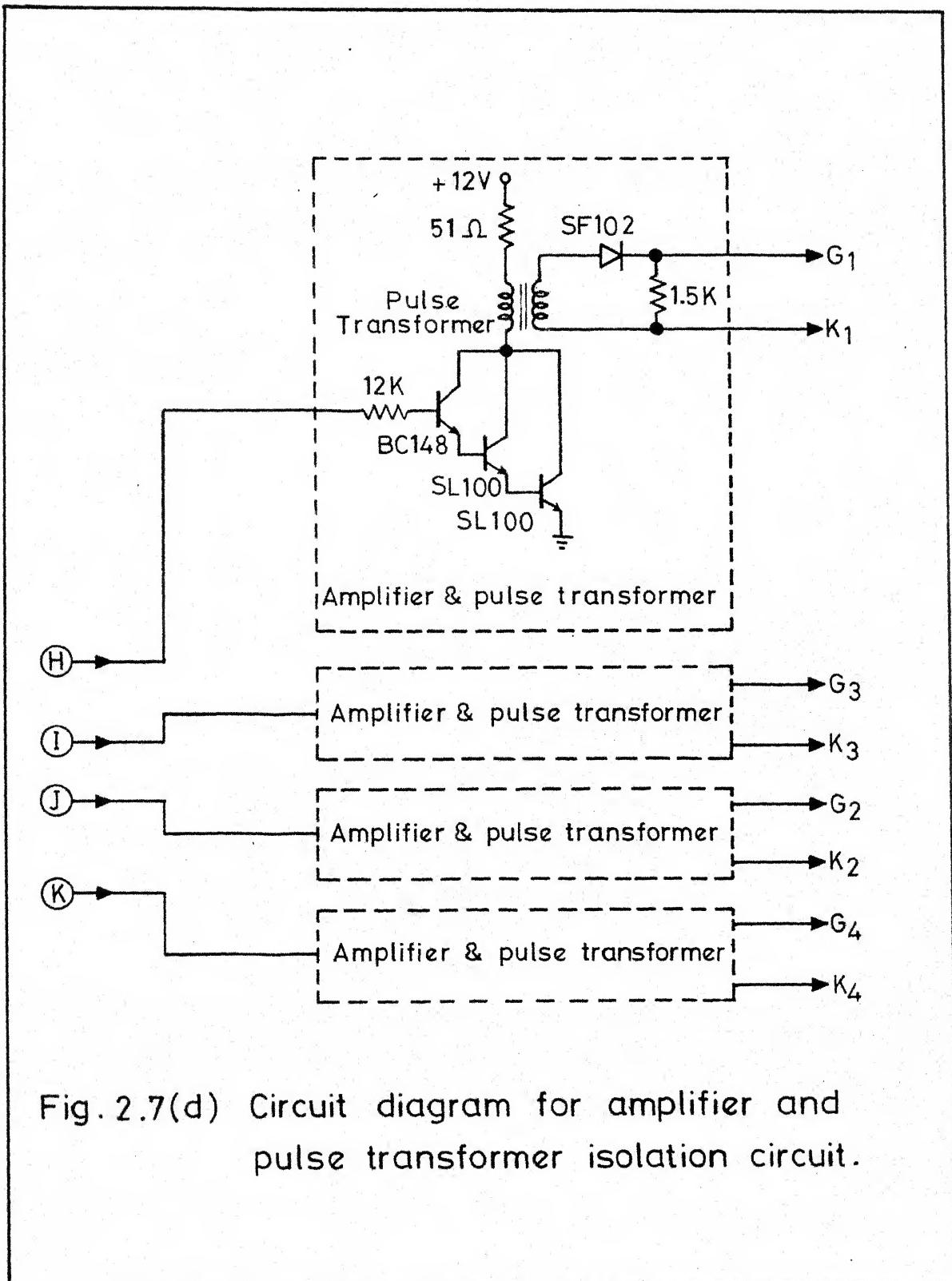
Fig. 2.7(d) Circuit diagram for amplifier and pulse transformer isolation circuit.
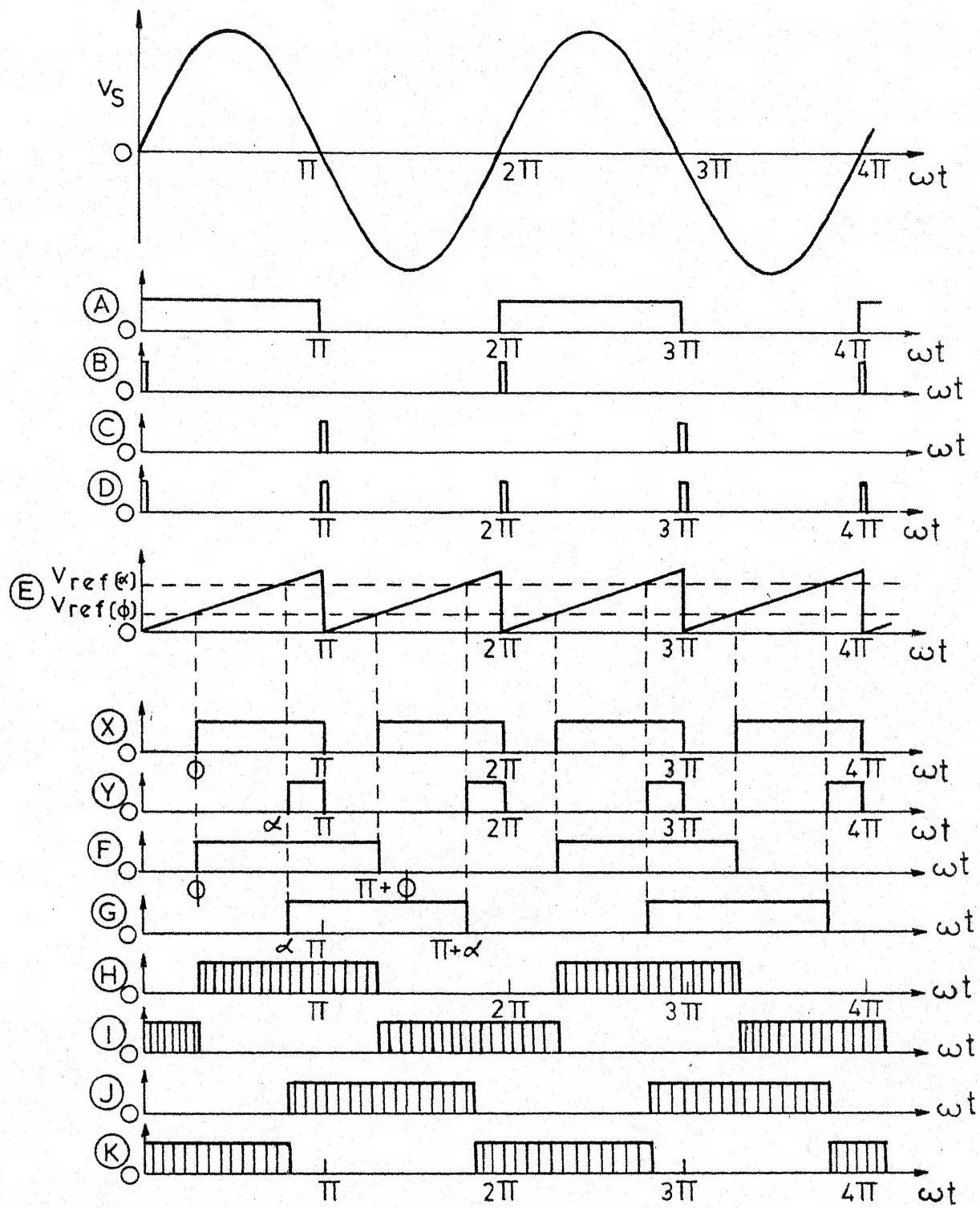
G. 2·8 WAVEFORMS AT DIFFERENT POINTS OF THE CONTROL CIRCUIT

The waveforms at different points of the circuit marked by capital alphabets are shown in Fig. 2.8.

Comparators : The comparator circuits used are shown in Fig. 2.7.(b) . An opamp in open-loop mode is used as the comparator. The ramp is fed to the non-inverting input and the dc reference voltage is given to the inverting input. The position of the leading edge of the output rectangular pulses at (X) and (Y) as shown in Fig. 2.7.(b) can be controlled from zero to π in each half cycle of the supply voltage by varying the reference voltage input with the help of potentiometers.

Pulse stretchers : The 180° pulse stretchers are easily realized using EXCLUSIVE-OR gates. The circuit details are given in Fig. 2.7.(c) . With the pulses at (X) and (A) as inputs to an EXCLUSIVE-OR gate, it gives an output square wave which has a width equal to one half cycle of the sine wave, the leading edge of which coincides with that of the rectangular pulse at (X) . Similarly, 180° stretching of the rectangular pulse at (Y) is also obtained. The stretched pulses at (F) and (G) are also shown in Fig. 2.8.

Inverters : The inversion of the square waves/at (F) and (G) are necessary to obtain the gate pulses at ($\pi + \emptyset$) and at ($\pi + \propto$) for the thyristors T_2 and T_4 respectively. This

is achieved using NAND gates as shown in Fig. 2.7.(c).

High frequency modulation circuit :   In order to include
the pulse transformers for isolation of the gate circuit
from the power circuit, high frequency modulation of the
gate pulses is necessary. The opamp astable circuit sho-
wn in Fig. 2.7.(c) is designed for approximately 10kHz
output. The high frequency signal is shaped and made TTL
compatible. The pulses are then modulated with the high
frequency signal. The resulting modulated gate pulses at
(H) , (I) , (J) ·and (K) are shown in Fig.
2.8.

Amplifier and pulse transformer isolation circuit :   In
order to trigger SCR's reliably, the gates have to be
driven hard and the pulse magnitude should be large but
within the maximum limits. Each pulse train at points
(H) , (I) , (J) and (K) is amplified and
isolated using individual Darlington's amplifier configu-
ration and pulse transformer and fed to the gate of res-
pective thyristor. The pulse transformer provides isola-
tion for gate pulses. The circuit details of this block
is shown in Fig. 2.7.(d).

2.5. EXPERIMENTAL RESULTS AND COMPARATIVE STUDY OF PERFORMANCES

The control circuit developed in section 2.4 is employed to study the performances experimentally for the converter circuit configuration with optional free-wheel control. Large inductance is inserted in the load circuit to make the load current constant as far as possible.

Table 2.1 gives the details of experimental set-up.

Table 2.1

Quantity	Value
Load resistance	13.5 Ω
Load inductance	3.72H
V_{sm}	99V
Load EMF for inversion mode	0-30V dc
1 pu output voltage	63.02V

By measuring input voltage, input current and input power from ac source, the total power factor is computed. A distortion analyser is used to measure the harmonic factor. Fig. 2.9.(a) shows oscillograms of input and output waveforms of voltage and current in the rectification mode while Fig. 2.9.(b) gives the same waveforms
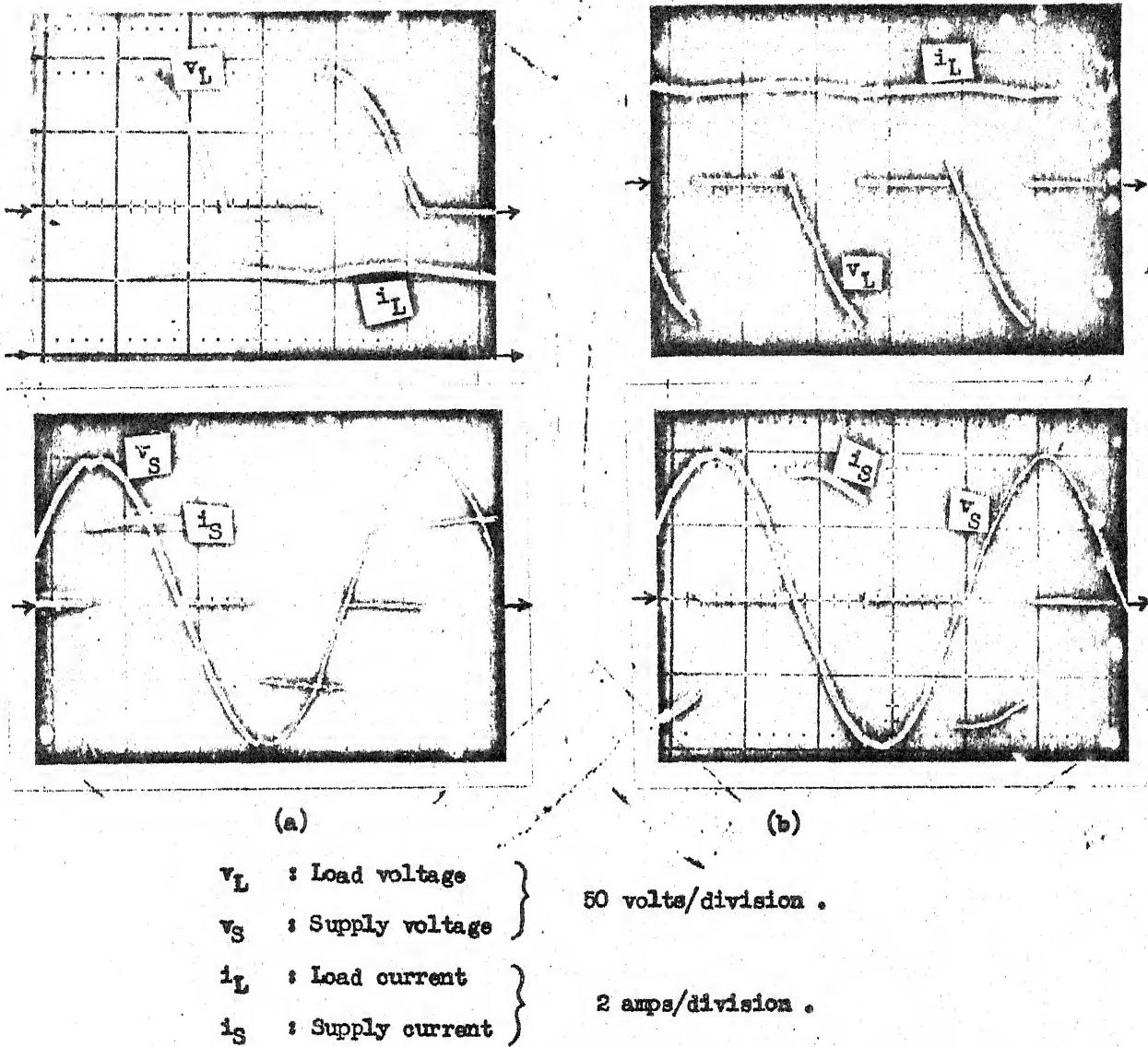
(a)   (b)

v_L : Load voltage   }
                                50 volts/division .
v_S : Supply voltage }

i_L : Load current   }
                                2 amps/division .
i_S : Supply current }

Fig. 2.9 Oscillograms of input and output voltage and current

waveforms for fully controlled converter with optional

freewheel control .

(a) Rectification operation with $\phi \approx 0°$.

(b) Inversion operation with $\alpha \approx 180°$.
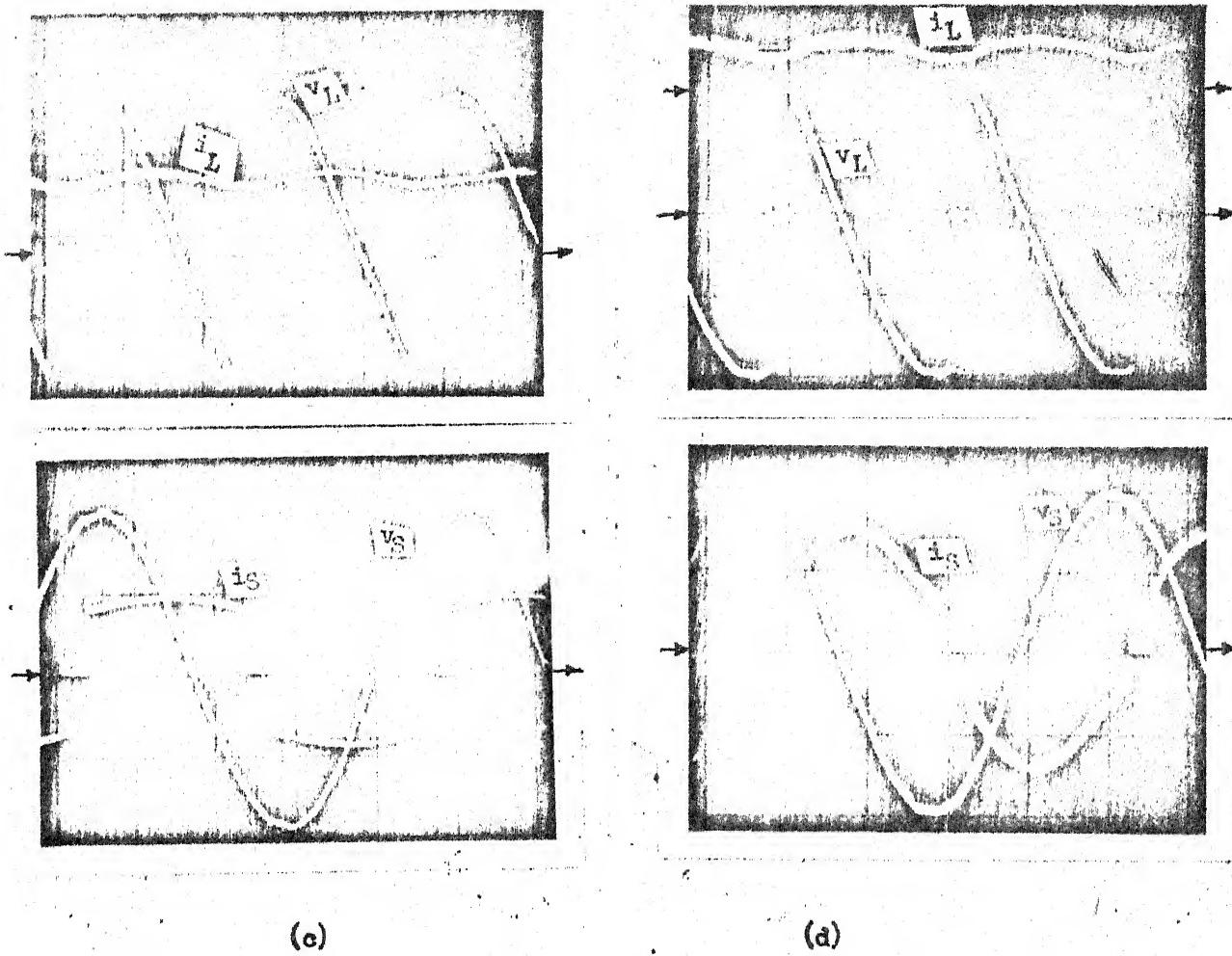
(c)   (d)

v_L : Load voltage   ⎫
                                ⎬ 50 volts/division .
v_S : Supply voltage   ⎭

i_L : Load current   2 amps/division .

i_S : Supply current   ⎰ 2 amps/division in (c) .
                             ⎱ 1 amp/division in (d) .

Fig. 2.9 Oscillograms of input and output voltage and current

waveforms for fully controlled converter with optional

freewheel control .

(c) Rectification operation with $\alpha = 60°$ and $\phi = 45°$.

(d) Inversion operation with $\alpha = 150°$ and $\phi = 105°$.

in the inversion mode. These waveforms correspond to maximum possible free-wheeling interval in rectification and inversion modes. The waveforms corresponding to optional free-wheel with particular values of α and $\emptyset$ in rectification and inversion modes are shown in Fig. 2.9.(c) and (d) respectively.

The expressions derived in section 2.3 are used to obtain different performances for fully controlled converter, fully controlled with optional free-wheel and forced commutated converter at various output voltages. A comparative study of the fundamental power factor, total input power factor, input harmonic factor and p - p voltage ripple factor for the same average voltage under different converter circuit configurations is presented.

The fundamental power factor (DSP) gives an idea of the active power requirement from the supply. This is shown in Fig. 2.10. for rectification and inversion modes. The symmetrical pulse-width control scheme offers maximum power factor of unity over entire output voltage range in both modes of converter circuit. As expected, it is minimum in the case of conventional full-controlled converter. Especially at light load conditions, that is corresponding to low output voltages, the fundamental power factor is very poor in this case. The performance of the

FIG. 2.10 FUNDAMENTAL POWER FACTOR VARIATION WITH LOAD VOLTAGE (P.U.)
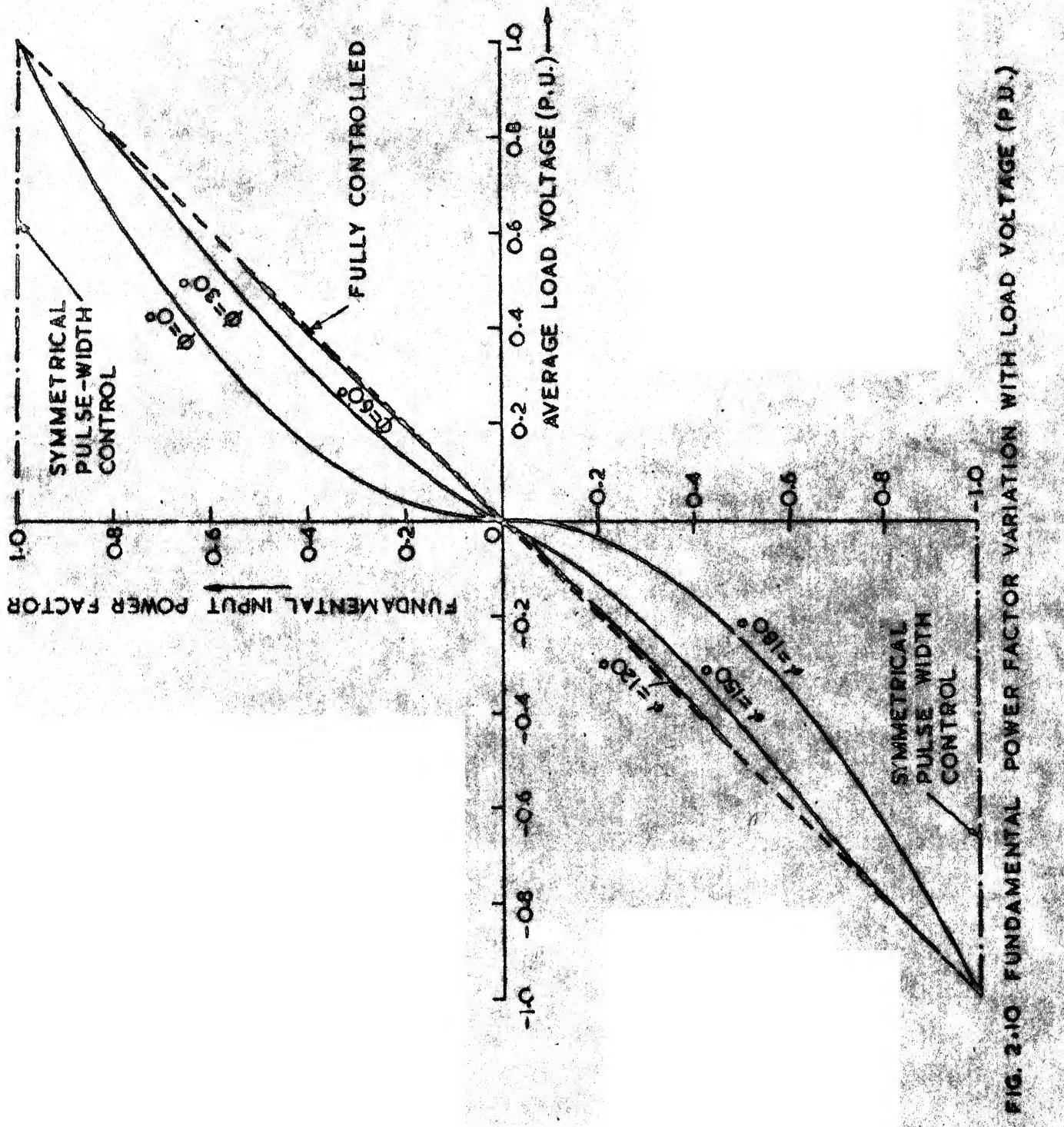
converter with optional free-wheel control with $\emptyset$ equal to zero for positive voltages and α equal to π for negative voltages shows significant improvement over that of the conventional converter. As free-wheel interval decreases with increasing values of $\emptyset$ and α in rectification and inversion modes respectively, there is less improvement in DSF compared to that in fully controlled converter.

The total input power factor is an important performance as it decides the volt-ampere requirement of input power apparatus. This is shown for the three converter circuit configurations in Fig. 2.11. The characteristics in the first quadrant correspond to rectification mode while those in the fourth quadrant correspond to regenerative mode. The symmetrical pulse width control compared to other schemes offers maximum power factor in the ac supply system. In this case also, the optional free-wheel with $\emptyset$ fixed at zero for positive output voltages or α fixed at π for negative output voltages provides better power factor compared to fully controlled circuit. The improvement in power factor decreases as the free-wheel interval decreases in the converter with optional free-wheel.

The harmonic factor is defined as the ratio of

47

FIG. 2.11   TOTAL   POWER FACTOR VARIATION   WITH   LOAD VOLTAGE (P.U.)

EXPTL. RESULTS:

RECTIFICATION WITH $\phi = 0°$
& REGENERATION WITH $\alpha = 165°$

RECTIFICATION WITH $\phi = 30°$
& REGENERATION WITH $\alpha = 150°$

RECTIFICATION WITH $\phi = 60°$
& REGENERATION WITH $\alpha = 120°$

INPUT (TOTAL) POWER FACTOR

AVERAGE LOAD VOLTAGE (P.U.)

SYMMETRICAL PULSE
WIDTH CONTROL

CONVENTIONAL FULLY
CONTROLLED

OPTIONAL FREEWHEEL
CONTROL
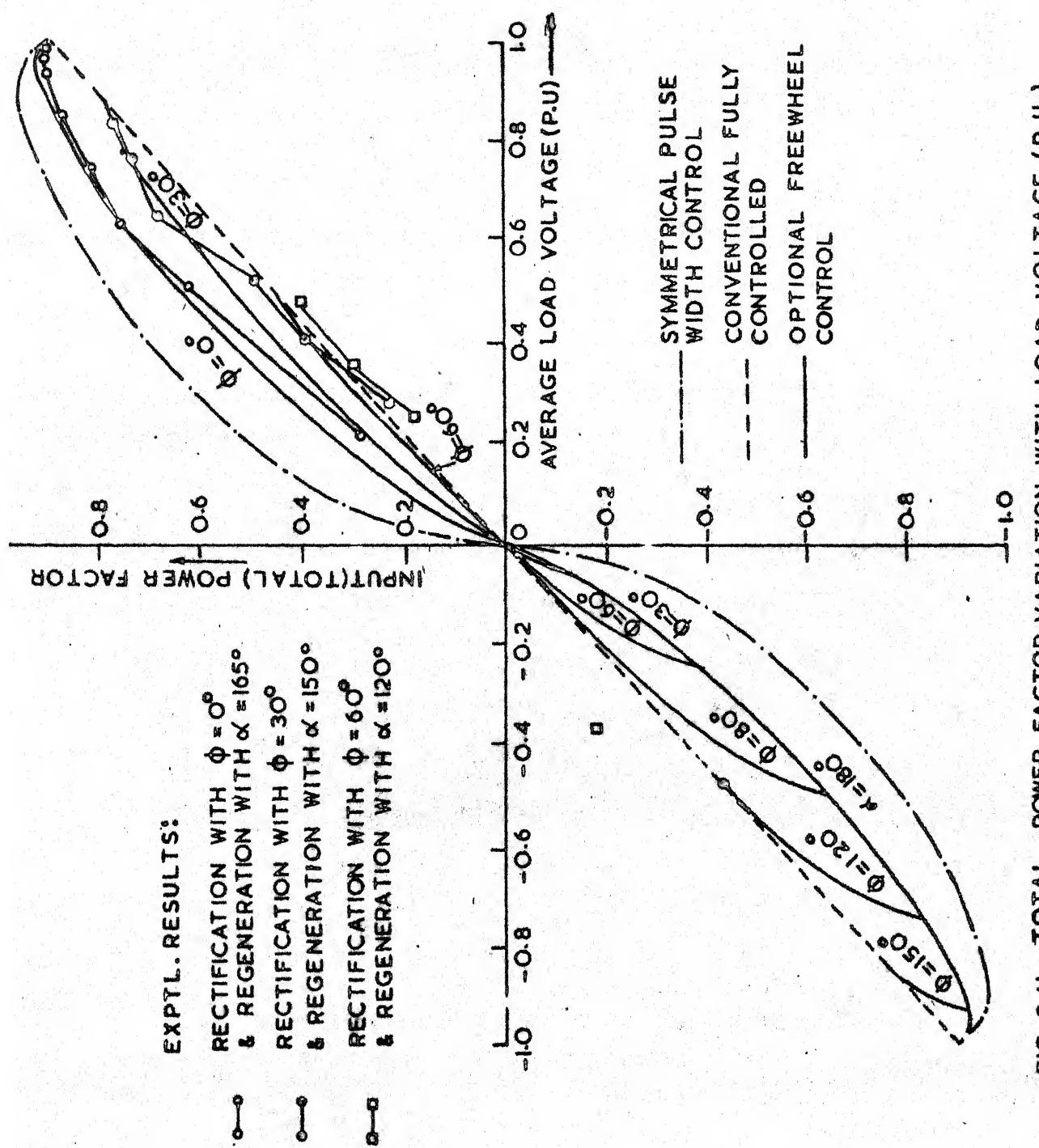
harmonic content to the rms fundamental component in the
ac supply current. This is illustrated in Fig.2.12 . It
remains constant over the entire range of the output vol-
tage in case of the conventional fully controlled scheme.
The harmonic factor increases astronomically as the out-
put voltage approaches zero in case of symmetrical pulse-
width control. It, of course, decreases with the increase
in the mean output voltage in rectification and inversion
modes. It is less than that of the conventional fully-
controlled bridge for higher output voltages. The harmo-
nic factor in case of fully-controlled bridge with half-
controlled characteristics, that is, $\emptyset$ equal to zero
for positive mean output voltages and α equal to π
for negative mean output voltages, is lesser than that of
the symmetrical pulse-width control scheme for a wide
range of the output voltage. At very large output voltages
does the difference between them become insignificant.
However, it is more than that of the conventional fully-
controlled scheme at lower output voltages. For higher
output voltages it is lesser than that of the conventional
full-controlled scheme. As free-wheeling interval decreas-
es with increasing values of $\emptyset$ in the rectification mode
and decreasing values of α in the inversion mode, the
harmonic factor decreases. For triggering angle $\emptyset$ less
than about 60° and for α greater than about 120° , the

EXPTL.RESULTS:

o RECTIFICATION WITH ϕ = 0°
   & REGENERATION WITH α = 165°

● RECTIFICATION WITH ϕ = 30°
   & REGENERATION WITH α = 150°

□ RECTIFICATION WITH ϕ = 60°
   & REGENERATION WITH α = 120°

SYMMETRICAL
PULSE-WIDTH
CONTROL

CONVENTIONAL
FULLY CONTROLLED
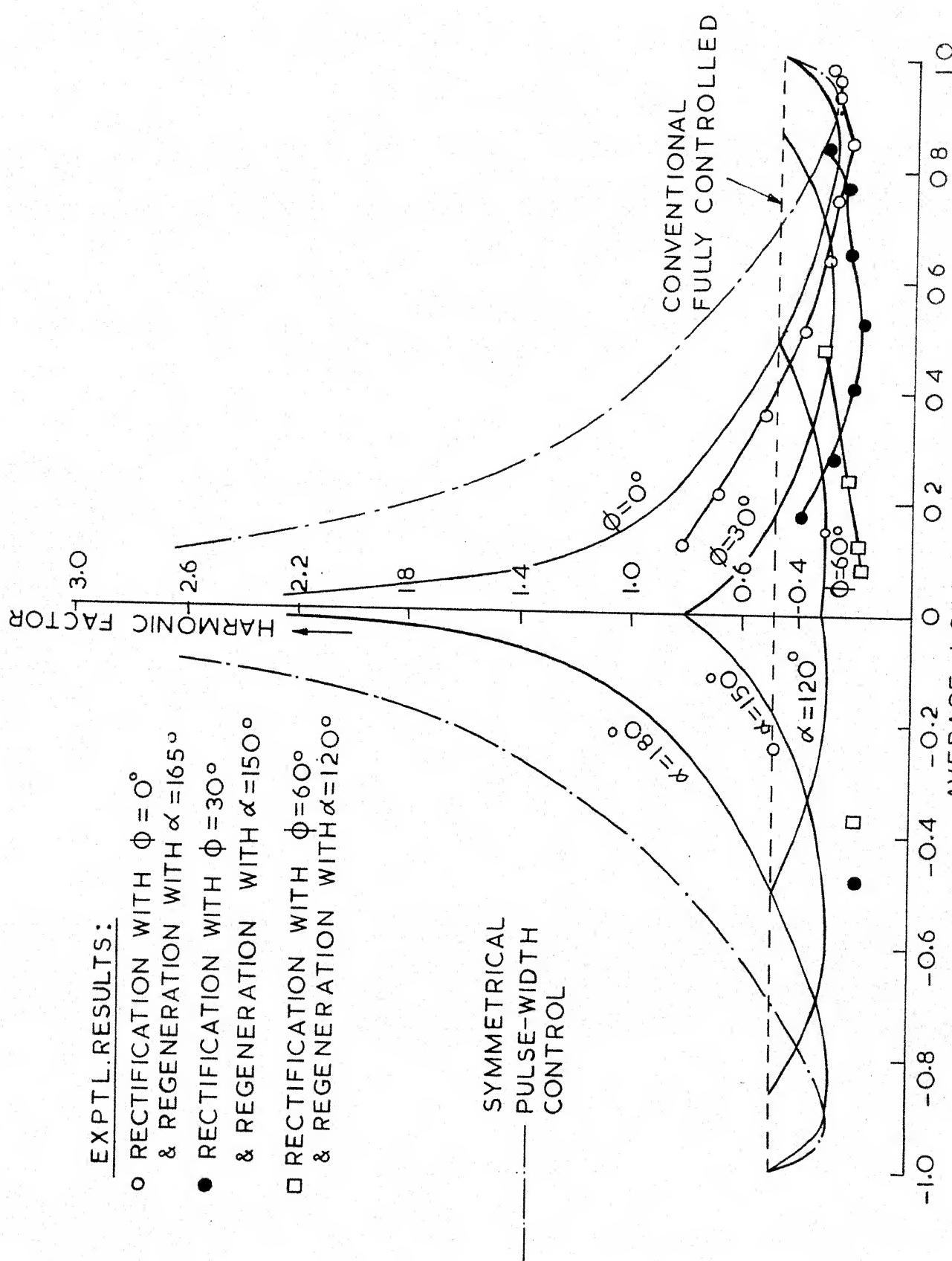
FIG. 2·12 INPUT HARMONIC FACTOR VERSUS AVERAGE LOAD VOLTAGE (P.U.)

harmonic factor decreases with increasing output voltages
in both rectification and inversion modes. However, for
higher values of $\emptyset$ or lower values of α , it appears
to be constant for low output voltages but increases
slightly with further increase in the output voltage for
a particular value of $\emptyset$ or α .

Experimental results are also shown for opt-
ional free-wheel. A good number of observations are re-
corded for the rectification mode. However, because of
non-availability of variable dc supply with wider range,
only a few readings are noted in the regenerative mode.
The theoretical results appear to be somewhat conservative
due to the assumption of constant current. In the actual
experimental set-up, the load current does consist of
some ripple, however small it may be. The discrepancy
between experimental and theoretical results may be
attributed to the finite ripple present in the load current.
Notice from Figs. 2.11. and 2.12. that there is good
agreement between experimental and theoretical results
at higher output voltages when the ripple in the load
current is negligibly small.

The peak-to-peak voltage ripple factor is shown
in Fig. 2.13 . The fully controlled converter with half-
controlled characteristics, that is, $\emptyset$ equal to zero
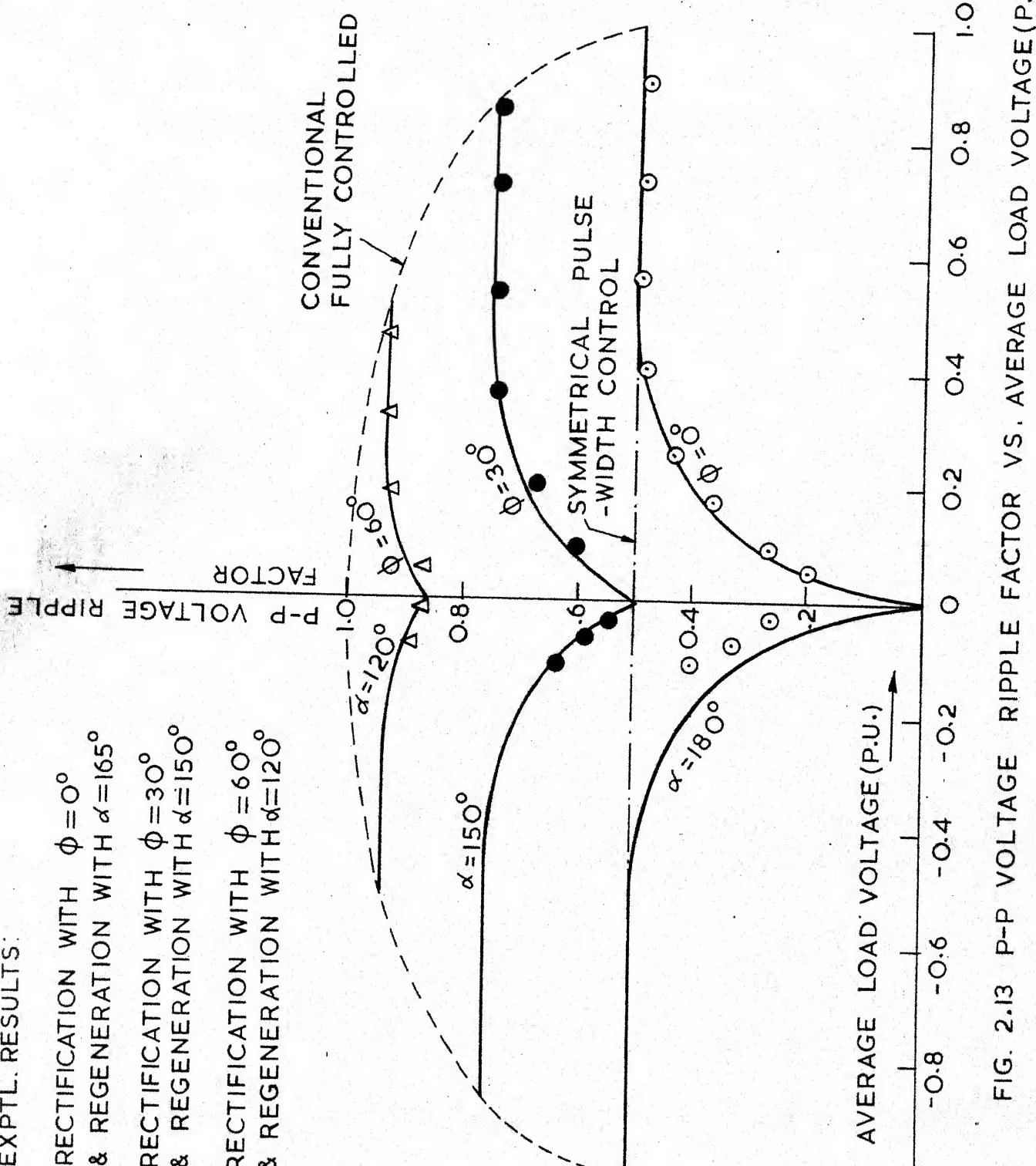
FIG. 2.13 P-P VOLTAGE RIPPLE FACTOR VS. AVERAGE LOAD VOLTAGE(P.U.)

EXPTL. RESULTS:

⊙ RECTIFICATION WITH $\phi = 0°$
   & REGENERATION WITH $\alpha = 165°$

● RECTIFICATION WITH $\phi = 30°$
   & REGENERATION WITH $\alpha = 150°$

△ RECTIFICATION WITH $\phi = 60°$
   & REGENERATION WITH $\alpha = 120°$

for positive output voltages and α equal to π for nega-
tive output voltages, shows the least p – p voltage
ripple factor. It is constant over half of the higher
output voltage range and decreases rapidly as the output
voltage decreases. For operation with other combinations
of α's and $\emptyset$'s the voltage ripple is always less than
that of the conventional fully controlled converter. The
ripple is constant over the entire voltage range in
symmetrical pulse-width control. For higher output voltag-
es, the ripple is the same in case of symmetrical pulse-
width control and fully-controlled converter with half-
controlled characteristics.

2.6. CONCLUSIONS

The comparative study of different circuit
configurations in traction power supply has revealed that
the symmetrical pulse-width modulation technique offers
maximum power factor. But it generates maximum distortion
in the source current especially at low output voltages.
Besides, it requires additional commutating elements and
complex control circuitry since it works on the principle
of forced commutation. On the other hand, the thyristor
converter configuration with optional free-wheel works on
line commutation requiring no additional commutating ele-
ments. For maximum power factor at low output voltages
in the rectification mode, the triggering angle $\emptyset$ is

held at zero and the triggering angle α is varied for variable output voltages. Alternatively, the triggering angle α is held constant at π and the triggering angle ϕ is varied for variable output voltage in order to realize maximum power factor in the inversion mode. This triggering strategy also offers least ripple in the output dc voltage. However, if harmonic distortion is to be minimised without affecting power factor much, it appears that both ϕ and α have to be controlled simultaneously. Further improvement in performances may be obtained by a series connection of several thyristor converter configurations [3, 6]. The single-phase fully-controlled thyristor converter configuration with optional free-wheel control provides better performance character-istics in traction power supplies compared to fully con-trolled thyristor converter and, therefore, can be regarded as an obvious choice in traction locomotives employing line commutated converter circuit configurations.

CHAPTER III

CONSTRUCTION OF OPERATING DIAGRAM AND
ESTIMATION OF MINIMUM INDUCTANCE IN FULLY
CONTROLLED CONVERTER WITH OPTIONAL FREEWHEELING

3.1 INTRODUCTION

In the preceding chapter the operating character-
istics of fully controlled converter with provision for
optional freewheel control have been obtained assuming the
load current to be continuous and constant. This assumption
can be made when the converter feeds a traction motor with
a large inductance in the armature circuit in addition to
the motor armature inductance. Furthermore, the possibility
of discontinuous armature current conduction is low with dc
series motors since the motor EMF is a function of the load
current. However, these converters are also widely used in
industry for the control of dc shunt motors which have
comparatively low armature inductance. Moreover, the motor
EMF is independent of load current. Hence, the load current
can be either continuous or discontinuous depending upon
the triggering angles and actual load circuit parameters,
namely, load phase angle and also load EMF. In case of
continuous current operation the load voltage waveform is
made up of portions of the ac supply voltage waveform and,

hence, determination of operating characteristics is tri-vial. In case of discontinuous current operation, however, different types of load voltage waveforms are encountered. These are recognised here as "modes". The expressions for voltage and current necessary to determine the operating characteristics are different for the different modes. Hence, a prior knowledge of the exact mode is desirable to determine the performance characteristics from the appro-priate set of equations. In this chapter, the different modes that are possible for the fully controlled converter with optional freewheel control in both rectification and inversion operations are identified. In the preceding chapter, it has been concluded that rectification operation is achieved with $\emptyset$ set to zero and variable α while inver-sion operation is achieved with α held constant at π and variable $\emptyset$ in order to realize maximum supply power factor. Hence, mode identification is carried out for these cases with the help of related operating diagrams [1].

In case of converter-fed motor drives, disconti-nuous current operation introduces adverse effects [14] like speed fluctuations, excessive instantaneous commutator bar-to-bar voltage and poor dynamic response. Also it requires a great deal of consideration for the control technique. These adverse effects can be overcome by

introducing additional inductance just sufficient to make
the current continuous. In this chapter, a graphical
procedure making use of the operating diagrams along the
lines given in reference [13] is presented for the deter-
mination of minimum inductance for the fully controlled
converter with optional freewheel for both rectification
and inversion operations.

3.2 OPERATING DIAGRAMS

The operating diagram of a converter defines
the possible and permissible conditions of operation of
the converter. In this diagram, the transition lines for
different load impedance angles separating the discontinu-
ous current region from that of the continuous current
are shown with the triggering angle and the normalised
load EMF as the variables [1] . In order to distinguish
the control variables α and $\emptyset$ of the converter circuit,
the operating diagrams are drawn separately for rectifier
and inverter operations. The thyristors in converter
circuits are generally provided with maintained trigger
pulses so that the devices turn on reliably with inductive
and back EMF loads. The gate pulses to the thyristors
are, therefore, assumed to be 180°-stretched while deriv-
ing the operating diagrams for the converter circuit. The
source impedance is neglected in the present analysis.

3.2.1 Computation

The operating diagrams are drawn on the basis of computational results. For different load impedance angles, θ , the load current is computed for various combinations of firing angles and normalised load EMFs to determine whether it is continuous or discontinuous. To obtain these results, it is necessary to compute the load current for only the first cycle of the supply voltage input to the converter circuit. In this section the expressions for the load current for different periods during the first cycle of the supply frequency are derived. These expressions are then used on a digital computer to obtain the operating diagrams of the converter circuit. In the following paragraphs the ac supply voltage is denoted by V_{Sm} sin ω t while the load comprises of a resistance, R, inductance, L, and EMF, E.

(i) Rectifier Operation:

In the first half cycle, the main thyristor pair T_1 and T_2 (Fig. 2.1) turn on at ω t = α_{act} (α_{act} denotes the actual turning on instant being equal to α or γ as the case may be). The operating circuit is as shown in Fig. 3.1 (a). The load current during the period $\alpha_{act} \leqslant \omega t \leqslant \pi$ is given by [1]
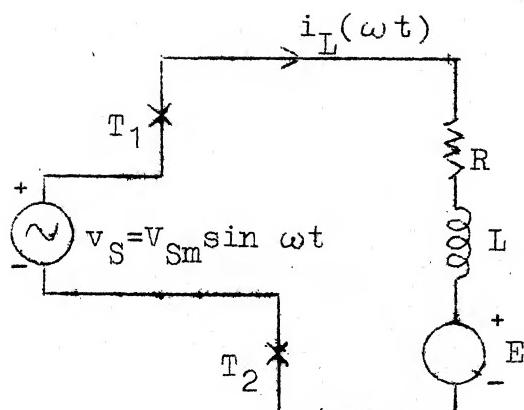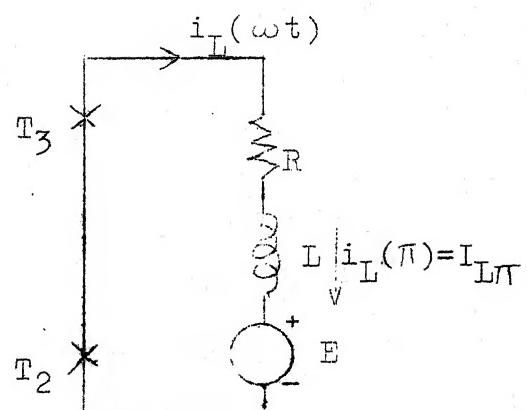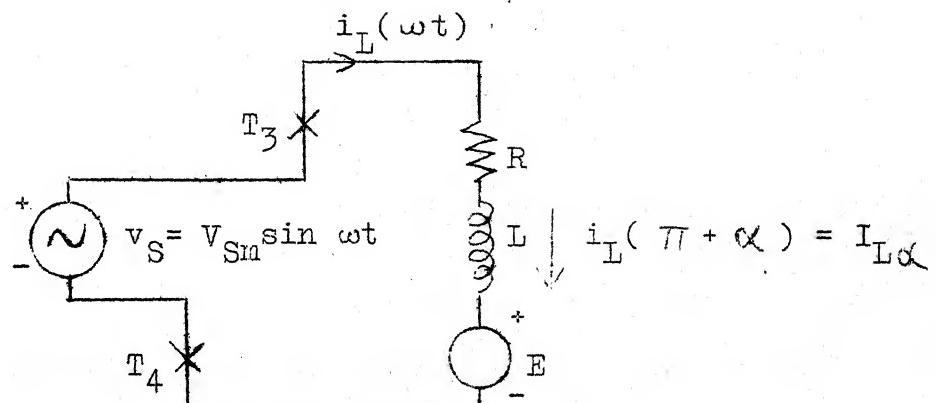
Fig. 3.1 Different operating circuits for rectifier operation

(a) Power interval ($\alpha_{act} \leqslant \omega t \leqslant \pi$)

(b) Freewheeling interval ($\pi \leqslant \omega t \leqslant \pi + \alpha$)

(c) Power interval ($\pi + \alpha \leqslant \omega t \leqslant 2\pi$)

$$i_L(\omega t) = (V_{Sm}/Z) \sin (\omega t - \theta) - (E/R) + A.\exp(-Rt/L)$$

where

$$Z = \left[R^2 + (\omega L)^2 \right]^{1/2}$$

$$\theta = \tan^{-1} (\omega L/R)$$

A is a constant and can be evaluated from the initial condition $i_L(\omega t) = 0$ at $\omega t = \alpha_{act}$. Substituting this initial condition in the above equation, we obtain,

$$i_L(\omega t) = (V_{Sm}/Z) \sin (\omega t - \theta) - (E/R) + \left[(E/R) \right.$$
$$\left. -(V_{Sm}/Z) \sin (\alpha_{act} - \theta) \right].\exp \left[-R(\omega t - \alpha_{act})/\omega L \right]$$

(3.1)

The normalised load current, $i_{LN}(\omega t)$, is obtained by dividing the actual load current by a factor V_{Sm}/Z (1 pu current). Also denoting the quantity E/V_{Sm} by the normalised load EMF, m, eqn.(3.1) reduces to

$$i_{LN}(\omega t) = \sin (\omega t - \theta) - (m/\cos \theta) + \left[(m/\cos \theta) \right.$$
$$\left. - \sin(\alpha_{act} - \theta) \right] .\exp \left[-(\omega t - \alpha_{act})/\tan \theta \right]$$

(3.2)

Freewheeling starts when the series-aiding thyristors are turned on at $\omega t = \pi$. Referring to the operating circuit of Fig. 3.1 (b) for this period

$\pi \leqslant \omega t \leqslant \pi + \alpha$, the load current is given by

$$i_L(\omega t) = - (E/R) + B . \exp (-Rt/L)$$

where B is a constant.

Solving the above eqn. with the initial condition $i_L(\omega t) = I_{L\pi}$ at $\omega t = \pi$. we get,

$$i_L(\omega t) = - (E/R) + \left[I_{L\pi} + (E/R) \right]$$
$$X \exp \left[- R (\omega t - \pi)/\omega L \right] \qquad (3.3)$$

Rewriting eqn. (3.3) in the normalised form, we have,

$$i_{LN}(\omega t) = - (m/\cos \theta) + \left[I_{L\pi N} + (m/\cos \theta) \right]$$
$$X \exp \left[- (\omega t - \pi)/\tan \theta \right] \qquad (3.4)$$

The thyristors T_3 and T_4 are triggered at $\omega t = \pi + \alpha$. The operating circuit for this period, $\pi + \alpha \leqslant \omega t \leqslant 2\pi$, is shown in Fig. 3.1 (c). The load current during this interval is given by,

$$i_L(\omega t) = - (V_{Sm}/Z) \sin (\omega t - \theta) - (E/R) + D$$
$$X \exp (-Rt/L)$$

where D is a constant and is obtained by putting the initial condition $i_L(\omega t) = I_{L\alpha}$ at $\omega t = \pi + \alpha$ in the above equation. We obtain,

$$i_L(\omega t) = - (V_{Sm}/Z) \sin (\omega t - \theta) - (E/R)$$

$$+ \left[(E/R) + I_{L\alpha} - (V_{Sm}/Z) \sin (\alpha - \theta) \right]$$

$$X \exp \left[-R (\omega t - \pi - \alpha)/\omega L \right] \qquad (3.5)$$

The normalised load current is given by

$$i_{LN}(\omega t) = - \sin (\omega t - \theta) - (m/\cos \theta)$$

$$+ \left[(m/\cos \theta) + I_{L\alpha N} - \sin (\alpha - \theta) \right]$$

$$X \exp \left[- (\omega t - \pi - \alpha)/\tan \theta \right] \qquad (3.6)$$

It should be noted that the above eqns. for the load current do not hold good for load impedance angle, $\theta = 90°$ as the term $m/\cos \theta$ becomes infinite for this case. Hence, the expressions for load current for this special case are derived by putting $R = 0$ in the basic differential equations [1]. Thus, for $\theta = 90°$, the expressions for the load current corresponding to eqns. (3.2) , (3.4) and (3.6) respectively are easily obtained as

$$i_{LN}(\omega t) = \cos \alpha_{act} - \cos \omega t - m (\omega t - \alpha_{act})$$

$$\alpha_{act} \leqslant \omega t \leqslant \pi \qquad (3.7)$$

$$i_{LN}(\omega t) = I_{L\pi N} + m (\pi - \omega t), \quad \pi \leqslant \omega t \leqslant \pi + \alpha \qquad (3.8)$$

and $i_{LN}(\omega t) = \cos \alpha + \cos \omega t - m (\omega t - \pi - \alpha) + I_{L\alpha N}$

$$\pi + \alpha \leqslant \omega t \leqslant 2\pi \qquad (3.9)$$

(ii) Inverter Operation :   At the instant $\omega t = 0$ in the

first half cycle when the main thyristor pair T_3 and T_4
(Fig. 2.1) is triggered, the source gets connected to the
load and the operating circuit is as shown in Fig. 3.2 (a).
The load current during this period, $0 \leqslant \omega t \leqslant \emptyset$, is
obtained as

$$i_L(\omega t) = (E/R) - (V_{Sm}/Z) \sin (\omega t - \theta) + A.\exp(-Rt/L)$$

where A is a constant and can be evaluated from
the initial condition $i_L(\omega t) = 0$ at $\omega t = 0$. We obtain,

$$i_L(\omega t) = (E/R) - (V_{Sm}/Z) \sin (\omega t - \theta) - [(E/R)$$
$$+ (V_{Sm}/Z) \sin \theta] . \exp (-R\omega t/\omega L) \qquad (3.10)$$

By normalising the load current, eqn. (3.10)
reduces to

$$i_{LN}(\omega t) = (m/\cos \theta) - \sin (\omega t - \theta) - [(m/\cos \theta)$$
$$+ \sin \theta] . \exp (-\omega t/\tan \theta) \qquad (3.11)$$

Freewheeling starts when the series-aiding
thyristor pair T_1 and T_4 is triggered at $\omega t = \emptyset$. The
operating circuit for the free-wheeling interval
$\emptyset \leqslant \omega t \leqslant \pi$, is shown in Fig. 3.2 (b) . Also, freewheeling
takes place through T_2 and T_3 during the interval,
$(\pi + \emptyset) \leqslant \omega t \leqslant 2\pi$. The eqn. for load current during
this period is given by

$$i_L(\omega t) = (E/R) + B . \exp (-Rt/L)$$

(a)

(b)

(c)
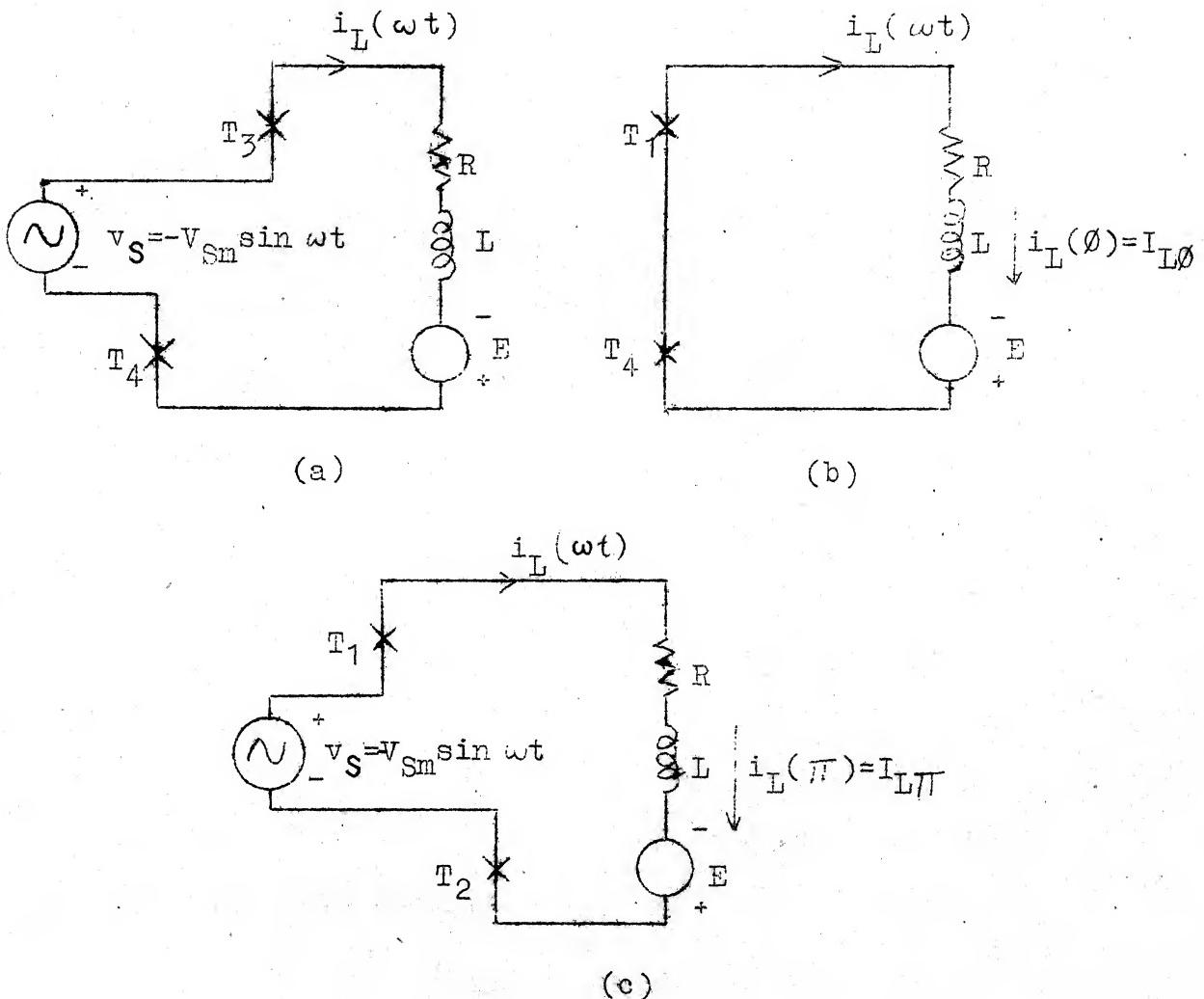
Fig. 3.2 Different operating circuits for inverter operation

(a) Power interval $(0 \leqslant \omega t \leqslant \emptyset)$

(b) Freewheeling interval $(\emptyset \leqslant \omega t \leqslant \pi)$

(c) Power interval $(\pi \leqslant \omega t \leqslant \pi + \emptyset)$

where B is a constant and can be evaluated from the initial condition $i_L(\omega t) = I_{L\emptyset}$ at $\omega t = \emptyset$. Thus the above equation reduces to

$$i_L(\omega t) = (E/R) + \left[I_{L\emptyset} - (E/R)\right].\exp\left[-R \ (\omega t - \emptyset)/\omega L\right]$$

(3.12)

Rewriting eqn. (3.12) in the normalised form, we have,

$$i_{LN}(\omega t) = (m/\cos \theta) + \left[I_{L\emptyset N} - (m/\cos \theta)\right]$$
$$X \exp\left[-(\omega t - \emptyset)/\tan \theta\right]$$

(3.13)

Freewheeling continues till $\omega t = \pi$ when the thyristors T_1 and T_2 are triggered to connect the source to the load. The operating circuit for this period $\pi \leqslant \omega t \leqslant \pi + \emptyset$, is shown in Fig. 3.2 (c). The load current during this interval is given by

$$i_L(\omega t) = (E/R) + (V_{Sm}/Z) \sin (\omega t - \theta) + D.\exp(-Rt/L)$$

where D is a constant which can be evaluated from the initial condition $i_L(\omega t) = I_{L\pi}$ at $\omega t = \pi$ as follows.

$$i_L(\omega t) = (E/R) + (V_{Sm}/Z) \sin (\omega t - \theta) + \left[I_{L\pi} - (E/R)\right.$$
$$\left. - (V_{Sm}/Z) \sin \theta\right].\exp\left[-R(\omega t - \pi)/\omega L\right] \quad (3.14)$$

The normalised load current is obtained from eqn. (3.14) as

$$i_{LN}(\omega t) = (m/\cos\theta) + \sin(\omega t - \theta) + [I_{L\pi N} - (m/\cos\theta)$$
$$- \sin\theta].\exp[-(\omega t - \pi)/\tan\theta] \qquad (3.15)$$

As pointed out in the case of rectification, eqns. (3.11), (3.13) and (3.15) will not hold good when $\theta = 90°$. They are to be drived from the first principles. It can be easily shown that the equations for the load current when $\theta = 90°$ are as given below.

$$i_{LN}(\omega t) = m.\omega t - 1 + \cos\omega t \;, \quad 0 \leqslant \omega t \leqslant \emptyset \qquad (3.16)$$

$$i_{LN}(\omega t) = I_{L\emptyset N} + m(\omega t - \emptyset) \;, \quad \emptyset \leqslant \omega t \leqslant \pi \qquad (3.17)$$

$$i_{LN}(\omega t) = I_{L\pi N} + m(\omega t - \pi) - 1 - \cos\omega t$$
$$\pi \leqslant \omega t \leqslant \pi + \emptyset \qquad (3.18)$$

The normalised equations are used to find the load current at different instants in the first cycle of the supply frequency. The flow-charts of the computer programs used to obtain data for constructing the operating diagrams are shown in Fig. 3.3 and 3.4 for rectifier and inverter operations respectively. In addition to the operating diagrams of the converter circuit, the different possible modes of current conduction are obtained using these flow-charts. The classification and identification of different modes is explained in the next section.
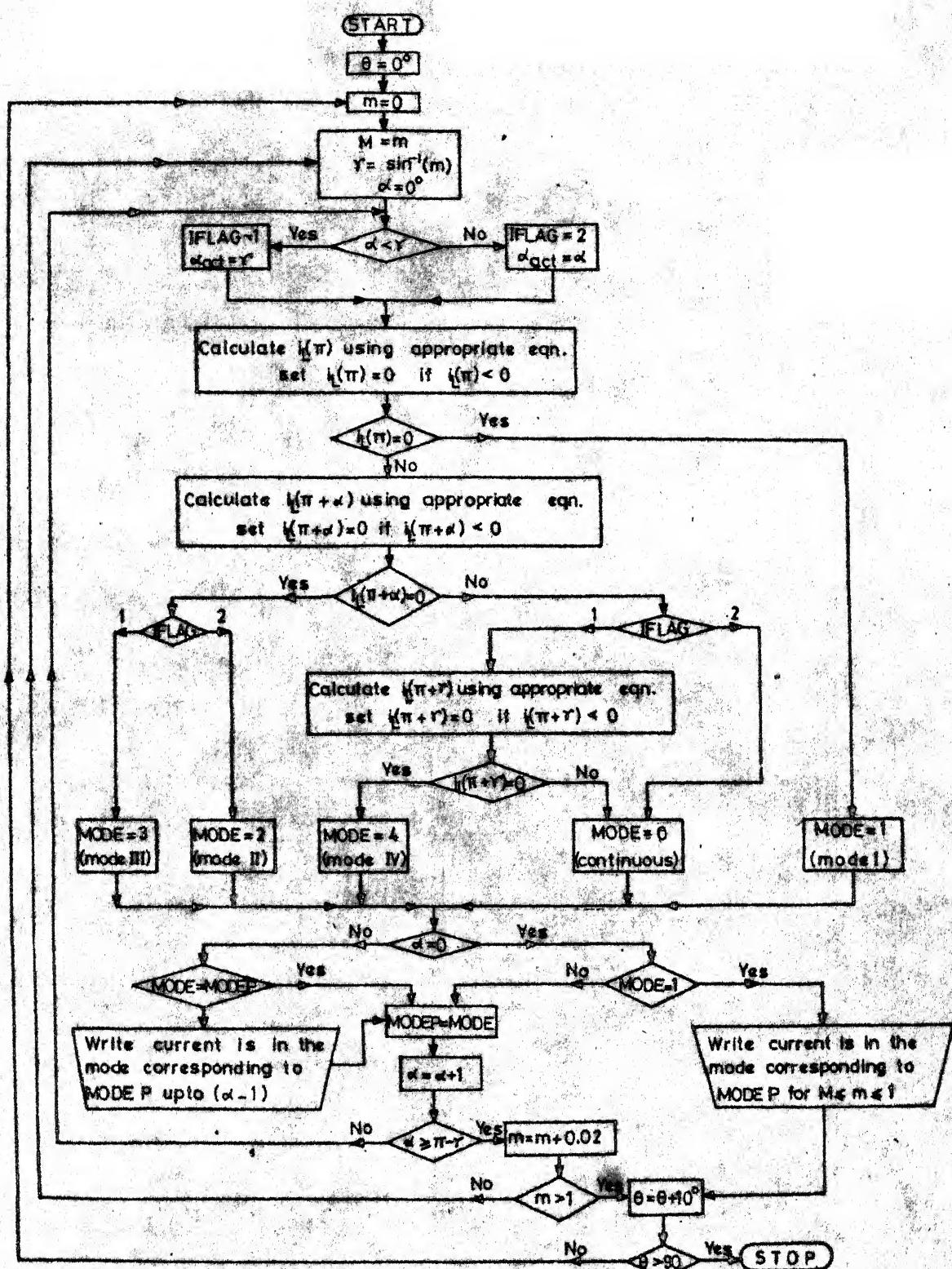
Fig. 3.3 Flow-chart of the computer program to obtain operating diagram and for identification of modes for rectifier operation.

START

$\theta = 0^\circ$

m = 0

$Y = \sin^{-1}|m|$
$\phi = 0^\circ$

$\phi \leqslant \pi - \Upsilon$ — Yes / No

Yes branch:

Calculate $i_L(\phi)$ using appropriate eqn.
set $i_L(\phi) = 0$ if $i_L(\phi) < 0$
IFLAG = 1 if $i_L(\phi) > 0$
IFLAG = 0 if $i_L(\phi) = 0$
Calculate $i_L(\pi)$ using appropriate eqn.
set $i_L(\pi) = 0$ if $i_L(\pi) < 0$

IFLAG — 1 / 0

Calculate $i_L(\pi + \phi)$ using appropriate eqn.
Set $i_L(\pi + \phi) = 0$ if $i_L(\pi + \phi) < 0$

$i_L(\pi + \phi) = 0$ — No / Yes

No branch:

Calculate $i_L(\pi - \Upsilon)$ using appropriate eqn.
set $i_L(\pi - \Upsilon) = 0$ if $i_L(\pi - \Upsilon) < 0$.

$i_L(\pi - \Upsilon) = 0$ — No / Yes

Calculate the values of $i_L(wt)$ for
$wt = \phi$, π and $(2\pi - \Upsilon)$
using appropriate eqn.
set $i_L(wt) = 0$ if $i_L(wt) < 0$.

$i_L(2\pi - \Upsilon) = 0$ — Yes / No

Calculate $i_L(\pi + \phi)$ using appropriate eqn.
set $i_L(\pi + \phi) = 0$ if $i_L(\pi + \phi) < 0$.

$i_L(\pi + \phi) = 0$ — Yes / No

MODE = 0 (continuous)

MODE = 1 (mode I)

MODE = 2 (mode II)

MODE = 0 (continuous)

$\phi = 0^\circ$ — Yes / No

MODE = MODE P — Yes / No

Write current is in the mode corresponding to MODE P upto $(\phi - 1)$

MODE P = MODE

$\phi = \phi + 1^\circ$

$\phi > 180^\circ$ — No / Yes

Write current is in the mode corresponding to MODE P upto $(\phi = 180^\circ)$

m = m − 0.02

m < −1 — No / Yes

$\theta = \theta + 10^\circ$

$\theta > 90^\circ$ — No / Yes

STOP

Fig. 3.4   Flow-chart of the computer program to obtain operating diagram and for identification of modes for inverter operation.

3.3 CLASSIFICATION OF MODES AND THEIR IDENTIFICATION ON THE OPERATING DIAGRAMS

3.3.1 Rectifier Operation

Apart from the continuous current mode, there are different modes of operation when the load current becomes discontinuous. The normalised equations for the load current derived in section 3.2.1 are used to construct the operating diagram. Fig. 3.5 shows operating diagram of the fully controlled converter with half-controlled characteristics in the rectifier operation. Operation of the converter is possible for any point below the boundary PQE . For any given values of θ and m, the solid curves in the diagram represent the transition from continuous current operation to discontinuous current operation as α is increased. For any given θ, any point lying below the corresponding curve represents continuous current operation, and any point above represents discontinuous current operation.

As an example, let us consider the load impedance angle $\theta = 60°$ in our discussion. SRE is the transition curve. Any point in the region SRETS represents operation with continuous current. The region SRTS corresponds to $\alpha \leqslant \gamma$ while the region TERT corresponds to $\alpha > \gamma$. In the continuous region the thyristors turn on the instant they
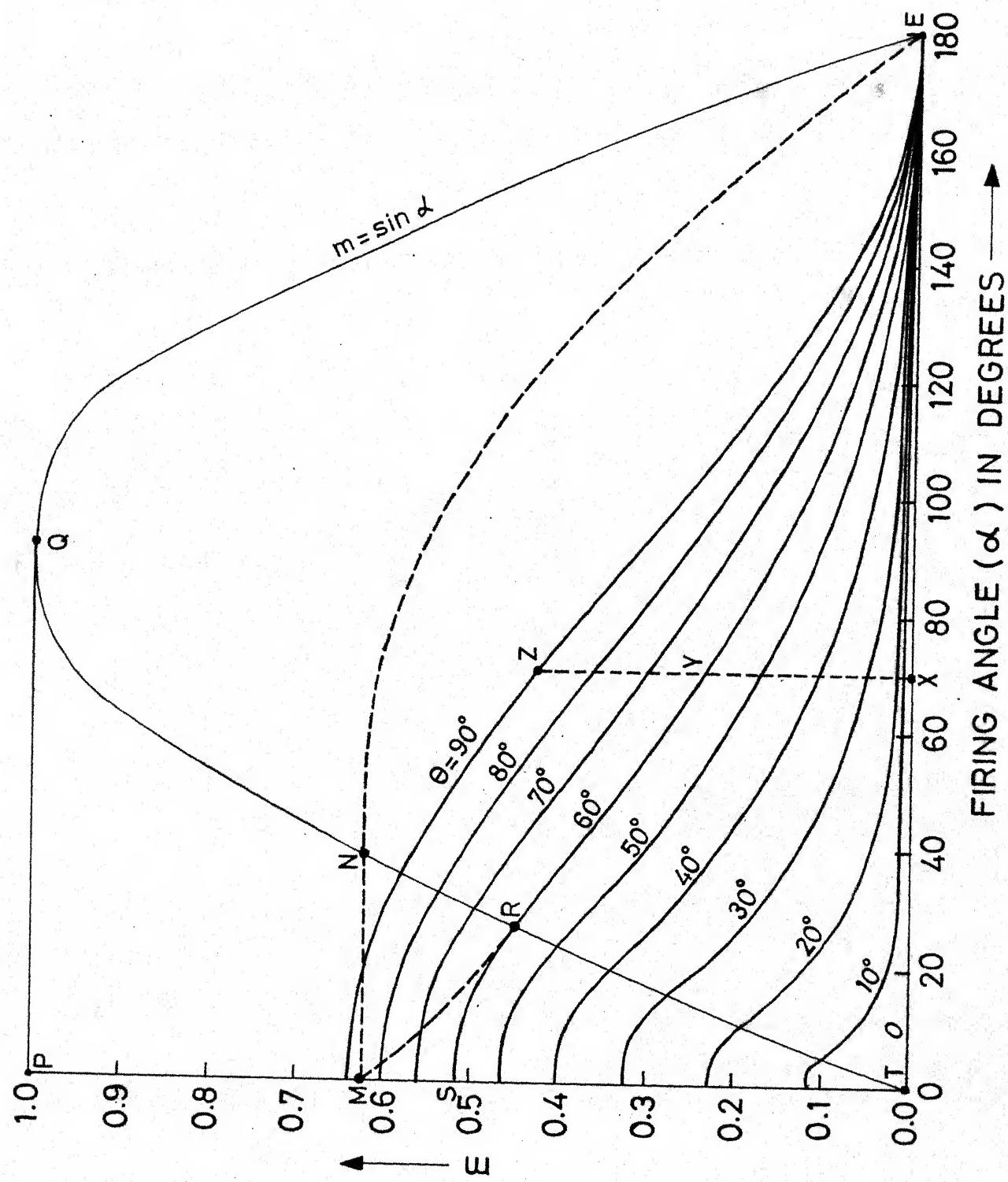
Fig. 3.5 Operating diagram for rectifier operation
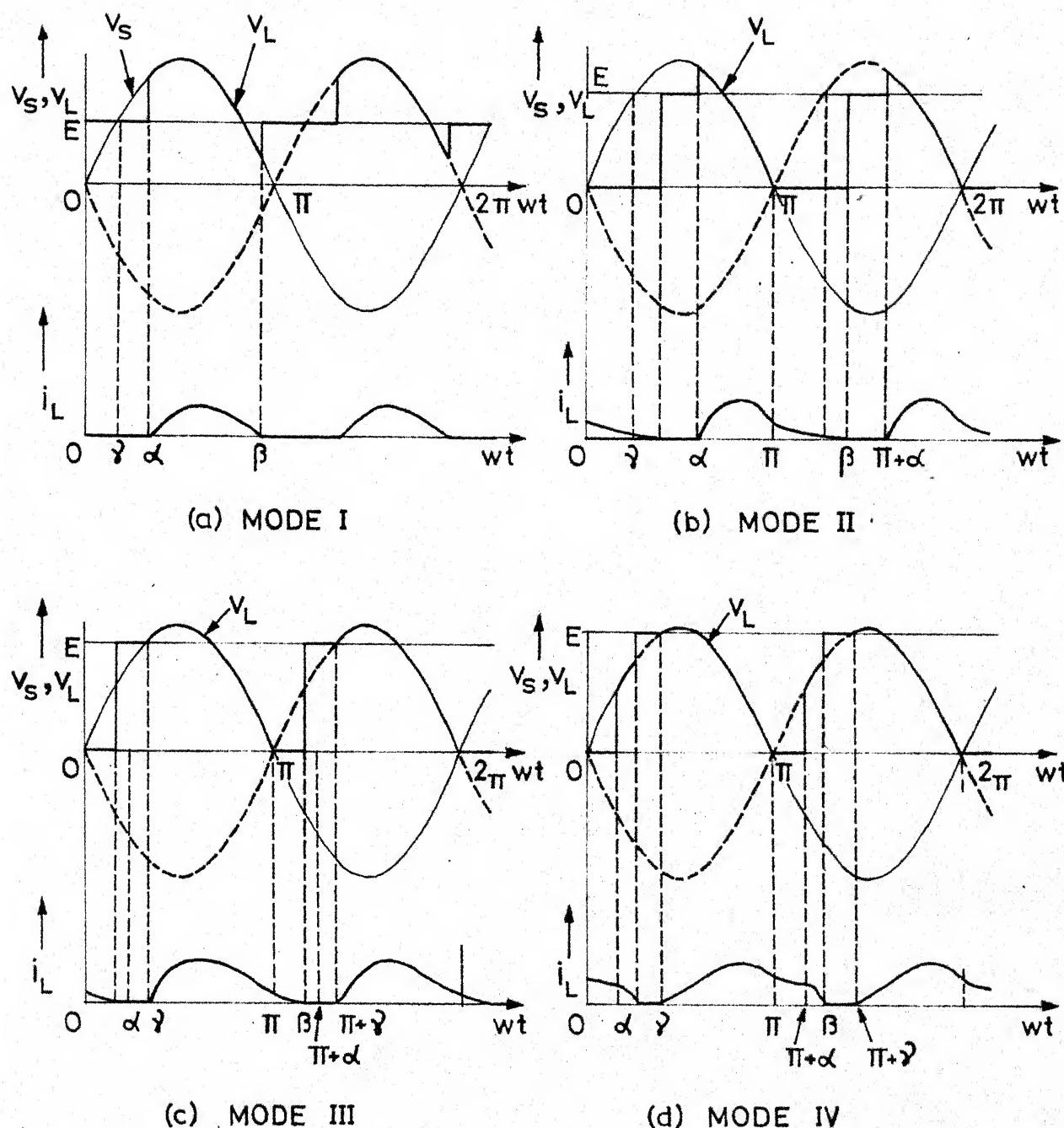
Fig. 3.6 Steady-state voltage and current waveforms
for different modes of discontinuous current
for rectifier operation.

are triggered whether the triggering is done before or
after $\omega t = \gamma$. A point in the region PQERSP represents
a condition of discontinuous current operation. There are
four distinct possible modes of operation in the disconti-
nuous region.

Mode I : The load voltage and load current waveforms
alongwith the supply voltage for this mode are shown in
Fig. 3.6 (a). The main thyristor pairs turn-on at α or γ
depending on whether $\alpha \gtrsim \gamma$ or $\alpha < \gamma$. Here , γ represents
the instant when instantaneous value of the supply voltage
equals the load circuit EMF as shown in Fig. 3.6 . This
mode is characterised by the load current falling to zero
before the next half cycle of the supply voltage starts.
This means there is no freewheeling of load current at all
and $\beta \leqslant \pi$. Here, β represents the extinction angle of
the load current. This mode is identified by the region
PQENMP in the operating diagram (Fig. 3.5) . .

Mode II : This mode exists when $\alpha \gtrsim \gamma$. The main
thyristor pair turn on when triggered at $\omega t = \alpha$ and
freewheeling commences at $\omega t = \pi$ by triggering the res-
pective series-aiding thyristors. The load current falls
to zero before the other main thyristor pair is turned on
at $\omega t = \pi + \alpha$ in the next half cycle, i.e., $\beta \leqslant \pi + \alpha$
for this mode. The associated waveforms are shown in

Fig. 3.6 (b) and the region NERN represents this mode in the operating diagram of Fig. 3.5 .

Mode III : This mode may occur for $\alpha < \gamma$. Though triggered earlier the main thyristor pair turn on only at $\omega t = \gamma$. However, the load current falls to zero before the other main thyristor pair is triggered at $\omega t = \pi + \alpha$ in the next half cycle as depicted in Fig. 3.6 (c) , This mode is identified by the region MNRM in the operating diagram as shown in Fig. 3.5 .

Mode IV : The different waveforms for this mode are shown in Fig. 3.6 (d) . The sequence of operations are same as those in mode III except that load current is present when the main thyristor pairs are triggered at α in each half cycle. Hence, these thyristors turn on and the source gets connected to the load at that instant. However, the load current falls to zero before the ac supply voltage reaches the load circuit EMF level. Thus, $(\pi + \alpha) < \beta < (\pi + \gamma)$ for this mode. In the operating diagram (Fig. 3.5), this mode is represented by the region MRSM.

3.3.2 Inverter Operation

Fig. 3.7 shows the operating diagram for inverter operation of the fully controlled converter with half-
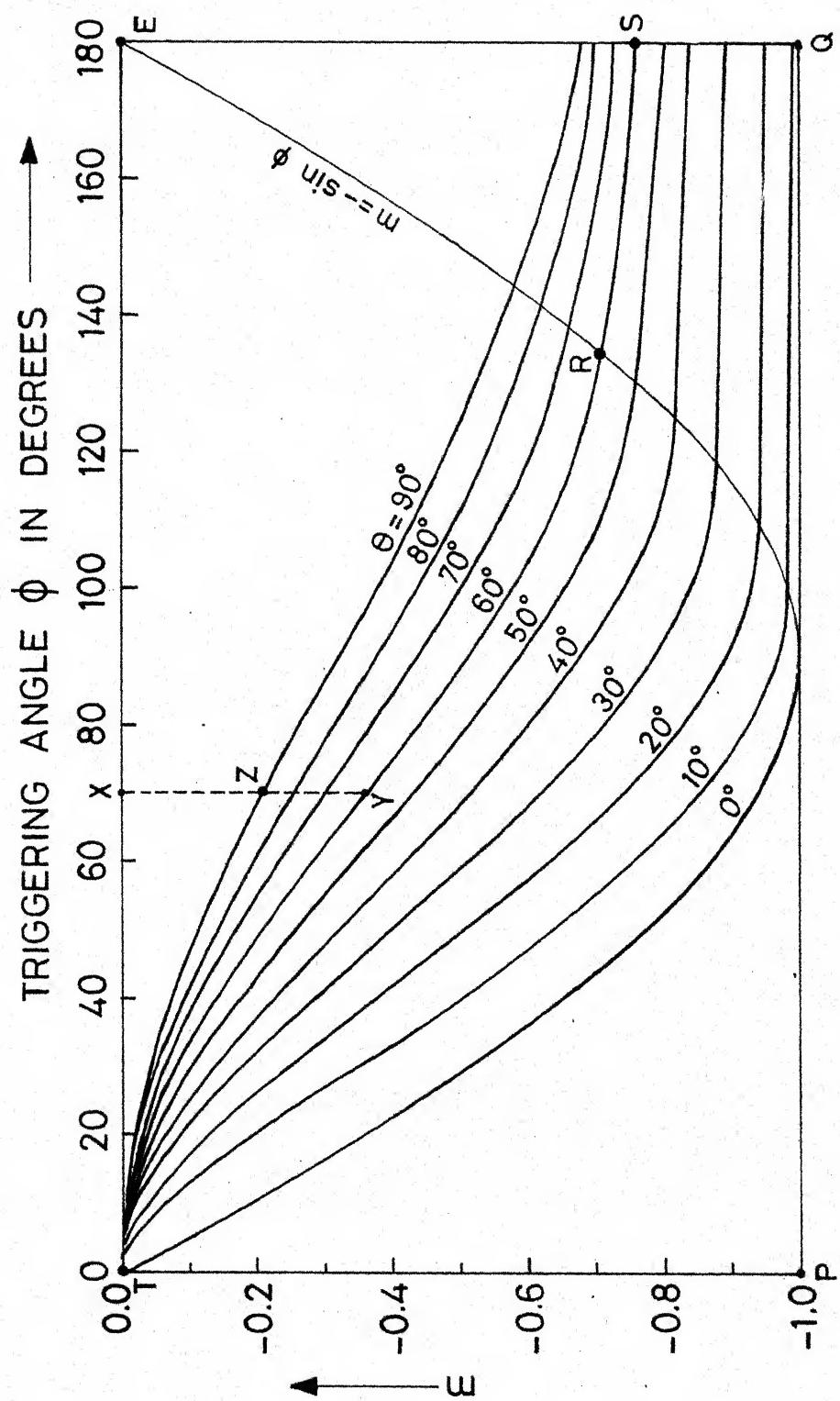
Fig.3.7 Operating diagram for inverter operation
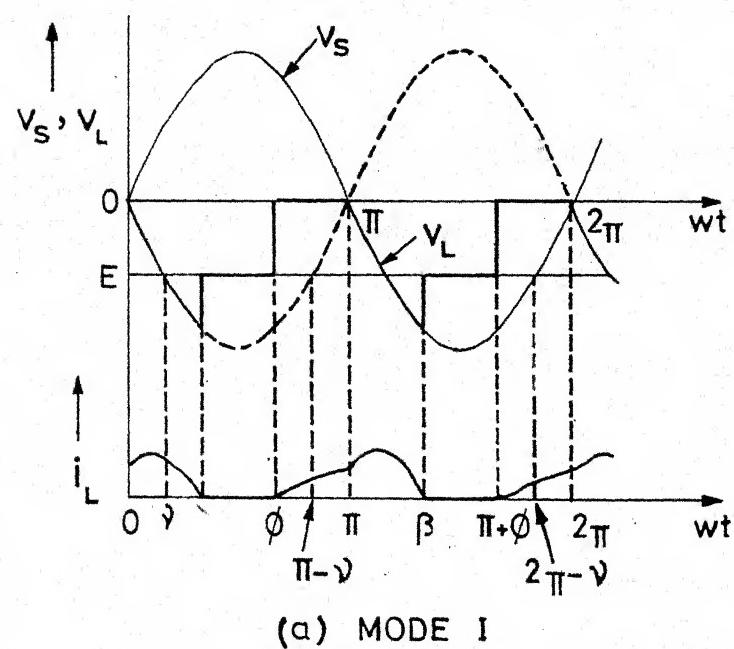
(a) MODE I
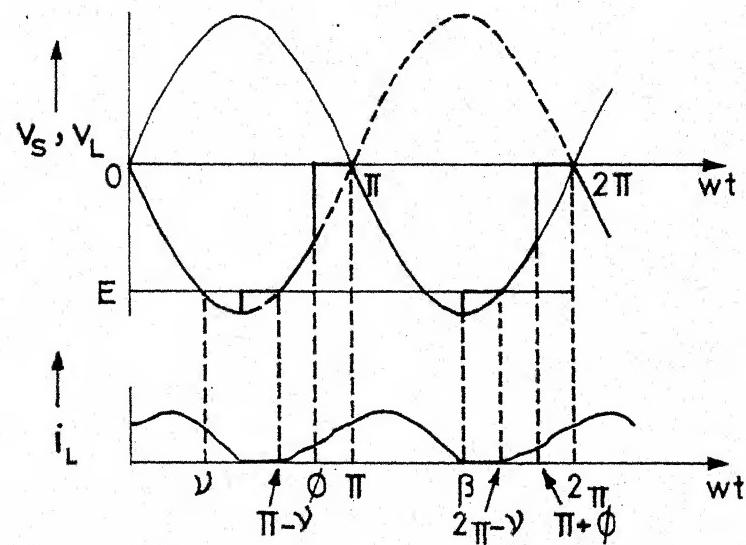
(b) MODE II

Fig. 3.8 Steady state voltage and current waveforms for different modes of discontinuous current for inverter operation.

controlled characteristics. Inverter operation is possible at any point inside the region TEQP. As in the case of rectifier operation for a given θ, any point lying below the corresponding curve represents continuous current operation, and any point above represents discontinuous current operation. As an example, let us again consider $\theta = 60°$ in our discussion. TRS is the separating curve.

Any point in the region TRSQPT represents a condition of continuous current operation while that in the region TESRT represents a condition of discontinuous current operation. In the discontinuous current region, there are two distinct possible modes.

Mode I : The associated waveforms for this mode are shown in Fig. 3.8 (a). The load gets connected to the source at $\omega t = 0$ when the main thyristor pair (T_3 and T_4) is triggered. However, the load current falls to zero before $\omega t = \emptyset$ when the freewheeling is initiated by triggering the corresponding series-aiding thyristor pair. Freewheeling continues till $\omega t = \pi$ when the other main thyristor pair (T_1 and T_2) is triggered to connect the load to the source and the process is repeated. This mode is identified by the sub-region TERT in the operating diagram as shown in Fig. 3.7 .

Mode II : This mode is possible for larger values

of $\emptyset$ when $\emptyset > (\pi - \gamma)$. The main thyristor pair (T_3 and T_4) is turned on at $\omega t = 0$ and current flows to the load from the source. The load current falls to zero before $\omega t = \pi - \gamma$. However, these thyristors are forward biased at $(\pi - \gamma)$. Since the thyristors are triggered by 180°-stretched pulses, they turn on once again in the same half cycle at $\omega t = (\pi - \gamma)$ thereby connecting the source to the load. Thus, some load current is present at $\omega t = \emptyset$ when the respective series-aiding thyristor pair is triggered so as to provide freewheeling path for the load current. The extinction angle $\beta < (2\pi - \gamma)$. This mode is demonstrated in Fig. 3.8 (b) while in the operating diagram of Fig. 3.7 the region ERSE represents this mode.

3.4 MINIMUM INDUCTANCE ESTIMATION

It may be desirable to insert additional inductance in the load circuit to avoid discontinuous current operation. An analytical method [14] describes calculation of minimum inductance necessary to achieve continuous current operation in conventional fully controlled converter system when the load resistance is negligible. The same method may be applied for minimum inductance estimation in case of fully controlled converter with half-controlled characteristics. The load resistance, however, cannot be neglected in some applications where the

converter is used for the control of a small dc machine.
A graphical method for estimating the minimum inductance
necessary to achieve continuous current operation is pre-
sented for the fully controlled converter with half-
controlled characteristics taking the load resistance
also into account. This graphical procedure is along the
lines given in the reference [13] .

For example, consider the operating diagram
for rectifier operation of the converter as shown in Fig.
3.5 . For certain triggering angle, α indicated by
the point X in the diagram, the ordinate XY gives the
normalised value of the load circuit EMF, E/V_{Sm} at the
limit of continuous current operation with $\theta = 90°$. The
ordinate XZ gives the normalised value of the average
output voltage, V_{LAV}/V_{Sm}, at the limit of continuous curr-
ent operation since the average voltage across a pure in-
ductor ($\theta = 90°$) is zero. Therefore, for the triggering
angle, X, the ordinate YZ equals the normalised value of
the average voltage drop, $I_L R/V_{Sm}$, across the load circuit
resistance. This is represented by point A in the plane
whose co-ordinates are α and $I_L R/V_{Sm}$ as shown in
Fig. 3.9 . Similarly, the normalised average voltage
drop across the resistance at the limit of continuous
current operation for other values of triggering angle
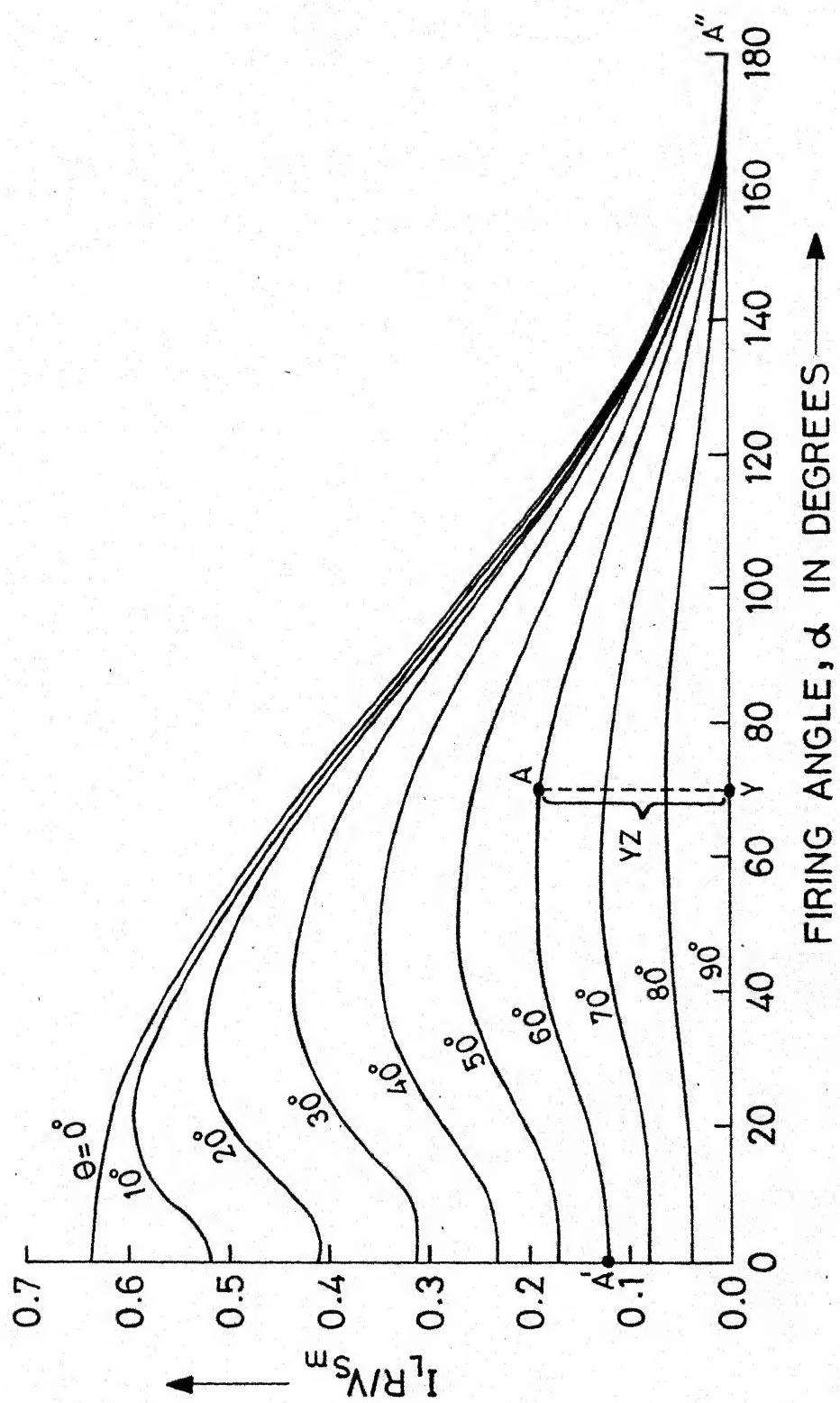
Fig. 3.9 Minimum load impedance angle for continuous current in rectifier operation.
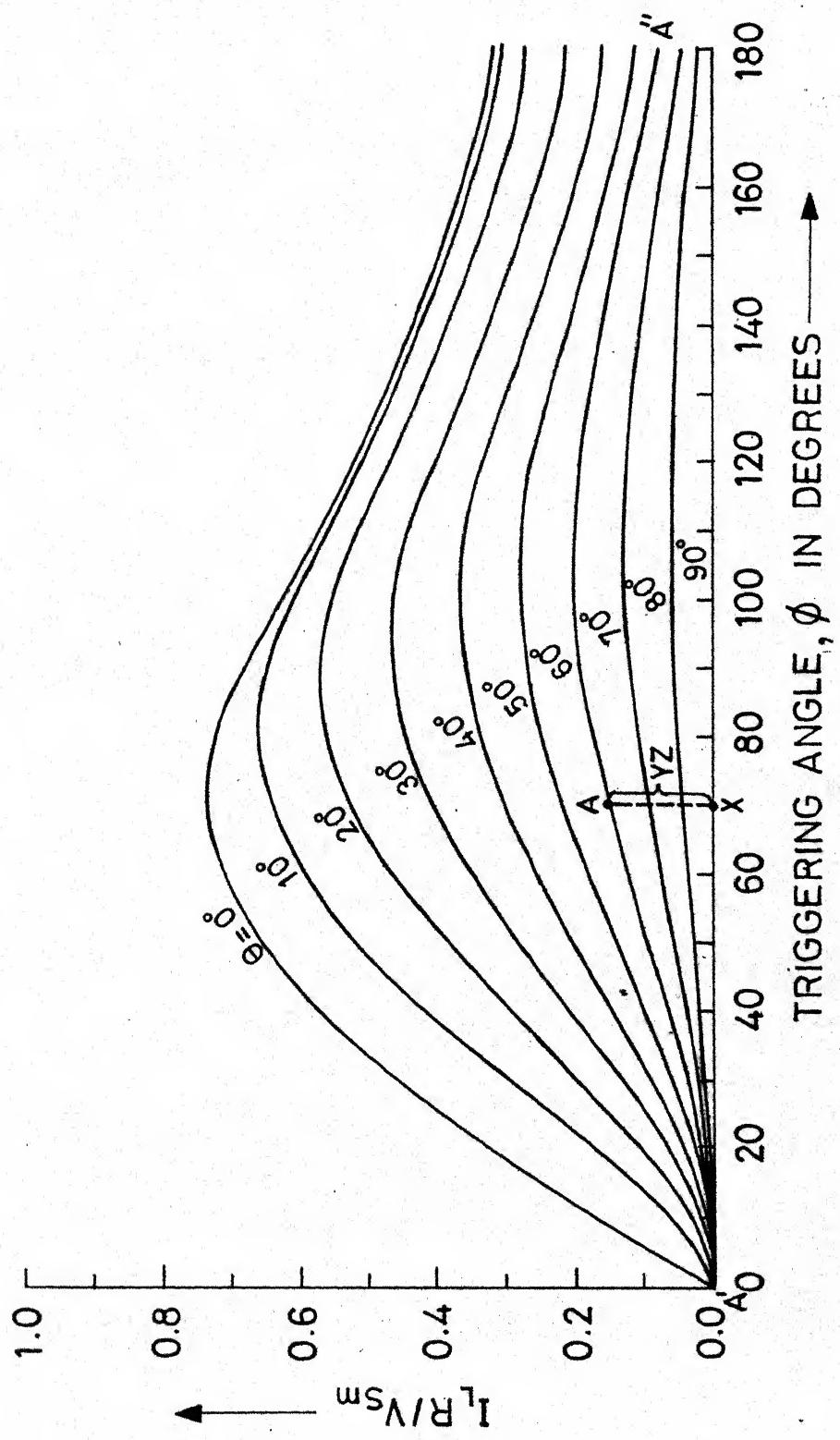
Fig. 3.10 Minimum load impedence angle for continuous current in inverter operation.

result in the curve $A'A\,A''$ in Fig. 3.9 . Using a simi-
lar procedure the curves in Fig. 3.9 for other values of
load impedance angle, θ, are obtained. The same method
when used with the operating diagram shown in Fig. 3.7
for inverter operation result in the curves shown in
Fig. 3.10 . The curves in Fig. 3.9 and 3.10 provide in-
formation regarding minimum inductance estimation for con-
tinuous current operation. As an example, let us consider
the rectifier operation of the converter on a dc motor
whose armature resistance, R_m , and armature inductance,
L_m , and hence armature circuit load angle, θ_m , are
known. For a particular firing angle, α , and back EMF ,
E , in the operating region of the motor, the load current
may become discontinuous which is known from the operating
diagram of Fig. 3.5 . In that case, the average load
current is calculated and the normalised average resistive
drop $I_L R/V_m$ is found out. Let the corresponding operating
point when located on the diagram of Fig. 3.9 fall on the
curve $A'A\,A''$. Since this curve represents the normalis-
ed value of average resistive drop at the limit of discon-
tinuous current operation for $\theta = 60°$, it means the mini-
mum value of θ for continuous current operation amounts
to 60°. If $\theta_m < 60°$, then the additional inductance, L_{add},
to be connected in series with the motor armature to make
the load current just continuous amounts to

$$L_{add} = (\tan 60° - \tan \theta_m) \cdot R_m / \omega \quad .$$

This gives the value of the additional induct-ance for a particular operating point. If the region of operation of converter-fed motor is known apriori for both rectification and inversion, the additional inductance can be calculated for different operating points in the entire region following the above procedure. Choosing the maximum value of these additional inductances would then assure converter operation in the continuous current mode.

3.5 CONCLUSIONS

The single-phase fully controlled converter with half-controlled characteristics is potentially suit-able for the control of not only traction drives but also industrial drives owing to improved performance character-istics. The industrial drives may also consist of sepa-rately excited dc motors. The load current is likely to become discontinuous more with these motors. Operating diagrams are established for the fully controlled conver-ter with half-controlled characteristics for both rectif-ier and inverter operations. Different possible modes of discontinuous current operation of this converter are recognised and identified on the operating diagrams. The single-phase converters are generally used to control

industrial drives of lower ratings upto about 7.5 kw where the motor resistance may not be negligible. A graphical procedure making use of the operating diagrams is described in this chapter to calculate the minimum inductance necessary to achieve continuous current operation.

CHAPTER IV

REACTIVE POWER COMPENSATION IN INDUSTRIAL POWER SYSTEMS

4.1 INTRODUCTION

The industrial load accounts for the maximum power consumption in the power system. Unlike household consumers, the industrial load comprising of mostly induction motors draws large amount of lagging reactive power from the power supply system. Transformers used in power transmission and distribution network also consume reactive power owing to magnetizing current drawn by them. The induction furnaces which are widely used in industries also draw large amount of lagging kVAR. The household consumers also require lagging kVAR, however small it may be compared to that of the bulk consumers, due to the extensive use of fluorescent lights, fans and various other appliances using fractional horse power ac motors. Thus, the reactive power requirement on the power system adds up to a large amount. This wattless power causes the system to operate at low power factor. There are many disadvantages as pointed out in Chapter I if the supply power factor is low.

These disadvantages can be overcome to a large

extent if the power factor is improved externally. In fact, it is a practice since the inception of ac power transmission to install reactive power compensators for power factor improvement. The reactive power compensators are external devices which supply and compensate the lagging reactive power consumed by the load thereby relieving the burden on the ac supply. These compensators are also known as power factor correcting devices. Obviously, these reactive power compensators are connected across the load terminals to relieve the transmission lines also from the excess current. Hence, they are called Shunt compensators.

With the passage of time, the shunt compensators have gone through several modifications with the rapid developments in the power system as regards the increase in the operating voltage level and complex interconnections of large networks. In what follows, a review of such reactive shunt compensators has been presented.

4.2 SHUNT REACTIVE POWER COMPENSATORS

4.2.1 Fixed Capacitor Banks

Shunt capacitors were first employed for power factor correction in the year 1914 [4]. The leading current drawn by the shunt capacitors compensates the lagging current drawn by the load. They are located at the service entrance of large industries or at the sub-

station supplying an industrial area. Initially, the use of capacitors was limited due to high cost per kVAR, large size and weight. However, over the years , capacitor usage has increased phenomenally due to reduction in selling price, improved design and manufacturing methods resulting in small size and weight and above all, better understanding of the system benefits that result from their use.

The selection of shunt capacitors is dependent on many factors the most important of which is the amount of lagging kVAR taken by the load. In the earlier days, this posed no problem since the reactive power requirements at a load bus could be very accurately determined as there were no complex interconnections of networks. Thus, the improvement in Power factor could be successfully achieved with the use of fixed shunt capacitors. However, with this interconnection of large power systems, the power flow at a particular substation also depends on loads at other buses of the system and the variation of kVAR occurs over a wide range. Thus, a fixed capacitor bank may lead to either over-compensation or under-compensation resulting in lower power factor in the ac power supply system.

4.2.2 Switched Capacitors

The wide range of variation in lagging kVAR on

the system has caused the necessity for dynamic VAR compensation, that is, controlled compensation of the reactive power to achieve desired power factor at all load conditions. This is achieved using switched capacitors. Depending on the total kVAR requirement, a number of capacitors are used which can be switched into or switched out of the system individually. The control is accomplished by continuously sensing the load kVAR. If more compensation is required, then the required number of capacitors are switched into the circuit so as to take the extra leading kVAR and, conversely, the required number of capacitors are switched out if the load kVAR falls. The smoothness of control is solely dependent on the number of capacitor switching units used. A very fine control over the power factor can be achieved at the expense of economy by using a large number of small such units. The switching is conventionally accomplished using relays and circuit breakers. One such method uses a master control relay in addition to a time-delay relay for each unit [4] . For one-step automatic control the master relay energizes the closing element of the time-delay relay, and if the master-relay contacts stay closed for the time required for the time-delay relay contacts to make, then the operating circuit is energized and the capacitor breaker closes. A similar process in reverse trips the capacitor breaker. For more accuracy and

reliability, multi-step control [4] is preferred.

However, these methods using mechanical switches and re-
lays invariably suffer from the drawbacks of being sluggish,
unreliable, introducing switching transients and requiring
frequent maintainance. With the advent of high power solid
state devices, thyristors have replaced the mechanical
switches. Sophisticated electronic circuits have made the
system highly reliable. Thyristors switching of static
capacitors has made it possible to achieve virtually conti-
nuous control of reactive power generation on a large scale
[15] . Each small unit of capacitors is switched on and
off individually using thyristors as switching elements as
shown in Fig. 4.1 (a). The switching-on transients are
avoided by selecting the switching-on instant at the time
when the network voltage corresponds in magnitude and pola-
rity to the capacitor voltage. Switching-off transients
are not a problem since turning-off of the thyristors
occurs at the next current zero after the removal of the
gate trigger. The capacitor then remains charged to either
positive or negative peak value of the network voltage and
is prepared for a new switching-on which will be free from
transients. The time required for switching-on or off is
made up of the time to detect the magnitude of the desired
change in reactive power (one-half cycle), plus a variable
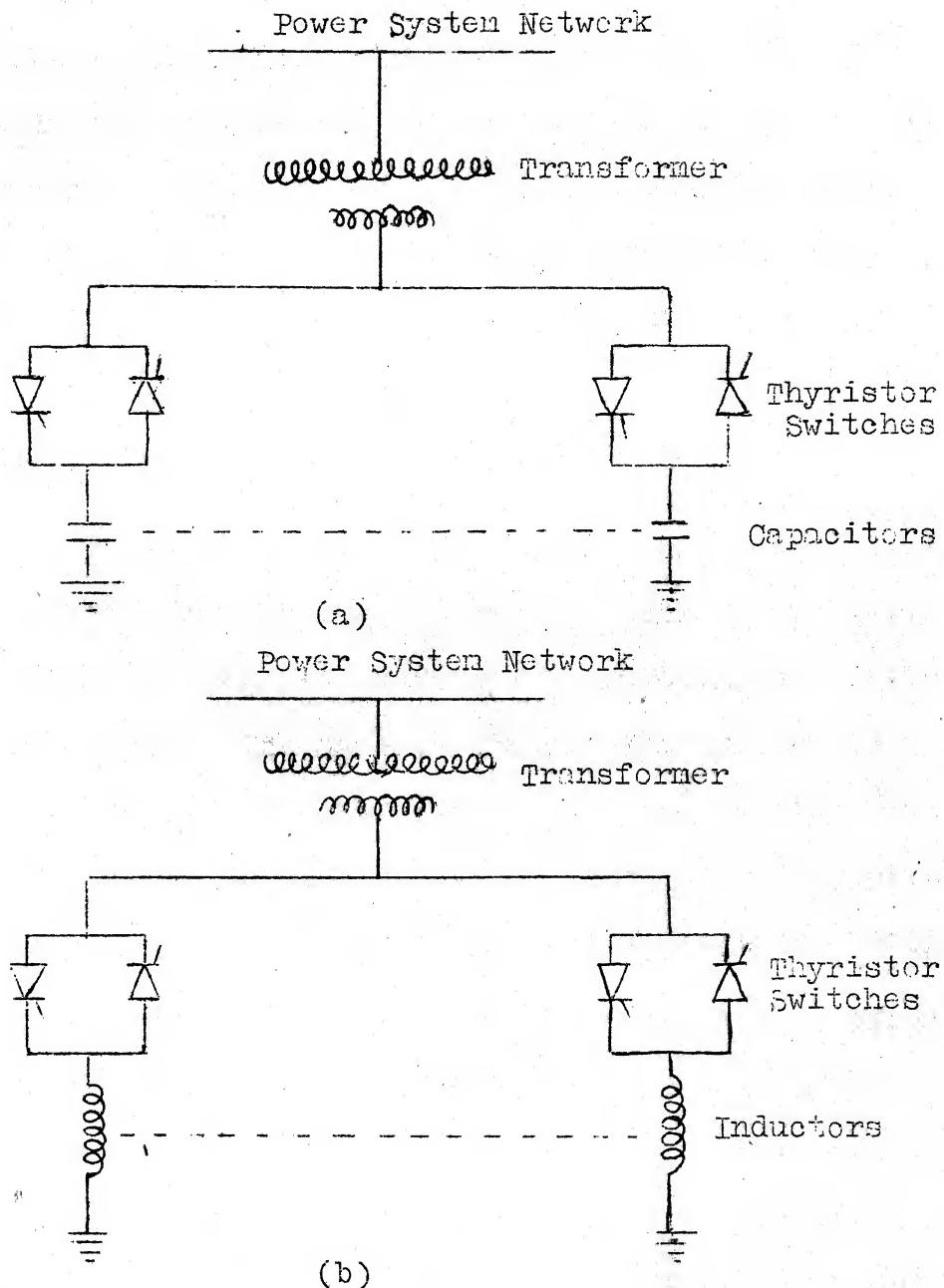
Fig. 4.1 (a)   Thyristor-Switched Capacitors.

(b)   Thyristor-Switched Inductors.

time (maximum of one-half cycle) waiting for suitable switching conditions. Switching-on or off is, therefore, achieved within one cycle of power frequency. Usually, a step-down transformer, as shown in Fig. 4.1 is necessary to suit the voltage ratings of thyristors and capacitors. Switched inductors working on the same principle are also extensively used in transmission systems for direct compensation of the charging capacitance of a line [15] .

4.2.3 Synchronous Condenser

The synchronous machine when over-excited draws leading current from the supply system. This characteristic particularly makes it useful as a dynamic power factor correction device. The machine can provide continuous kVAR balance when used with proper automatic exciter control system. The short time overload capacity of synchronous compensator is larger than that of capacitors. The synchronous condenser has also greater stabilizing effect upon system voltages. However, it has also many drawbacks as compared to the shunt capacitors. The losses in the synchronous condensers are much greater. For synchronous condensers the full-load losses vary from about 1½ percent to 3 percent of the kVA rating whereas for capacitors the losses are about 1/3 percent of the kVA

rating [4] . The capacitors are more effective since they lend themselves to distribution at several locations closer to the load throughout the network. It will be very costly to distribute small synchronous condensers throughout the system. The kVAR rating of a capacitor installation can be easily changed with the variation in loads and system requirements day by day, which is impractical with synchronous condensers. The failure of a synchronous condenser compared to a single unit in a bank of capacitors is less likely to occur. However, any such failure in a sychronous condenser completely affects entire ability to produce kVAR. This is not so in capacitor banks since there are several other capacitors in a bank even if a particular unit fails. Synchronous condensers increase the short-circuit current of a system and thus higher rating breakers are required. The response of the synchronous condenser is slow due to the inherent mechanical inertia.

4.2.4 Static Reactor Compensator

The aim to achieve fine control over the entire kVAR range as in case of the synchronous condenser without sacrificing the advantages of static capacitors has been fulfilled by the development of static reactor compensator. This essentially consists of a controllable reactor in parallel to a shunt capacitor as shown in Fig. 4.2 . By

choosing proper values for the capacitor and the inductor,
it is possible to achieve smooth and stepless control of
kVAR from lagging to leading over a wide range to compen-
sate for the wide variations in the load kVAR. This is
accomplished by continuous control of the effective funda-
mental reactance of the inductor. Since there is greater
requirement for leading kVAR, preferably a number of capa-
citors are switched in steps to provide a wide range of
leading kVAR [16] . The controllable reactor can be realiz-
ed using different methods some of which are listed below.

(a) Reactors with dc current-controlled saturation : The
current in a reactor can be controlled by a direct current
fed into a control winding mutually coupled to the main
reactor winding. In power systems, a transformer is usually
preferred to ordinary reactor. The alternating current in
the primary is controlled by a direct current fed into
secondary control winding coupled to normally delta-connect-
ed secondary. The arrangement is shown in Fig. 4.3 . By
varying the control current, the primary alternating current
can be controlled from practically zero when the cores are
unsaturated to a maximum at fully saturated cores [15] .
The primary is connected to the high voltage power system
without an auxiliary transformer. The dc control current
thus changes the effective reactance posed to the power
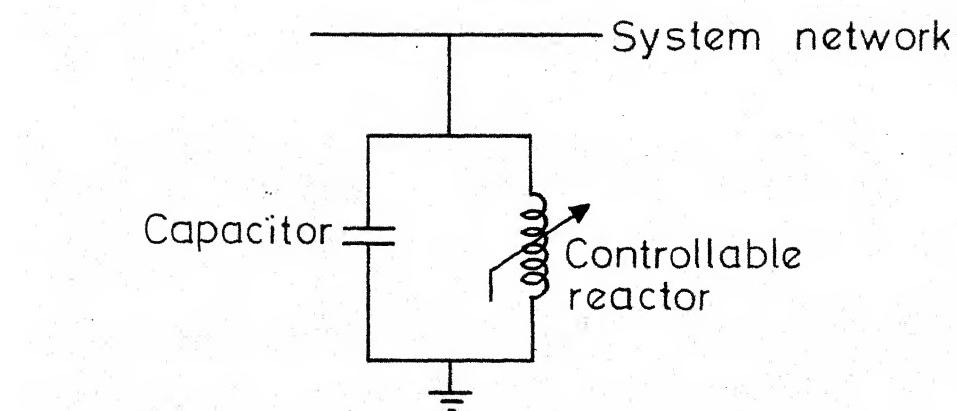
Fig. 4.2   Basic static reactor compensator
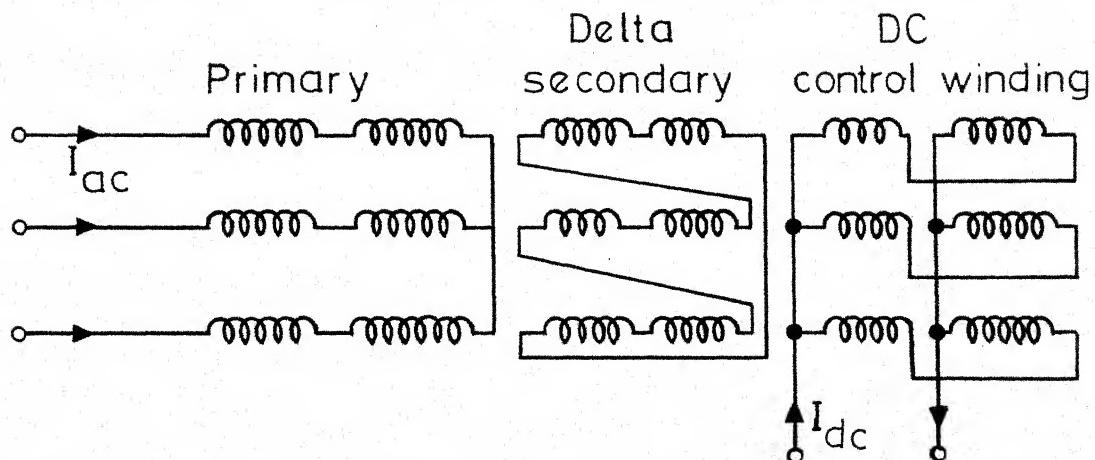
Fig. 4.3   Reactor using dc current-controlled saturation.

(a)   (b)
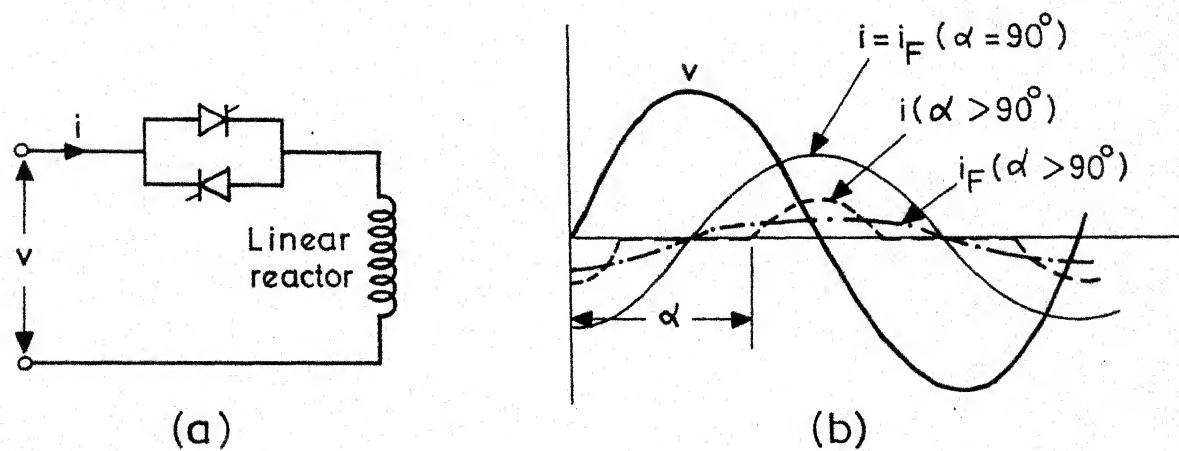
Fig. 4.4   Thyristor-controlled reactor
    (a) Line diagram
    (b) Voltage and current waveforms.

system [17] . Though the operating principle is very simple, the transient behaviour of the reactor with dc current-controlled saturation is very complicated and cannot be characterised by a simple time constant. However, with special techniques [15] the time for changing the primary currents by control actions can be minimized to a fraction of a second. In addition, a dc source, usually a thyristor rectifier of relatively low power rating, is necessary for its operation.

(b) Thyristor-controlled shunt reactors : With the increase in the size and complexity of power system, fast reactive power compensation has become necessary in order to maintain the stability of the system. The thyristor-controlled shunt reactors make it possible to reduce the response time to a few milliseconds. Thus, reactive power compensators utilizing the thyristor-controlled shunt reactors are becoming increasingly popular. The basic operating principle of a thyristor-controlled reactor is illustrated in Fig. 4.4 . A reactor operating in its linear region is connected to the ac system in series with back-to-back connected thyristors as shown in Fig. 4.4 (a). The inductive reactive current is continuously controlled by phase-control of the thyristors, one being fired in the positive half cycle of the supply frequency and the other in the

negative half cycle. Thyristors operating in this mode
are known as ac controllers [1]. Fig. 4.4 (b) shows the
supply voltage and current waveforms for two different
firing angles. For firing angle, α = 90° , maximum
current is drawn from the supply. If the firing instants
of the thyristors are delayed beyond 90° , current becomes

discontinuous. This is illustrated by the dotted line in
Fig. 4.4 (b). The conduction interval decreases as the
firing angle, α increases and finally no current flows
for α = 180° . The fundamental component of the current
which is shown by chain curve in Fig. 4.4 (b) , however,
always lags the voltage by 90° and it is this component
which accounts for the effective reactive power compensa-
tion. Due to the discontinuous conduction, the current has
a certain finite harmonic content. A detailed treatment to
static shunt reactor compensator utilizing thyristor-contro-
lled reactor is presented in section 4.3.2 . Normally
for linear operation over a wide range, gapped core type
reactors are used [15]. Economics show that a step-down
transformer is necessary to connect the reactors and the
thyristors to the low voltage winding. The transient res-
ponse time of thyristor-controlled reactors is within one
cycle of power frequency [15].

(c) Thyristor-controlled high-impedance transformer : Since a transformer is necessary for connection of thyristor-controlled reactors, it is economical to construct a transformer with high leakage reactance and to control the primary current by phase-control of thyristors connected to the secondary windings, thus eliminating separate reactors [15]. The transformer is designed for linear magnetic characteristic with 100% leakage reactance between primary and secondary windings [16]. The primary winding is star-connected with the star point grounded. The secondary winding connection and its voltage are determined such as to match to voltage and current ratings of the thyristors [16]. Controlling the secondary current by phase-control inherently introduces harmonics in the current of the compensator under partial loading conditions. Only at full load (corresponding to α = 90°) and no load (α = 180°) are the harmonics zero. The actual harmonic content, however, depends on the type of connection of both secondary windings and thyristors. Table 4.1 gives a brief summary of the properties of three different connections. They are

(1) The secondary winding as well as the thyristors are star-connected. The star points are inter-connected and grounded.

(2) Star connection of the secondary windings and thyristors, but there is no connection between star points.

(3) The secondary winding as well as the thyristors are delta-connected.

Table 4.1

Connection	Thyristor rating		Maxm. harmonic currents in %				
	Voltage X $\sqrt{2}/\sqrt{3}$	Current r.m.s	3	5	7	9	11
1	1.0	1.0	13.7	5.0	2.55	1.55	1.0
2	1.5	1.0	–	9.5	3.4	–	1.7
3	$\sqrt{3}$	$1/\sqrt{3}$	–	7.6	3.85	–	1.5

The triplen harmonics in connection (1) can be eliminated by providing an additional delta-connected tertiary winding closely coupled to the secondary. Thus, connection (1) is the most suitable one as regards harmonic generation and thyristor rating though with some extra cost. Where even the remaining higher order harmonic content cannot be tolerated, it can be further reduced by using additional filters connected to the delta tertiary winding [16].

4.3 APPLICATIONS OF STATIC THYRISTOR-CONTROLLED SHUNT COMPENSATORS FOR LOAD COMPENSATION

4.3.1 Fundamentals of load compensation

Due to their fast response and very smooth VAR control, there has been a rapid increase in the number of static thyristor-controlled shunt compensators in industrial and utility systems for load compensation, transmission line voltage regulation and other purposes [16, 18]. In industrial power systems load compensation means cancellation of the reactive power demand of large and fluctuating industrial loads such as electric arc furnaces, induction furnaces, rolling mill drives used in steel industries etc., and to balance the real power drawn from the three phases of the ac supply system. In simpler terms, load compensation involves two distinct acts; one being power factor correction and the other load balancing in the three phases. If both are carried out, they determine together the total reactive power needed for compensation.

Any 3-phase unbalanced linear steady state load can be compensated by three appropriate reactive impedances (capacitive and inductive) connected between the three phases [18]. The load on a power system varies with time which can be represented by a series of "steady state" impedances at discrete time instants close to one another.

The compensation, therefore, requires variable reactances that can be adjusted according to the load variation.

4.3.2 Practical Approach

Under steady-state conditions the compensating susceptances can be expressed in terms of the load imped-ance [18] . Since the load impedances are directly measur-able, the compensating susceptances can always be deter-mined by direct use of appropriate analytical expressions. However, the parameters of a transmission network in which changes both in loads and generations can take place frequently cannot be known accurately. Hence, for effect-ive dynamic compensation of kVAR in power systems, the following are required:

(i)   rapidly variable compensating susceptances

(ii)   fast measurement of load parameters

(iii)   rapid signal processing and fast-acting feed-back control.

A static shunt compensator using thyristor-controlled reactor (TCR) is capable of meeting all the three desired requirements and, hence, has found extensi-ve use.

Realization of variable reactances :   The different schemes for realizing variable reactance (or susceptance)

have been outlined in section 4.2 . The basic scheme using a fixed capacitor in parallel with a TCR is illustrated in Fig. 4.5 .

Since the capacitor draws a fixed amount of current from the source, the resultant current drawn from the source is effectively controlled by controlling the conduction interval of thyristor switches using phase-control. The supply voltage and inductor current waveforms are shown in Fig. 4.6 for a particular value of firing angle, α . The range of variation of triggering angle, α , is from 90° to 180° .

The current, i_{TCR} through the inductor when thyristor T_1 is fired at delay angle, α is given by

$$L \, di_{TCR}(\omega t)/dt = \sqrt{2} \, V_{SRMS} \sin \omega t \qquad (4.1)$$

Solving the differential equation (4.1) with the initial condition $i_{TCR} = 0$ at $\omega t = \alpha$ and after simplification, the current through the TCR is obtained as

$$i_{TCR}(\omega t) = (\sqrt{2} \, V_{SRMS}/ \, \omega L)(\cos \alpha - \cos \omega t)$$
$$\alpha \leqslant \omega t \leqslant \beta \, . \qquad (4.2)$$

The current i_{TCR} is again zero at the extinction angle, β as seen from Fig. 4.6 . Substituting this condition in eqn. (4.2) , we obtain
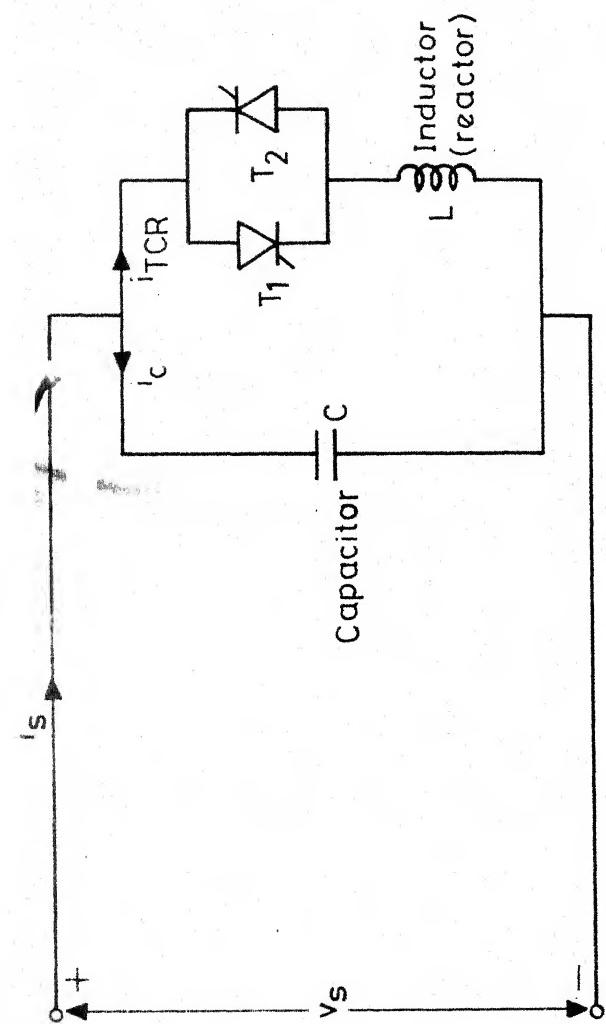
Fig. 4.5   Basic fixed capacitor, thyristor-
controlled reactor type compensator.
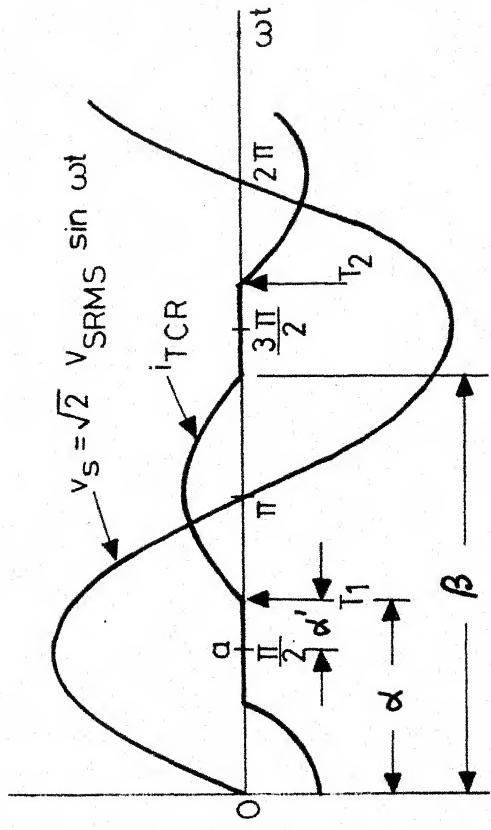
Fig. 4.6   Supply voltage and TCR
current waveforms.

$$\cos \alpha = \cos \beta$$

Since the extinction angle is greater than the firing angle, but less than 2π radians, we obtain

$$\beta = 2\pi - \alpha \tag{4.3}$$

Similarly, considering the thyristor T_2 which is fired in the other half cycle of the supply frequency, we obtain

$$i_{TCR}(\omega t') = (\sqrt{2}\, V_{SRMS}/\omega L)(\cos \alpha - \cos \omega t')$$

$$\alpha \leq \omega t' \leq \beta \tag{4.4}$$

where $\omega t' = \omega t + \pi$

The current is sinusoidal and lags the voltage by 90° when $\alpha = 90°$, neglecting commutation intervals of thyristors. The current becomes discontinuous for $\alpha > 90°$. And the discontinuous period increases with increase in firing angle, α. The TCR current can be expressed by the Fourier series ;

$$i_{TCR}(\omega t) = \frac{a_0}{2} + \sum_{n=1}^{\infty} (a_n \cos n\omega t + b_n \sin n\omega t)$$

The Fourier coefficients are obtained as follows:

$$a_0/2 = \frac{1}{2\pi} \int_0^{2\pi} i_{TCR}(\omega t)\; d(\omega t)$$

$$a_n = \frac{1}{\pi} \int_0^{2\pi} i_{TCR}(\omega t) \cos n\omega t \; d(\omega t)$$

$$b_n = \frac{1}{\pi} \int_0^{2\pi} i_{TCR}(\omega t) \sin n\omega t \; d(\omega t)$$

The fundamental and harmonic coefficients are given below.

$$a_1 = (\sqrt{2}\, V_{SRMS}/2\pi\omega L)\left[\sin 2\alpha - \sin 2\beta -(2\beta -2\alpha)\right.$$
$$\left. -4\cos\alpha\left\{-\sin\beta + \sin\alpha\right\}\right] \qquad (4.5)$$

$$b_1 = (\sqrt{2}\, V_{SRMS}/2\pi\omega L)\left[-\cos 2\alpha + \cos 2\beta\right.$$
$$\left. -4\cos\alpha(\cos\beta - \cos\alpha)\right] \qquad (4.6)$$

$$a_n = (\sqrt{2}\, V_{SRMS}/2\pi\omega L)\left[\{2/(n+1)\}\left\{\sin (n+1)\alpha\right.\right.$$
$$\left. - \sin (n+1)\beta\right\} -\{2/(n-1)\}\left\{\sin (n-1)\alpha - \sin (n-1)\beta\right\}$$
$$\left. -(4\cos\alpha/n)\left\{-\sin n\beta + \sin n\alpha\right\}\right], \quad n > 1 \quad (4.7)$$

$$b_n = (\sqrt{2}\, V_{SRMS}/2\pi\omega L)\left[\{2/(n+1)\}\left\{-\cos (n+1)\alpha\right.\right.$$
$$\left. + \cos (n+1)\beta\right\} -\{2/(n-1)\}\left\{-\cos (n-1)\alpha + \cos (n-1)\beta\right\}$$
$$\left. -(4\cos\alpha/n)\left\{\cos n\beta - \cos n\alpha\right\}\right], \quad n > 1 \quad (4.8)$$

The rms value of the n-th order harmonic and its phase angle, ψ_n are then given by

$$I_{nRMS} = (a_n^2 + b_n^2)^{1/2}/\sqrt{2}$$

$$\psi_n = \tan^{-1}\left| a_n/b_n \right|$$

The per-unit values of the fundamental and different harmonics are computed for different α's and are shown in Fig. 4.7 .

Substituting the value of β from eqn. (4.3) in eqns. (4.5) and (4.6) , we obtain,

$$a_1 = (-\sqrt{2}\ V_{SRMS}/\pi\omega L)(2\pi - 2\alpha + \sin 2\alpha)$$

$$b_1 = 0$$

Hence, the fundamental component,

$$I_{1RMS} = I_{TCRF}(\alpha) = (a_1^2 + b_1^2)^{1/2} / \sqrt{2}$$

$$= (V_{SRMS}/\pi\omega L)(2\pi - 2\alpha + \sin 2\alpha)$$

$$\pi/2 \leqslant \alpha \leqslant \pi \tag{4.9}$$

Phase angle, $\psi_1 = \tan^{-1}\left| a_1/b_1 \right| = 90°$ (lagging)

The TCR (thyristor-controlled reactor) current changes from its maximum value to zero when the firing angle, α is varied from 90° to 180° . It may be more convinient to fix the reference point or origin at 90° as indicated by point 'a' in Fig. 4.6 . Let us recognise a new firing angle notation , α' such that

$$\alpha' = \alpha - (\pi/2) \tag{4.10}$$
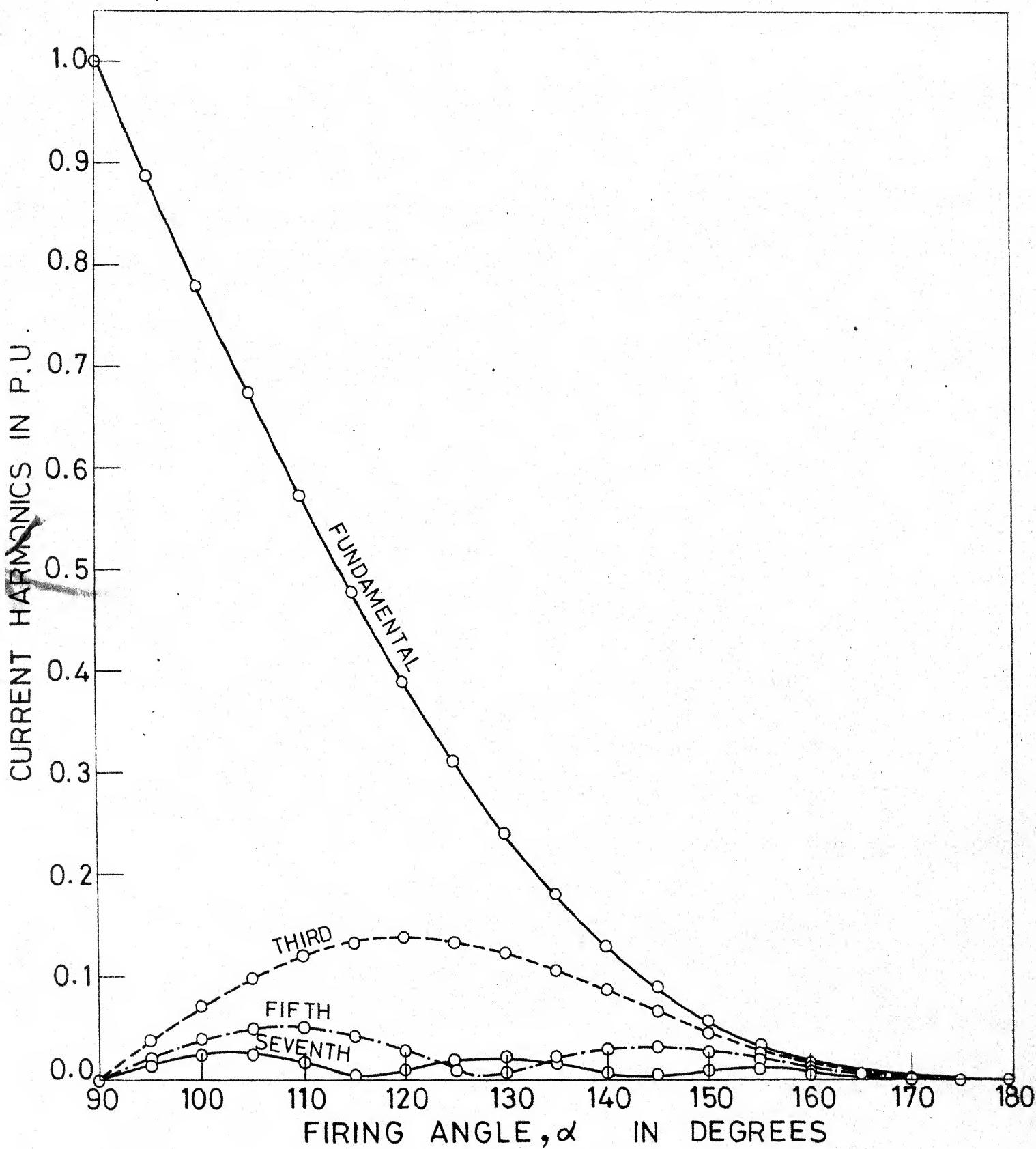
Fig. 4.7 Fundamental and harmonics values in TCR current.

Substituting the relation (4.10) in the expression (4.9) , the fundamental component of TCR current is obtained as :

$$I_{TCRF}(\alpha) = (V_{SRMS}/\omega L)\left[1 - (2/\pi)\alpha' - (1/\pi)\sin 2\alpha'\right]$$
$$0 \leqslant \alpha' \leqslant \pi/2 \qquad (4.11)$$

Thus, the magnitude of the total fundamental current drawn by the static compensator is

$$I_{SF}(\alpha) = I_C - I_{TCRF}(\alpha) \qquad (4.12)$$

$$= V_{SRMS}\left[\omega C - (1/\omega L)\left\{1 - (2/\pi)\alpha'\right.\right.$$
$$\left.\left. - (1/\pi)\sin 2\alpha'\right\}\right] \qquad (4.13)$$

By controlling the fundamental component of TCR current, it can be seen from eqn. (4.12) that the static reactor compensator draws either net capacitive or inductive current from the ac supply depending upon whether the current $I_{SF}(\alpha)$ is positive or negative respectively.

The control process is illustrated in Fig. 4.8 . The controlled inductor current, $i_{TCR}(\alpha)$, the fixed capacitor current, i_C , and the total current drawn from the ac supply, $i_S(\alpha)$, with its fundamental component, $i_{SF}(\alpha)$ are shown together with the applied voltage, v_S as α' is increased from 0° to 90° gradually. The inductive reactance, ωL has been assumed to be smaller than the
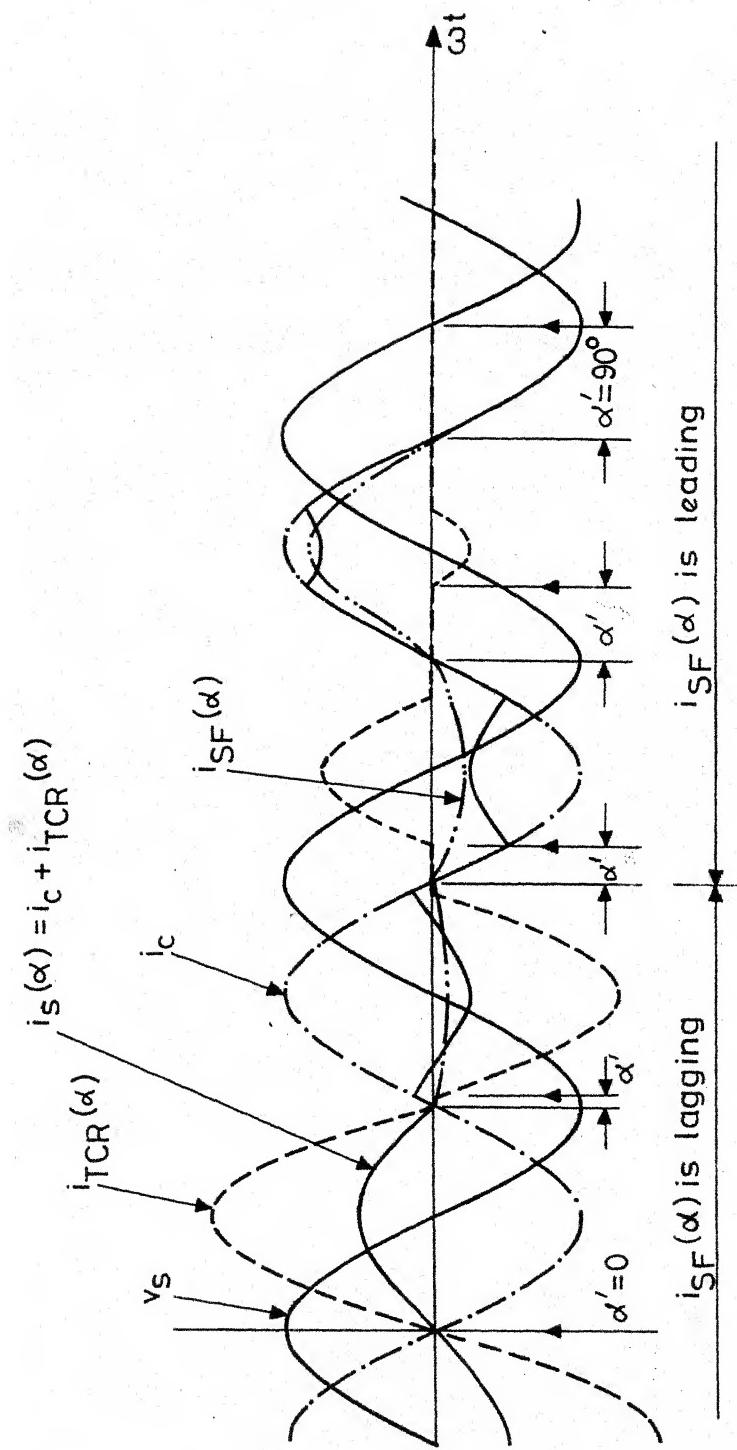
Fig 4.8   Associated waveforms for TCR compensator illustrating control process.

capacitive reactance, $1/\omega C$ in this illustration so as to achieve range of control in both the inductive and capacitive domains. As is evident, the effective reactance and the compensating current can be adjusted at discrete instants of time, not more often than once in each half-cycle. However, it should be noted that the current can be changed from maximum leading to maximum lagging in one half-cycle. So, in practice, the thyristor-controlled reactor scheme can be made to achieve a very fast dynamic response using fast measuring circuits and control devices.

Control approaches: For control of reactive power in the thyristor-controlled inductor scheme, α' has to be computed and controlled accordingly. For computing α', three basic control approaches are generally employed which are outlined in the following paragraphs.

The first one is of direct computational type which is called "feed forward" control. This control approach is based on the fundamental assumption that the load is in the steady state between any two consecutive instants of time at which the current in the compensator is changed. Thus, between these time instants the relevant load currents (or powers, or impedances) can be sensed and, from these, the required compensating currents can be computed using appropriate steady state relations.

In 3-phase systems, the processing of each of the three
steady state equations for the three phases, expressing
the required compensating current in terms of quantities
characterizing the load (currents, power or impedances),
is carried out over time intervals which are mutually
displaced by one third of the period of the ac system vol-
tage. The three compensating currents are measured indep-
endent of each other and the required firing angle, α' is
determined using the relation (4.13) . Thus, the feedfor-
ward control scheme requires two main functional elements
as illustrated by the block diagram of Fig. 4.9 : one to
compute the desired inductor current and the other to
determine the firing angle corresponding to the desired
inductor current.

The second control approach utilizes feedback
concept for the control of compensating power. Though
this approach is mainly used for regulating the terminal
voltage of a transmission line network [16, 18], it can
also be used for load compensation. The basic principle
is to control the TCR with an appropriate error signal.
The error signal represents the difference between a chosen
reference and a corresponding parametric value of the
variable to be controlled (voltage or power factor) , A
change in the error signal results in an opposing change
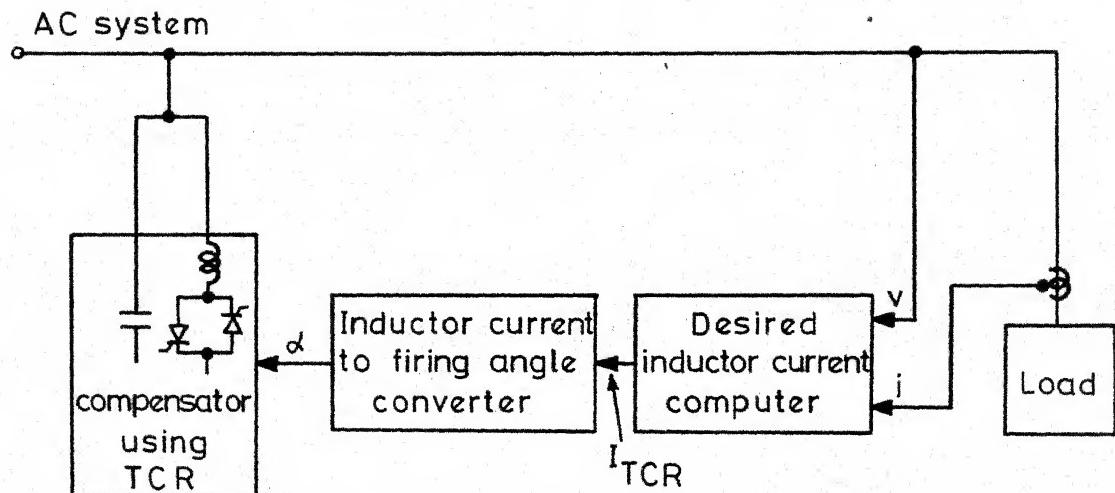
Fig. 4.9   Major functional elements in a general feedforward control scheme
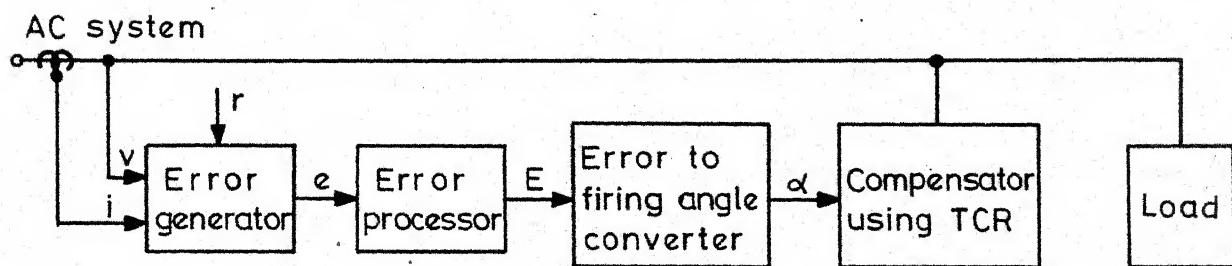
Fig. 4.10   Major functional elements in a general feedback control scheme.
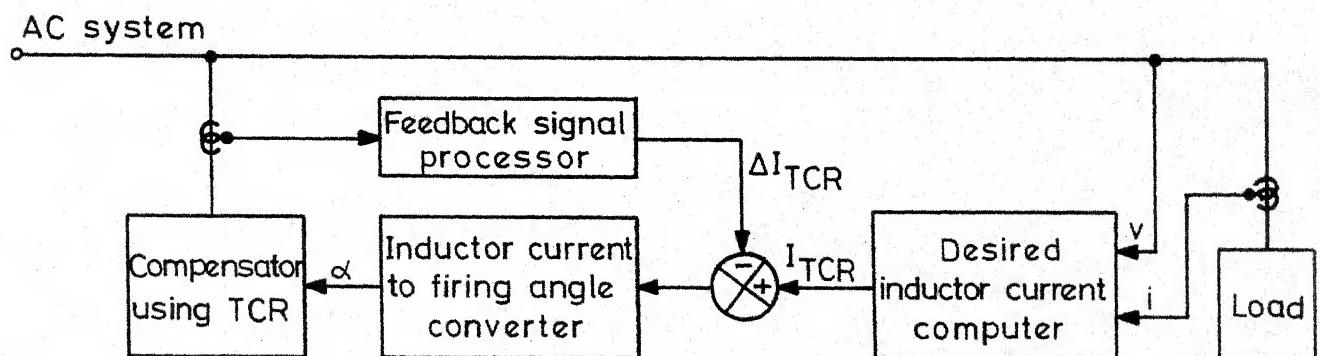
Fig. 4.11   Major functional elements in an overall feedforward control scheme using negative feedback.

in the effective susceptance value of the TCR. This tends
to keep the error signal close to zero. The block diagram
of a typical feedback control scheme is shown in Fig. 4.10.
There are three main functional elements in the feedback
loop. The function of the error generator is two-fold.
First, it derives a parametric value of the variable, x,
to be controlled (e.g., voltage components, reactive power
etc.) from the input signals which are the line currents
and voltages of the system. Secondly, it generates an
error signal, e, by comparing the derived parametric value
of the variable with the reference signal, r. The output
signal, E of the error processor is proportional to the
error signal, e, and the derivative and/or integral of the
error signal may be incorporated to get better control [16].
The Error to Firing Angle Converter converts E to the desir-
ed firing angle of the thyristor.

The feedforward and feedback control approaches
are complementary. The former is inherently stable and
fast whereas the latter can be made very accurate. The
third control approach combines the good features of both
feedforward and feedback control. For example, the accu-
racy of the desired inductor current to firing angle con-
verter can be improved and made independent of the circuit
parameters by providing a negative feedback from the

actual inductor current as shown in Fig. 4.11 . The output of the feedback signal processor, ΔI_{TCR} represents the deviation of the actual inductor current from the desired value.

4.4 CONCLUSIONS

It is possible to change the current flow through the static shunt compensator using thyristor-controlled inductor from maximum leading to maximum lagging in one half cycle of the supply frequency. Such a fast response is not possible with other types of compensators. Therefore, the thyristor-controlled compensator is finding widespread application not only in industrial power systems for load compensation but also in the utility systems for transmission line voltage regulation. In the next chapter, the details of a single-phase thyristor-controlled static shunt compensator have been presented. The experimental results regarding steady state and dynamic response of the same are also discussed in detail.

CHAPTER V

SINGLE-PHASE THYRISTOR PHASE-CONTROLLED
REACTIVE POWER COMPENSATOR

5.1 INTRODUCTION

In chapter IV the basic principles of static
reactive shunt compensator employing thyristor controlled
reactor (TCR) for load compensation have been explained in
detail. In this chapter, a static reactive shunt compensa-
tor has been practically realized for improvement of power
factor of a single-phase load on those principles. Simple
but novel control circuit has been developed for this pur-
pose. Fundamentally, the information regarding reactive
load current must be known in order to improve the supply
power factor. The feedforward or computational type control
approach [18] is adopted. The details of experimental set-
up including control circuits are explained. The experimen-
tal results showing supply power factor with and without the
TCR compensator are presented. Moreover, the dynamic response
of the TCR regulator whenever load is changed is presented
by oscillograms (traced from storage oscilloscope) obtained
from the experimental set-up.

The experimental results show that the power

factor is improved substantially and the regulator requires
only one cycle to implement the desired improvement in
power factor from the instant the load is changed. Further-
more, the experimental results showing the dynamic response
of the TCR regulator point out that there is scope for
improvement in the control circuit.

5.2 PRACTICAL CONTROL APPROACH USING FEEDFORWARD SCHEME

The block diagram of the control scheme based
on the main functional block diagram of Fig. 4.9 is shown
in Fig. 5.1 . The instantaneous values of system voltage,
V_S, load current, i_L, and capacitor current, i_C, are
measured and fed to the signal processing unit which basi-
cally consists of a Reactive Current Detector and a differ-
ence amplifier. The output of the signal processing unit
is the difference between the rms value of the capacitor
current, I_C , and the rms value of the reactive component
of the load current, $I_L \sin \theta$. This difference also gives
the fundamental component of the desired TCR current, I_{TCRF}.
The "Inductor current to firing angle converter" block of
Fig. 4.9 essentially consists of a function circuit and a
comparator as shown in Fig. 5.1 . The function circuit
generates the function relating fundamental rms TCR current,
I_{TCRF}, with firing angle, α' , in real time. Referring to
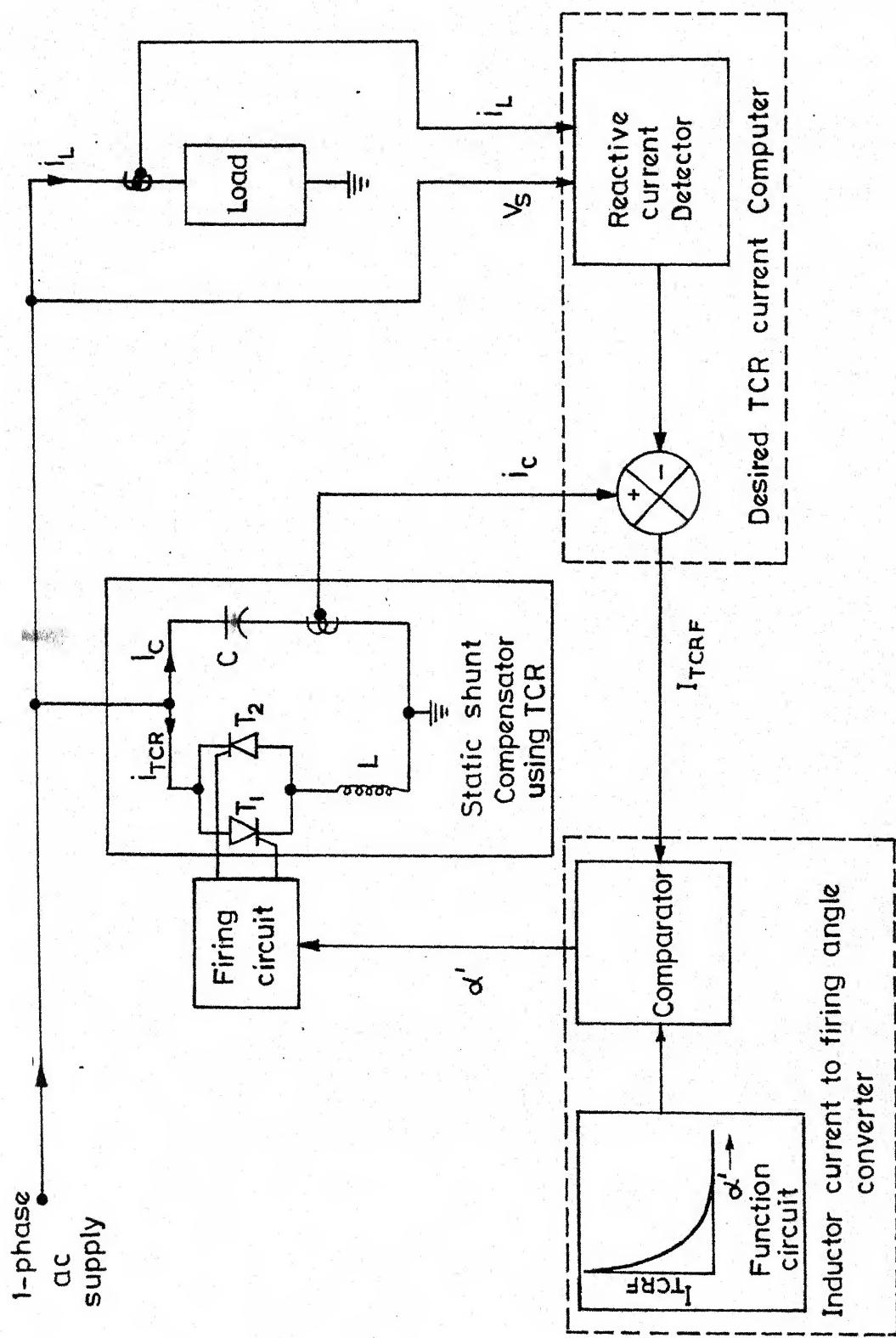
Fig. 5.1 Block diagram of the control scheme.

section 4.3.2 , we have,

$$I_{TCRF}(\alpha) = (V_{SRMS}/\omega L)\left[1 - (2/\pi)\alpha' - (1/\pi)\sin 2\alpha'\right]$$

$$(5.1)$$

The desired TCR current, I_{TCRF}, is compared with the output of the function generator to get information about the firing angle, α', in real time. This information is finally passed on to the 'Firing Circuit' block to produce the gate pulses at the desired instants for the thyristors, T_1 and T_2, connected back to back in series with the reactor, L.

The different waveforms and processed control signals illustrating the control process is depicted in Fig. 5.2 taking the system voltage as the time reference. Let us consider, for example, the kth steady state interval. The instantaneous values of the load current and the capacitor current are measured and the rms values of I_C and $I_L\sin\theta$ are computed during the kth steady-state interval of computation where k represents the number of supply cycles. The difference between these two signals which gives the value of the required TCR current, I_{TCRF}, is also computed during this interval. During the kth firing interval the function relating fundamental rms TCR current with the firing angle, α' is generated and this is compared with the desired I_{TCRF}. Thus, the firing
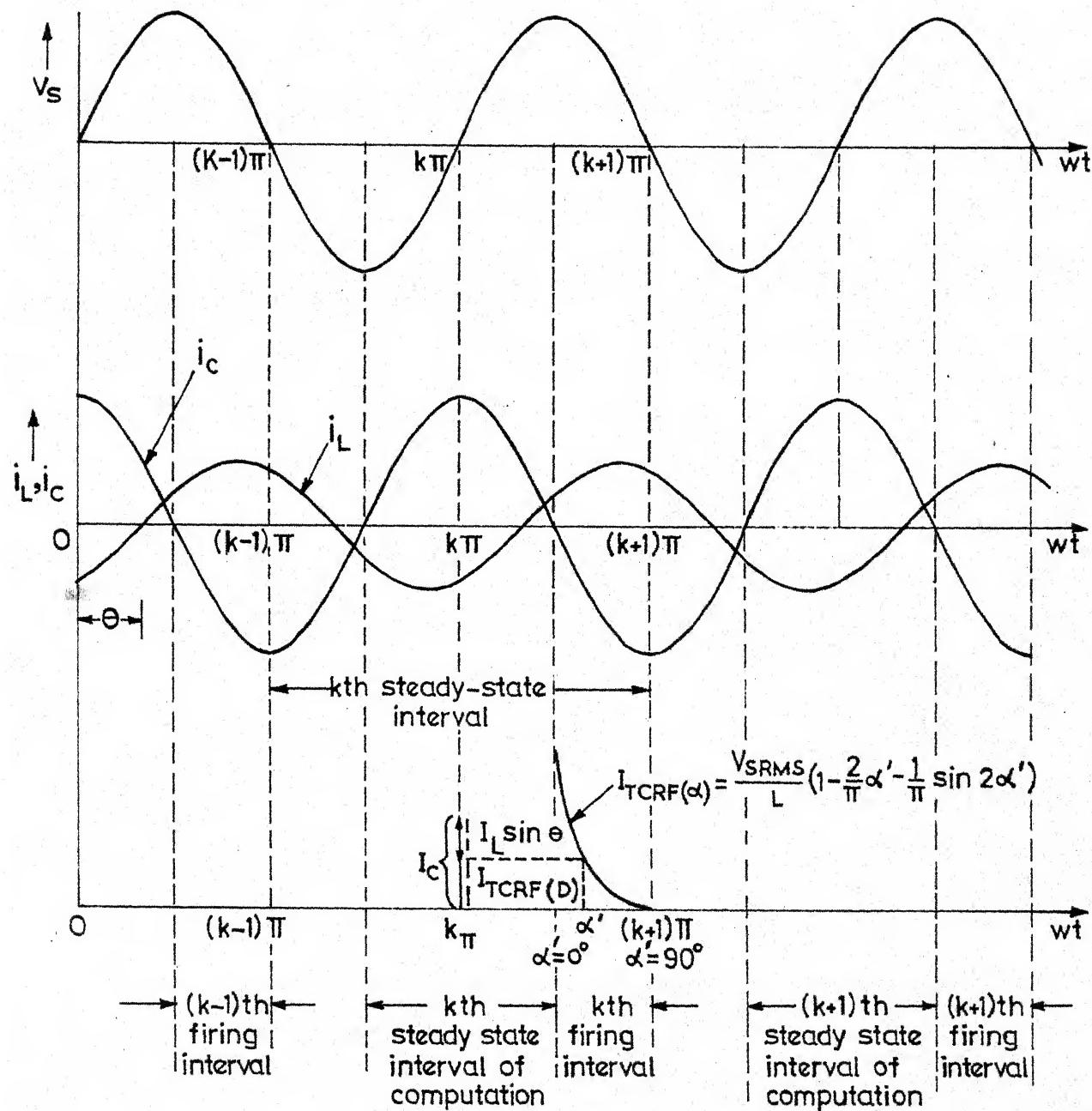
Fig.5.2 Voltage and current waveforms and control signals to describe the control process.

angle, α', is determined in real time and T_1 is triggered accordingly in the kth firing interval. The thyristor T_2 is triggered just half a time period after T_1 is triggered. The TCR current, thus, can be controlled in each cycle of the supply frequency.

5.3 CONTROL CIRCUIT

The control circuits used in different blocks of Fig. 5.1 are explained in this section. The instantaneous values of the load current and the capacitor current are measured using sensing resistors. Voltage followers using opamps are provided to present high input impedance to the power circuit. The supply voltage is sensed using a potential divider. These signals are required to produce the desired TCR current. Fig. 5.3 (a) shows complete details of the TCR Current Computer. The desired TCR Current Computer is designed assuming that the load current and the capacitor current are purely sinusoidal. With this assumption the reactive component of the load current is easily computed by using sample and hold technique. The load current is first inverted using an inverting amplifier and fed to the sample and hold circuit. The output tracks the negative load current during the negative half cycle of the supply voltage and its value at the voltage zero, $I_{Lm}\sin\theta$ (I_{Lm} and θ being the peak value

118
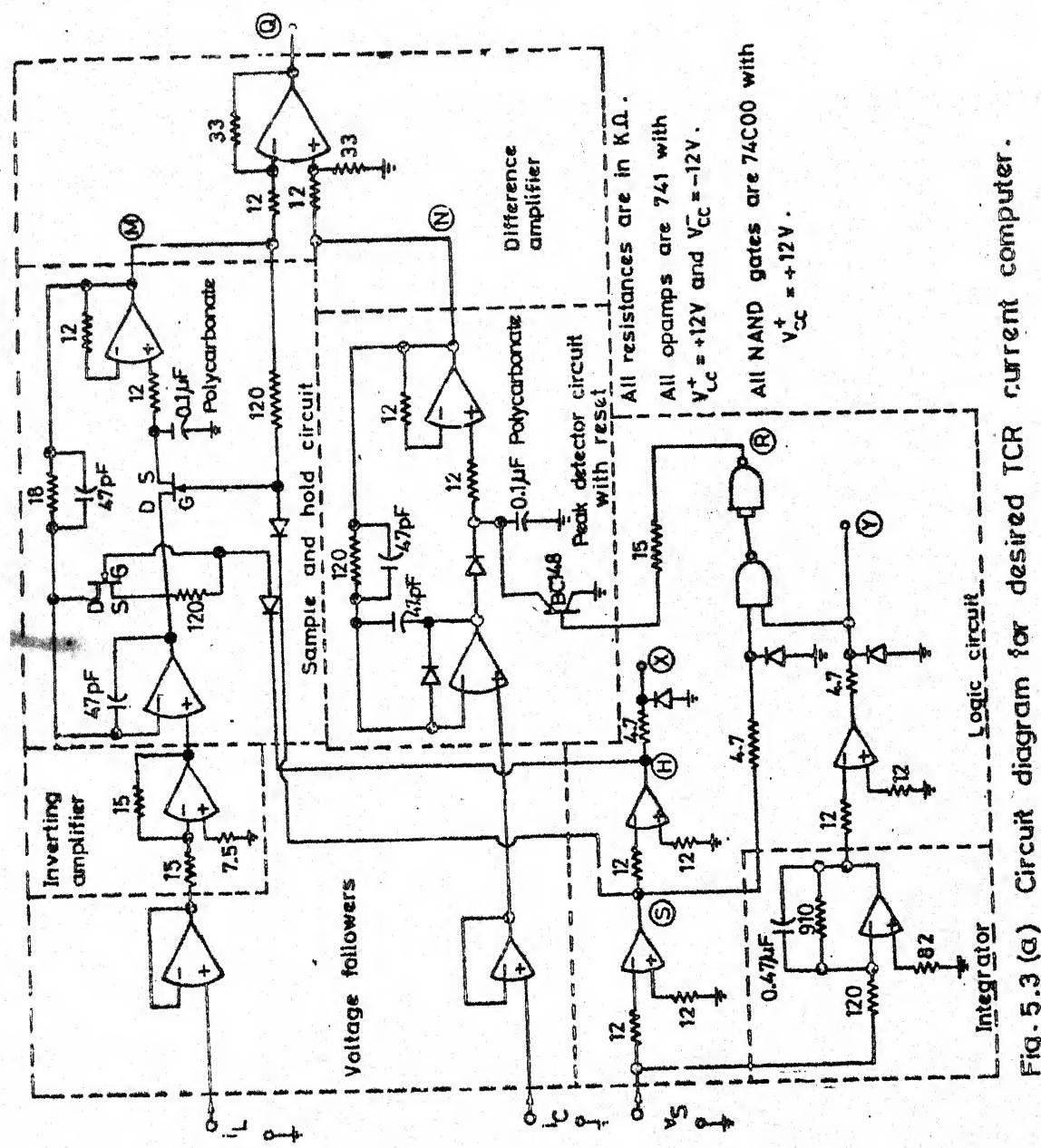
Fig. 5.3 (a) Circuit diagram for desired TCR current computer.
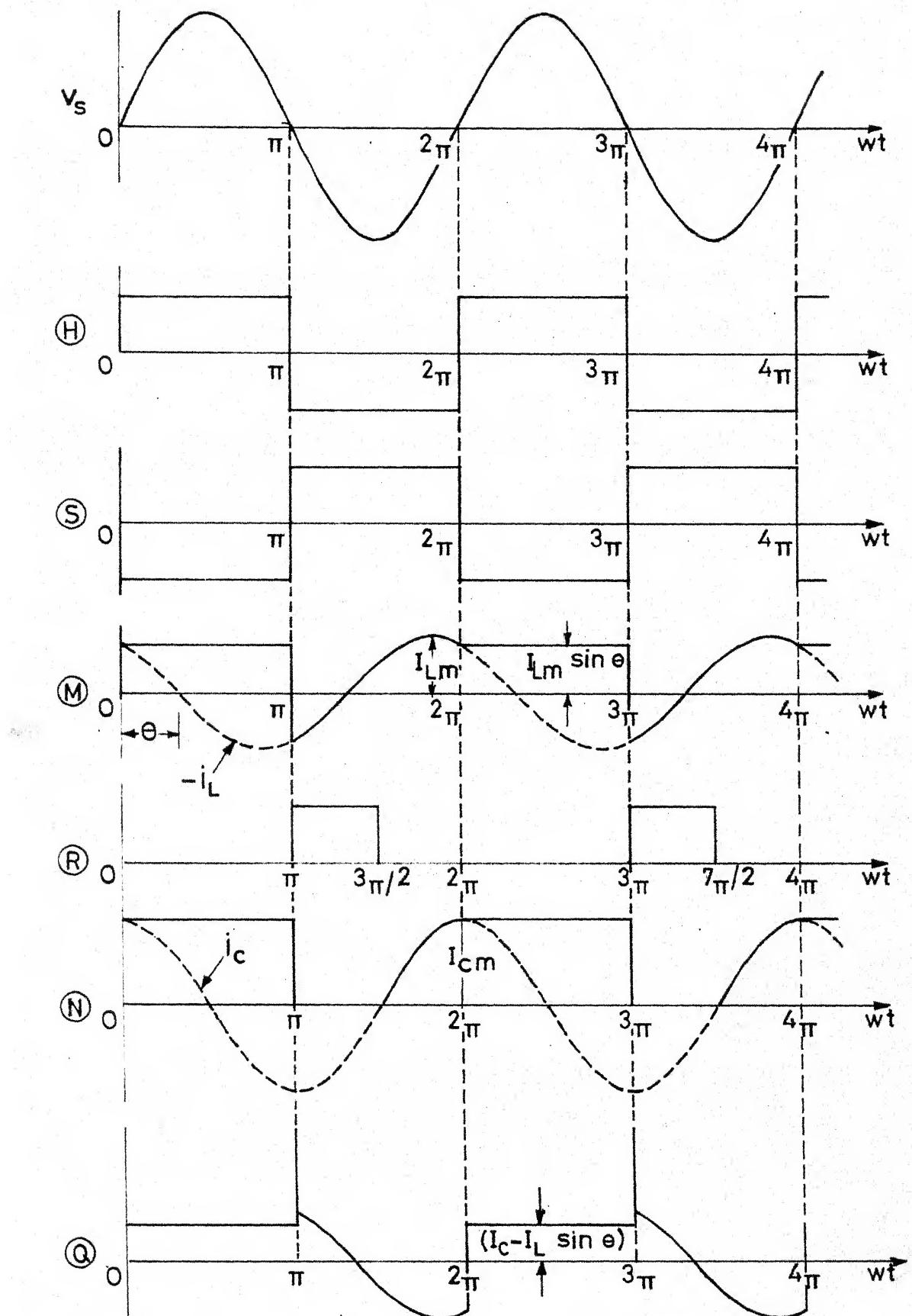
Fig.5.3(b) Waveforms at different points of the desired TCR current computer circuit.

and the phase angle respectively of the load current) is held during the positive half cycle. The output waveforms of different stages of Fig. 5.3 (a) are shown in Fig. 5.3 (b). For example, the waveform (H) of Fig. 5.3 (b) shows the output of the sample and hold circuit at the point marked (H) . A non-inverting two-opamp sample and hold circuit [19, 20] is used. The sample and hold signals fed to the gates of the FET switches are obtained at point (S) and (H) . These are derived from the supply voltage. The rms value of the load current , $I_L \sin \theta$, is subsequently obtained by multiplying the quantity $I_{Lm} \sin \theta$ with the form factor of a sine wave (0.707). In a similar way, the rms value of the capacitor current, I_C , is obtained by first measuring the peak value, I_{Cm} , and then multiplying with the form factor. A peak detector circuit with reset [20] as shown in Fig. 5.3 (a) is used to determine the peak value. The waveform (N) (Fig. 5.3 (b)) shows the output of peak detector. Since the capacitor current may vary with the fluctuations in the supply voltage, the circuit is reset at the end of each cycle so that actual peak value is obtained in each cycle. The reset takes place when the transistor across the "memory" capacitor is driven into saturation by pro- viding the reset pulse obtained at the point (R) of the

logic circuit (Fig. 5.3 (b)) to the base of the transistor.
The output of the sample and hold circuit, $I_{Lm}\sin\theta$, and
that of the peak detector with reset circuit, I_{Cm} , are
given to the inverting and non-inverting inputs of a differ-
ence amplifier [20] respectively. The difference amplifier
is designed with a gain equal to the form factor (0.707)
of a sine wave so that the difference between the rms value
of the capacitor current and that of the reactive component
of the load current, $(I_C - I_L\sin\theta)$, is obtained at its
output during the positive half cycles of the supply vol-
tage. The waveform (Q) (Fig. 5.3 (b)) illustrates the
output of difference amplifier at the point marked (Q)
in Fig. 5.3 (a).

The function circuit for generating the functional
relationship between I_{TCRF} and α' in real time is shown
in Fig. 5.4 (a) and the waveforms at different stages are
illustrated in Fig. 5.4 (b). As seen from the right hand
side of eqn. (5.1) , the function consists of a constant
term, 1 , a ramp term, $(2/\pi)\alpha'$, and a sine term,
$(1/\pi)\sin 2\alpha'$ .Since $\alpha' = 0$ when the supply voltage
reaches its peak value, it implies that to generate the
function in real time, a ramp has to be generated such that
it starts at $\alpha' = 0°$ and reaches its peak value of $2/\pi$
at $\alpha' = 90°$. Also, a sine function has to be generated
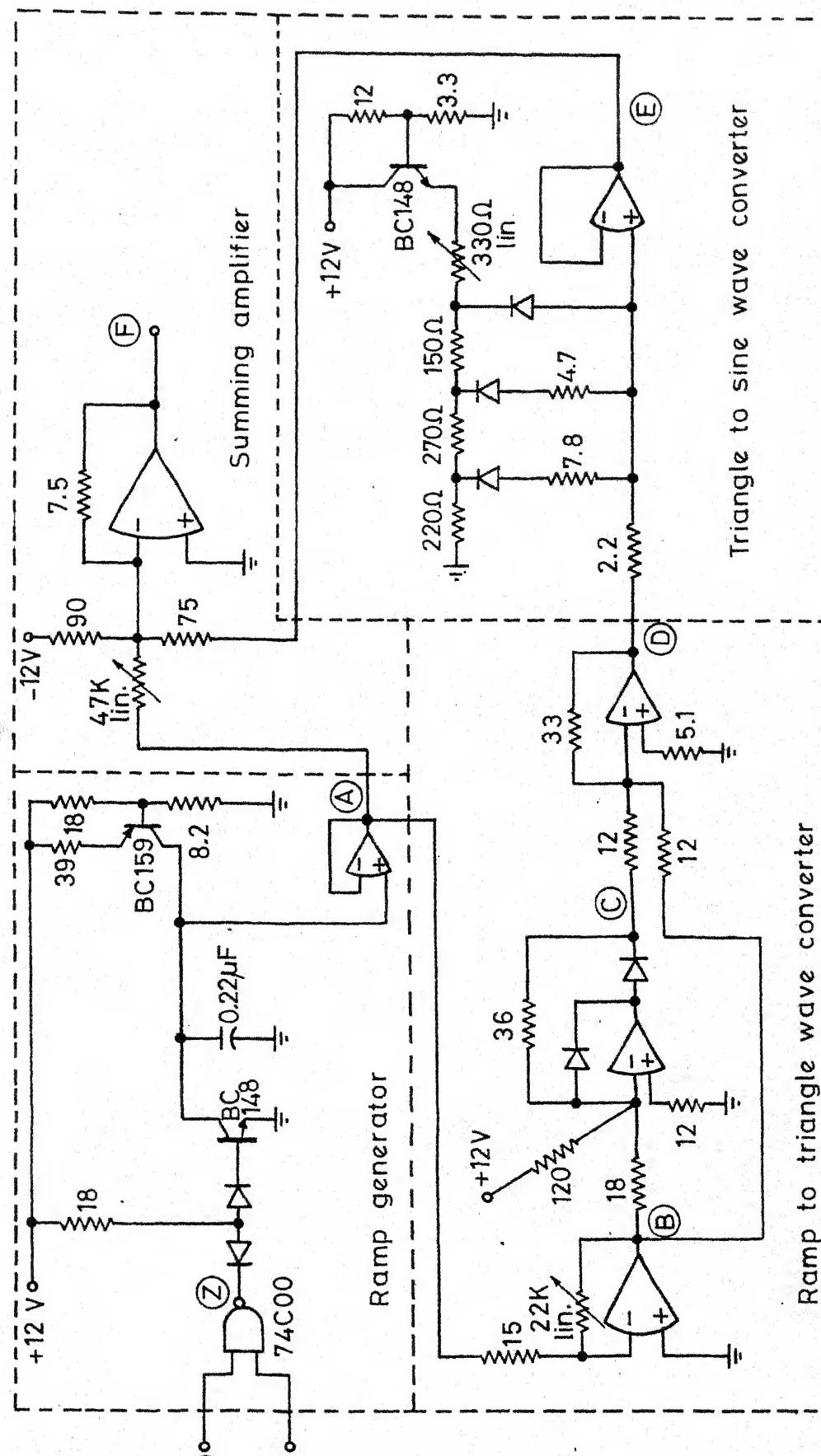
Fig. 5.4 (a)   Circuit diagram for the function circuit.

122
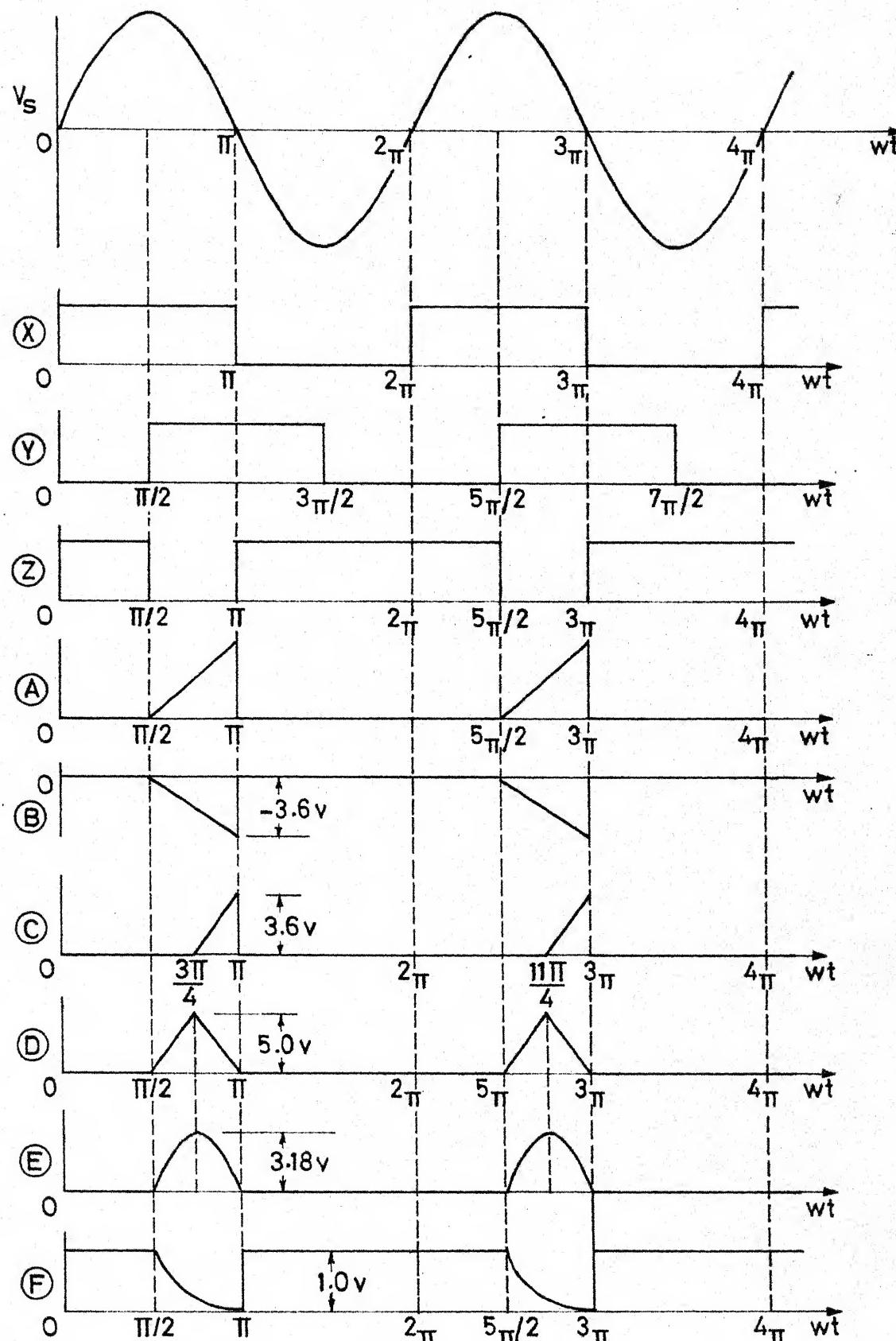
Fig. 5.4(b) Waveforms at different points of the function circuit

which starts at $\alpha' = 0°$, reaches its positive peak value
of $1/\pi$ at $\alpha' = 45°$ and again becomes zero at $\alpha' = 90°$.
With these considerations in mind, the function circuit is
realized as described below.

The logic signals derived at points (X) and
(Y) of the circuit shown in Fig. 5.3 (a) are fed to a
NAND gate to get the pulse at (Z) which serves as the
timing pulse for discharging the capacitor in the ramp
generator as shown in Fig. 5.4 (a) . A linear ramp output
is obtained at the point marked (A) .

The desired sine function is obtained by first
converting the ramp to triangular wave and then the tri-
angle to sine wave. A current-biased zero-bound circuit
[20] is used for converting the ramp to triangular wave.
These waveforms are illustrated by (B) , (C) and (D)
of Fig. 5.4 (b). A simple triangle to sine converter using
the principle of piece-wise approximation is used [21] .
The circuit is designed for three break points as shown in
Fig. 5.4 (a). The waveform (E) (Fig. 5.4 (b)) corres-
ponds to the output sine wave converter at the point marked
(E) (Fig. 5.4 (a)). The outputs of the ramp generater
and that of the triangle to sine wave converter along with
a dc supply of -12V magnitude are fed to the inverting
input of an opamp used as a summing amplifier. The input

resistances are chosen so as to get the desired gains for the three input signals. At the output marked $\boxed{F}$ of the summing amplifier, we get a signal, v_F , given by

$$v_F = 1 - (2/\pi)\alpha' - (1/\pi) \sin 2\alpha' \quad , 0 < \alpha' < 90°$$

$$(5.2)$$

The output at $\boxed{F}$ is then fed to a non-inverting amplifier with gain equal to $V_{SRMS}/\omega L$ (assumed constant) where V_{SRMS} is the rms value of the supply voltage and ωL is the fundamental reactance of the thyristor controlled reactor. This is shown in Fig. 5.5 (a) . Thus, at the output $\boxed{F'}$ of the non-inverting amplifier the desired function given by equation (5.1) is obtained. The waveform at $\boxed{F'}$ is shown by the chained curve of Fig. 5.5 (b). This is then compared with the desired value of TCR current given by the signal output at $\boxed{Q}$ (Fig. 5.3 (b)). An opamp in open-loop mode is used as the comparator. The comparator output at the point $\boxed{G}$ provides the information regarding the firing angle. As seen from the waveforms of Fig. 5.5 (b) , the leading edge of the output pulse at $\boxed{G}$ fixes the value of α' in real time. This pulse is then fed to a monostable. The monostable is realized by using a TIMER. The output pulse of the monostable has width equal to half a cycle. This pulse-stretching is necessary to ensure reliable
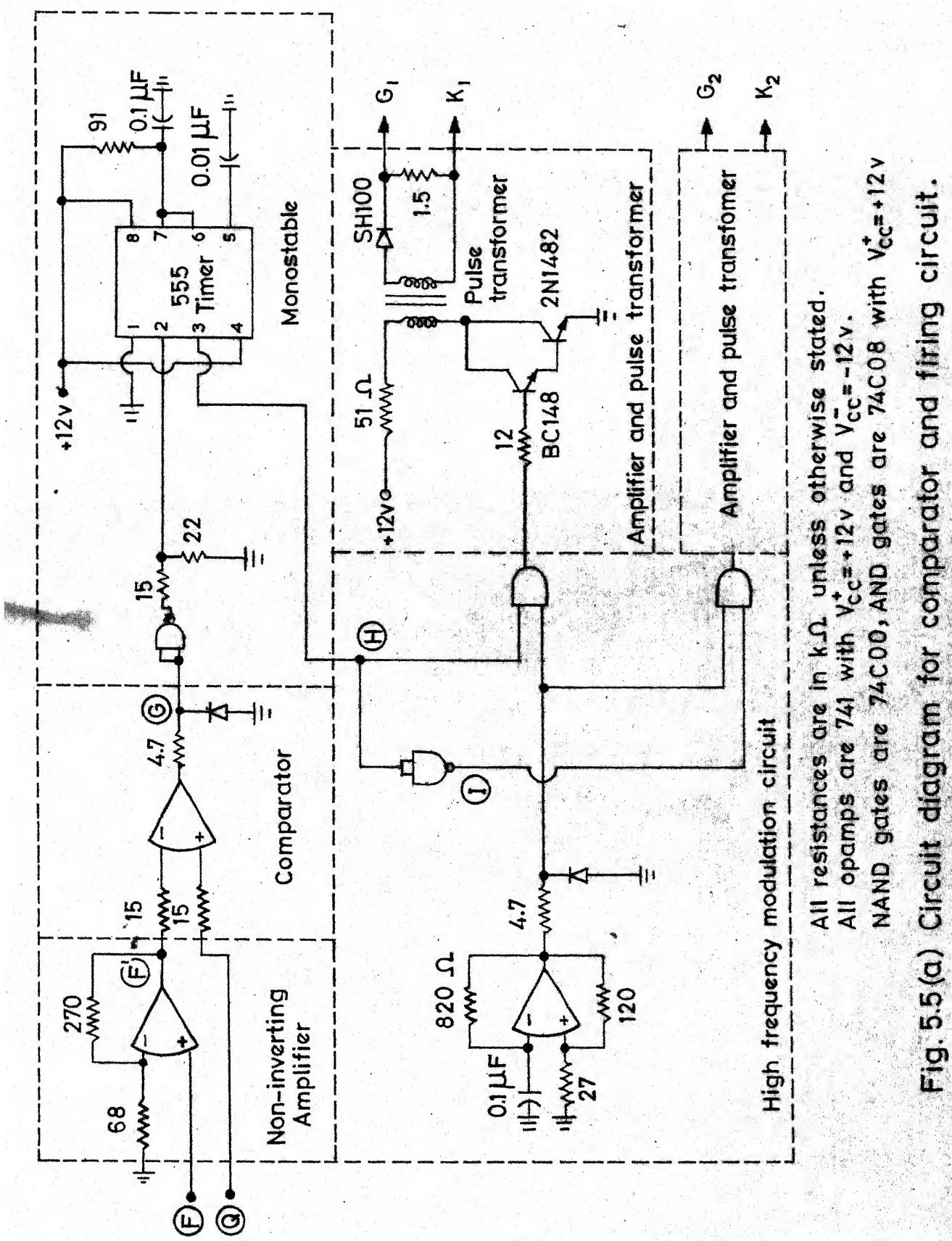
Fig. 5.5(a) Circuit diagram for comparator and firing circuit.

All resistances are in kΩ unless otherwise stated.
All opamps are 741 with $V^+_{CC}=+12v$ and $V^-_{CC}=-12v$.
NAND gates are 74C00, AND gates are 74C08 with $V^+_{CC}=+12v$

$(I_C - I_L \sin\theta)$

$\dfrac{V_{SRMS}}{\omega L}(1 - \dfrac{2}{\pi}\alpha' - \dfrac{1}{\pi}\sin 2\alpha')$
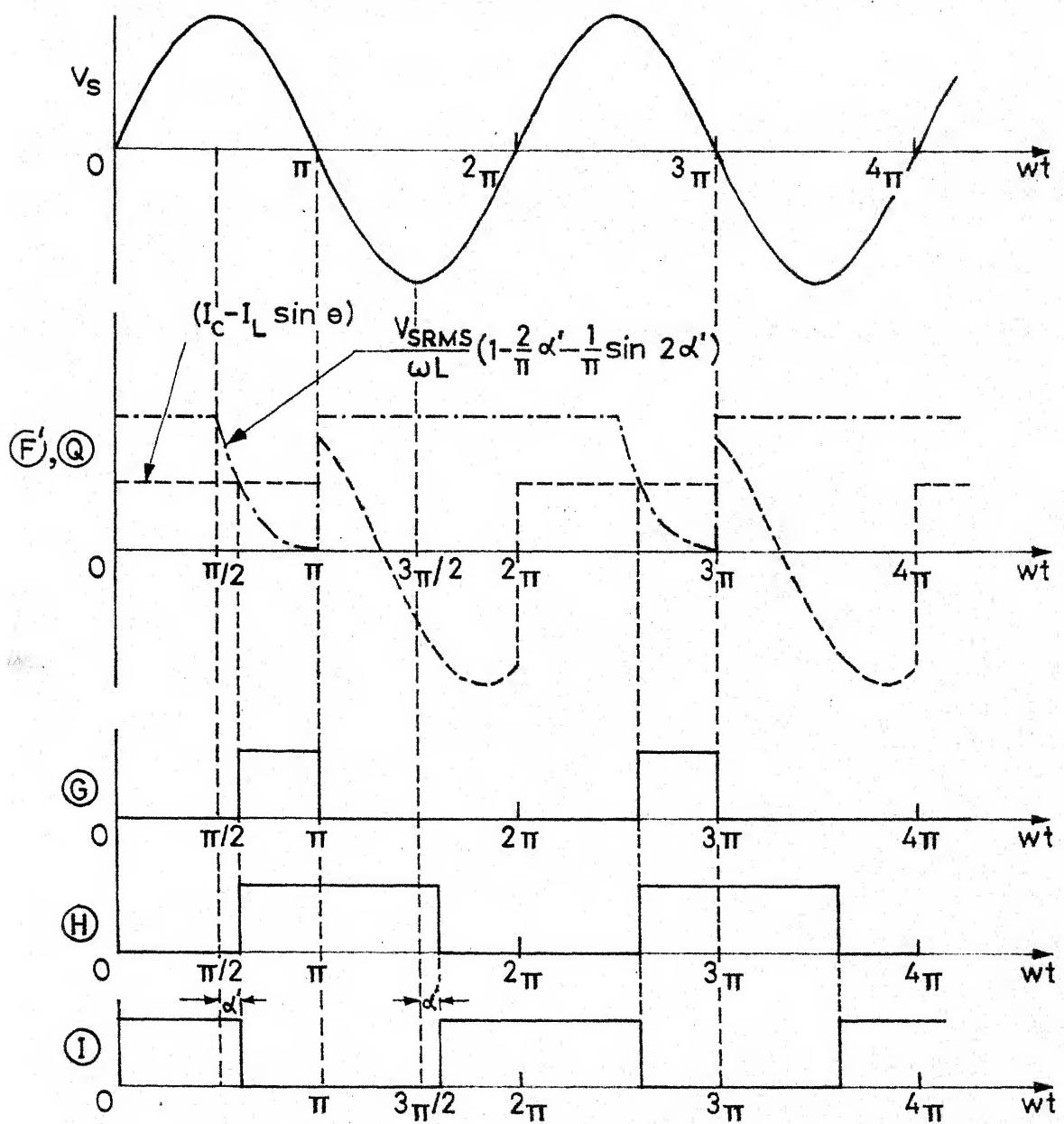
Fig. 5.5(b) Waveforms at different points of comparator and firing circuit.

firing of the thyristors since they are in series with an inductor. The monostable output at $\left(H\right)$ is the gate pulse for the thyristor, T_1 while its complement $\left(I\right)$ (Fig. 5.5 (b)) is the gate pulse for the thyristor T_2. These gate pulses, however, go through high frequency modulation, amplification stages to achieve reliable triggering. Pulse transformers are also used at the output stage to provide isolation.

5.4 EXPERIMENTAL RESULTS AND DISCUSSIONS

5.4.1 Details of experimental set-up

The response of the static shunt reactive compensator is determined experimentally in the laboratory on an R - L load supplied from a single-phase 230V, 50Hz supply. The load current is varied by varying the load resistance. The reactance of the load inductor is 100 Ω while the load resistance can be varied from 0 to 220 Ω . The load draws a maximum reactive current of 2.3Amp when the load resistance value is zero. This must be compensated by the current drawn by the capacitor. Hence, a capacitor is chosen which draws 2.3Amp from the 230V ac supply. Again, when the load is purely resistive, the TCR current (corresponding to full conduction) should compensate for the full capacitive current. Thus, another inductor having a reactance of 100 Ω is chosen to be used as the TCR .

The design of the inductor is presented in Appendix I.

5.4.2 Steady state response

The power factor of the input current for various values of the load current are calculated by measuring the supply voltage, supply current and the input power. For the same load current, the power factor is determined with and without the compensator. Table 5.1 shows substantial improvement in power factor with the compensator. It is close to unity over a wide range of cariation of load current. For large load current, the current drawn by the TCR is small resulting in large firing angle delay for the controller. Since the harmonic content is high when the triggering angle is large, the power factor is, therefore, not improved significantly for large load currents as seen from Table 5.1 .

Table 5.1

Supply voltage, V_{SRMS} = 231 volts

Load current, I_L (Amps)	Supply current, I_S (Amps)		Input power, W (Watts)		Input power factor $\cos\theta = W/(V_{SRMS}I_S)$	
	Without Compensator	With Comptr.	Without Comptr.	With Comptr.	Without Comptr.	With Comptr.
1.1	1.1	1.02	205	225	0.8075	0.955
1.5	1.5	1.08	237.5	250	0.6860	1.0
1.7	1.7	1.09	235	250	0.5980	0.993
1.8	1.8	1.07	230	245	0.5535	0.991
1.9	1.9	1.05	220	240	0.5020	0.990
2.1	2.1	0.90	175	195	0.3605	0.937
2.2	2.2	0.77	130	150	0.2555	0.843
2.3	2.3	0.28	22.5	30	0.0423	0.464

5.4.3 Transient response

Whenever the load current is changed, the thyristor controlled reactor regulator immediately responds to the load changes and tends to maintain the supply power factor at unity. The response of the regulator is presented in the form of oscillographic results both for an increase and decrease in the load current. Depending upon the load impedance angle before load change and also the instant in the ac supply cycle at which the load change is initiated, it may take a few cycles for the load current to settle down to the steady operating point corresponding to the new load condition. This is also confirmed by the oscillograms obtained from the experimental set-up. However, the regulator corrects the firing angle at the end of each cycle from the instant the load change is initiated. In order to study the transient response of the regulator, it is appropriate to present ac transient analysis. Fig. 5.6 (a) shows a R - L load fed by an ac supply. The load inductor has a winding resistance of R_L ohms. In what follows, the transient process of the thyristor regulator is explained when the load resistance is completely cut-off. Initially, the switch is in the open position. Assuming that steady-state has been reached, the load current, i_L , is given by
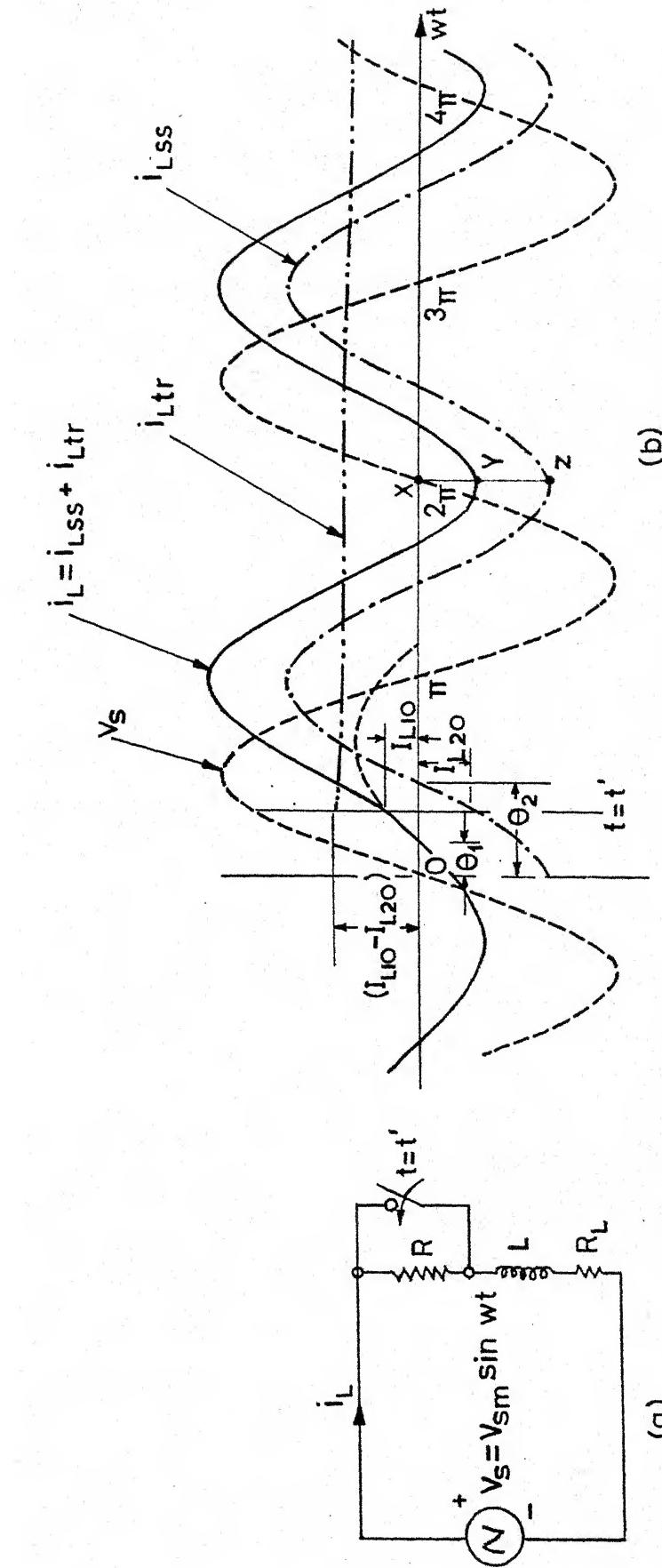
Fig.5.6 Transient process in the load current

(a) Circuit diagram
(b) Waveforms

$$i_L(\omega t) = (V_{Sm}/Z_1) \sin (\omega t - \theta_1) \qquad (5.3)$$

where
$$Z_1 = \left[(R + R_L)^2 + (\omega L)^2 \right]^{1/2}$$

$$\theta_1 = \tan^{-1} \left[\omega L/(R + R_L) \right]$$

Let the switch be closed at, say, $t = t'$ short-circuiting the load resistance, R. The resulting load current after the switching instant is given by

$$i_L(\omega t) = (V_{Sm}/Z_2) \sin (\omega t - \theta_2)$$

$$+ A \cdot \exp (-R_L t/L) \qquad\qquad t \geqslant t' \quad (5.4)$$

where
$$Z_2 = \left[R_L^2 + (\omega L)^2 \right]^{1/2}$$

$$\theta_2 = \tan^{-1} (\omega L/R_L)$$

The first term on the right hand side of eqn. (5.4) is the steady-state component, i_{Lss}, and the second term is the transient component, i_{Ltr}. The coefficient A is a constant and can be evaluated from the initial condition at $t = t'$. The current at the instant $t = t'$ can be obtained from eqn. (5.3). Let is be I_{L10}. Substituting this in eqn. (5.4), we obtain,

$$I_{L10} = (V_{Sm}/Z_2) \sin (\omega t' - \theta_2) + A \cdot \exp (-R_L t'/L)$$

$$= I_{L20} + A \cdot \exp (-R_L t'/L) \qquad (\text{say})$$

Hence,

$$A = (I_{L10} - I_{L20}) \cdot \exp(-R_L t'/L)$$

Substituting the value of A in eqn. (5.4) , we obtain,

$$i_L(\omega t) = (V_{Sm}/Z_2) \sin(\omega t - \theta_2)$$
$$+ (I_{L10} - I_{L20}) \cdot \exp\left[-R_L(t - t')/L\right]$$
$$t \geqslant t' \qquad (5.5)$$

For qualitative explanation, the waveforms of steady state (i_{Lss}), transient (i_{Ltr}) and total (i_L) load currents are shown in Fig. 5.6(b) ; the suply voltage, is taken as the reference; some arbitrary values are chosen for θ_1, θ_2 and t' . However, the load impedance angle, θ_2 , will be almost equal to 90° since R_L is small. These wave-forms are then referred while discussing the operation of the controller. The reactive component of the current is measured at the instant $\omega t = 2\pi$. As seen from Fig. 5.6 (b) , the reactive component, $I_{Lm}\sin\theta$, is given by the ordinate XZ in the absence of transient component. Thus, the desired TCR current which is equal to the difference between the capacitor current and the measured react-ive component of the load current is very small (the reactances of the capacitor and that of the load reactor being chosen equal). This results in large firing angle, α'

approaching nearly 90° as may be seen from Fig. 5.5 (b).

However, due to the presence of transient compo-
nent, i_{Ltr}, the reactive component of load current is given
by the ordinate XY. Since the desired TCR current is thus
high, it requires a small value of firing angle, α', and
therefore, the thyristors are triggered earlier. This
action of the TCR regulator is demonstrated by the oscillo-
grams of Fig. 5.7 (a) - (c) . Notice from these wavefroms
that the firing angle, α', increases in successive cycles
as the transient component, i_{Ltr}, decays gradually to zero.

The transient component depends on the load
impedance angle before switching and also on the instant
of switching. Depending on these values, the point Y in
the Fig. 5.6 (b) may lie above the horizontal axis and
therefore there will be a large positive swing for the
load current, i_L. In this particular case, the TCR current,
$(I_C - I_L \sin\theta)$, will have a value higher than $V_{SRMS}/\omega L$;
and this will not intersect the output characteristic of
the function generator as seen from Fig. 5.5 (b). This
will, therefore, result in continuous triggering of the
thyristor T_1 till the desired TCR current decreases and is
within the control range of the regulator. This is demon-
strated by the waveforms shown in the oscillograms of Figs.
5.7 (d) - (e) . The trigger pulse to the thyristor T_1 is

The arrow indicates
approximate instant
of switching
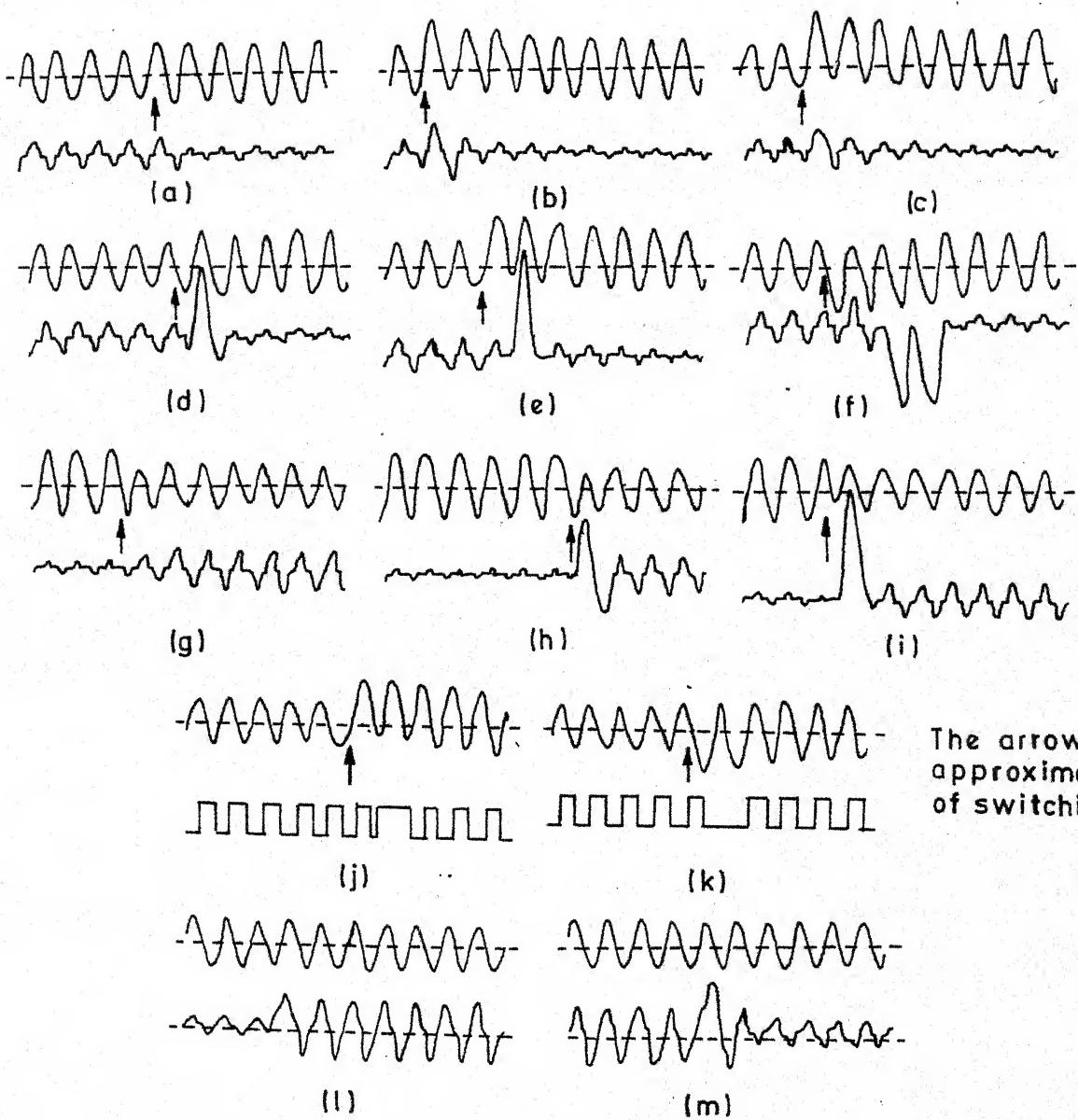
FIG. 5·7   Different waveforms illustrating transient process.
        (a) through (i): Upper trace – Load current
                         Lower trace – TCR current
        (j) and (k)   Upper trace – Load current
                         Lower trace – Gate trigger pulse to thyristor T_1
        (l) and (m)   Upper trace – Supply voltage
                         Lower trace – Supply current

also obtained under such conditions and is shown in Fig.
5.7 (j) .

Let us consider a situation when the load
resistance is cut-off at $\omega t = \pi$. That is, the switch
in Fig. 5.6 (a) is closed at the end of positive half
cycle. The transient component under this condition will
have a high negative component. Since the steady state
component remains the same, there will be a larger negative
swing of load current at the end of one half cycle. The
ordinate XY in Fig. 5.6 (b) may well exceed XZ. In this
case, $(I_C - I_L \sin \theta)$, becomes negative and, hence, the
thyristor T_1 does not get any firing pulse. Since the
gate pulses to the thyristors T_1 and T_2 are complementary,
the thyristor T_2 is continuously triggered. This is demon-
strated by the waveforms of the oscillogram shown in Fig.
5.7 (f) . And Fig. 5.7 (k) shows load current and firing
pulses to the thyristor, T_1 . The control circuit provides
gate pulses to the thyristor T_1 after the amplitude of
$(I_C - I_L \sin \theta)$ becomes zero and/or positive in subsequent
cycles.

The waveforms describing the transient response
of the regulator when the load resistance is suddenly
introduced are shown in Figs. 5.7 (g) - (i) . The asymmet-
tical nature of the load current before the steady state

clearly shows the presence of transient component. In this case also, the regulator changes the firing angle, α' , in the successive cycles until the transients die down and the load current settles down to the new steady state condition. These waveforms can be analysed in a similar manner.

The waveforms of the supply voltage and the supply current are shown in Fig. 5.7 (1) when the load resistance is shorted and in Fig. 5.7 (m) when the load resistance is introduced suddenly. It may be noted that in steady state the supply current is almost in phase with the supply voltage denoting nearly unity power factor. The distortion in the source current is due to the distortion in the capacitor current and/or the harmonics present in the TCR current.

5.4.4 Suggested modifications for improved control circuit

The experimental study of transient response of the TCR regulator has revealed some limitations of the control circuitry. These can be overcome by incorporating the following modifications in the control circuit.

The asymmetrical nature of the load current, whenever the load is changed, has caused continuous conduction of either T_1 or T_2 for a few cycles. The thyristor

T_1 conducts if there is a large positive swing of transient component in load current. On the other hand, if there is a large negative swing, the thyristor T_2 conducts. As explained in section 5.4.3 , this results in asymmetrical TCR current and possibly in core saturation. This can be eliminated if limits (0 and $V_{SRMS}/\omega L$) are provided for the desired TCR current computer. With this modification in the control circuitry, the firing angle, α' , will always be controlled within the range 0° to 90° for all load changes and the TCR current waveform will always be symmetrical.

In the present control circuitry, the function circuit is designed assuming constant magnitude of supply voltage. This may not provide complete compensation of load reactive power if the system voltage fluctuates. Improvements in the control circuit can be incorporated by continuous measurement of supply voltage in the design of the function characteristic. This, however, requires analog multipliers.

In this control circuit, there is a maximum delay of 20 msecs before the controller can act after necessary measurements whenever the load is changed. This is due to the fact that the firing pulses to T_2 are derived by complementing the gate pulses to T_1 and the function

characteristic is employed only to determine the triggering pulse for T_1 . The maximum delay can be reduced to 10 msecs if T_1 and T_2 are controlled independently by separate function characteristics. This requires duplication of control circuitry and the number of components is increased. In such a scheme, measurements are made in every half cycle and the required changes in the firing angle, α' , are implemented in the successive half cycles.

5.5 CONCLUSIONS

The experimental study of static reactive power compensator has shown that the load reactive power can be compensated and the power factor can be improved significantly over the expected range of load variation. By choosing proper values of the compensating capacitor and the controlled inductor, nearly unity power factor can be achieved over a wide range of load variation. These compensators can be installed by individual consumers for their appliances and by bulk power consumers they can be placed at the service entrance of large industrial centres. Significant savings may accure by their usage. The thyristor controlled reactor compensator provides fast response. With the control circuit developed here, there is a maximum delay of 20 msecs before the controller can act to compensate load reactive power from the instant the

load is charged. By a suitable modification of the con-
trol circuitry, the delay time can be reduced to 10 msecs.
Such a fast response is not possible with other compensa-
tion schemes. This feature makes the static shunt compen-
sator using thyristor phase-controlled reactor very much
suitable for power factor improvement particularly in
fast varying loads, such as, arc furnaces and rolling mill
drives used in steel industries.

CHAPTER VI

CONCLUSIONS

6.1 SUMMARY

The investigations carried out in this thesis
on the different converter configurations show that with
a slight change in the triggering strategy of fully con-
trolled converter, the power factor is improved substanti-
ally both in rectification and inversion operations.
Further improvement in power factor may be obtained using
ac pulse width modulation technique. But this involves
forced commutation of the thyristors, thereby increasing
the cost and complexity. Hence, the fully controlled con-
verter with optional freewheel facility looks promising
not only for traction locomotives but also for the control
of other dc drives in industry. The study has revealed,
depending upon the triggering angles, α , $\emptyset$, and load
circuit parameters, the fully controlled converter with
half-controlled characteristics has four possible disconti-
nuous current modes of operation in rectification while it
operates in two discontinuous modes in inversion. The dis-
continuous current has many adverse effects. The operating
diagrams obtained here are quite useful to determine the

possible modes of operation of the converter for a particular application and also to estimate the additional inductance necessary for continuous current operation.

The static reactive power compensators using thyristor phase-controlled reactors and fixed capacitors can efficiently change the power factor in industrial power systems to unity over a wide range of variation in the load reactive power from leading to lagging. They are very effective for fast varying loads owing to their extremely fast response. Economically and technically, they are superior to synchronous compensators. In the recent years they have found wide applications in the utility systems for fast reactive power control to achieve quality voltage regulation.

6.2 SUGGESTIONS FOR FURTHER RESEARCH

The improvement in different performances may be investigated by the series connection of two or more fully controlled converters with optional freewheeling. These performances may be compared with those obtained with the converter configurations studied in this thesis. Closed loop control of dc motor using the converter with optional freewheel may be investigated. Furthermore, the concept of optional freewheeling may be extended to three-phase fully controlled converter circuit and the improvement

in power factor may be studied.

There is also great scope for further work to be done on the static reactive power compensator. Analog multiplication and advanced digital techniques may be incorporated for the measurement of actual load reactive power. Additional feedback control as mentioned in section 4.3.2 may be introduced in the overall feedforward scheme.

Research is already in progress [22] to use the static reactive power compensator employing thyristor controlled reactor for voltage regulation in utility systems. The dynamic and transient responses of the static VAR compensator may be compared with those of a synchronous condenser for load changes and faults in the power system. The stability studies when static VAR compensators are employed may also be carried out. The switching transients on the transmission lines are likely to be reduced with the use of TCR type static VAR compensators. This aspect may also be a topic for further study. These studies can be undertaken on a digital computer or using ac transient network analyser.

LIST OF REFERENCES

(1)   S.B. Dewan and A. Straughen ; Power Semiconductor
      Circuits ; Wiley - Interscience publication, John
      Wiley and Sons , New York , 1975.

(2)   M. Ramamoorty ; An Introduction to Thyristors and
      Their Applications ; Affiliated East-West Press
      Pvt. Ltd. publication, New Delhi , 1977.

(3)   B.R. Pelly ; Thyristor Phase-Controlled Converters
      and Cycloconverters ; Wiley-Interscience publication,
      John Wiley and Sons , New York , 1971.

(4)   Electrical Transmission and Distribution Reference
      Book ; Westinghouse Electric Corporation publicat-
      ion , U.S.A. , 1964.

(5)   H. Zander ; "Self-Commutated Rectifier to Improve
      Line Conditions," Proc. IEE , Vol. 120 , No. 9 ,
      pp. 977-981 , 1973.

(6)   W. Farrer and D.F. Andrew ; "Fully Controlled Regen-
      erative Bridges with Half-Controlled Characteristics,"
      ibid Vol. 125 , No. 2, pp. 109-112 , 1978.

(7)   S.R. Doradla and P.C. Sen ; "Solid-State Series
      Motor Drive," IEEE Trans. Ind. Electron. Contr.
      Instrum. , IECI-22 , No.2 , pp. 164-171 , May 1975.

(8)   P.C. Sen and S.R. Doradla ; "Symmetrical and Extin-
      ction Angle Control of Solid-State Series Motor
      Drive," ibid IECI -23, No. 1, Feb. 1976.

(9)   K.A. Krishnamurthy ; G.K. Dubey and G.N. Revankar ;
        "Converter Control with Selective Reduction of Line
        Harmonics ," ibid Vol. 125 , No. 2 , pp. 141-145,
        1978.

(10)   P.C. Sen and S.R. Doradla ; "Evaluation of Control
        Schemes for Thyristor-Controlled DC Motors"," IEEE
        Trans. Ind. Electron. Contr. Instrum. , IECI - 25,
        No. 3 , pp. 247-255 , August 1978.

(11)   T. Kataoka, K. Mizumachi and S. Miyairi ; " A Pulse-
        Width Controlled AC to DC converter to Improve Power
        Factor and Waveform of AC Line Current ," ISPCC-1977
        Conference paper.

(12)   V. Subbiah and S. Palanichamy ; "Investigations on
        Operation of Fully Controlled Thyristor Converters,"
        Proc. IEE, Vol. 125 , No. 1 . pp. 58-59, December
        1978.

(13)   V. Subbiah and S. Palanichamy ; "Mode Identification
        and Minimum Inductance Estimation for Fully Controll-
        ed Thyristor Converters," IEEE Trans. Ind. Electron.
        Contr. Instrum. , IECI - 26 , No. 1, pp. 49-50 ,
        Feb. 1979.

(14)   G. Moltgen ; Line Commutated Thyristor Converters ;
        Pitman publishing, London, 1972. .

(15)   L.O. Barthod, H. Becker, J. Dalzell, et al , "Static
        Shunt Devices for Reactive Power Control," CIGRE
        Report 31-08 , 1974.

(16)   K. Reichert, J. Kauferle and H. Glavitsch, "Controll-
        able Reactor Compensator for More Extensive Utilisa-
        tion of High Voltage Transmission System," CIGRE
        Report 31-04, 1974.

(17)   H. Becker, et al , "Three-phase Shunt Reactors with
       Continuously Controlled Reactive Current," CIGRE
       Report 31-13, 1972.

(18)   L. Gyugyi, R.A. Otto, T.H. Putman ; "Principles and
       Applications of Static Thyristor-Controlled Shunt
       Compensators," IEEE Trans. on PAS , Vol. 97, No. 5,
       pp. 1935-1945, Sept./Oct. 1978.

(19)   J.G. Greame, G.E. Tobey and L.P. Huelsman; Operation-
       al Amplifiers Design and Applications; McGraw-Hill
       Kogakusha Ltd. publication, Copyright 1971 by Burr-
       Brown Research Corporation.

(20)   John I. Smith ; Modern Operational Circuit Design ;
       Wiley-Interscience publication, John Wiley and Sons,
       New York, 1971.

(21)   U. Tietze, Ch. Schenk ; Advanced Electronic Circuits;
       Springer-Verlag Berlin Heidelberg New York publica-
       tion, 1978.

(22)   R.L. Hauth, T. Humann and R.J. Newell ; "Application
       of a Static VAR System to Regulate System Voltage in
       Western Nebraska," IEEE Trans. on PAS, Vol. 97,
       No. 5, pp.1955-1964,Sept./Oct. 1978.

(23)   A.K. Sawhney ; A Course in Electrical Machine
       Design ; Dhanpat Rai & Sons , Jullunder-Delhi
       publication , 1972 .

APPENDIX I

DESIGN OF REACTOR [23]

An inductor with an air gap is designed to be connected to the supply system as the thyristor controlled reactor (TCR) . The design details are given here.

Voltage rating, V = 250 v ac

Current rating, I = 2.5 Amp

Hence,   VA = 250X2.5 = 625 VA

Core

Corresponding to this VA, turns per volt,

T_e = 2.0

Flux in the core, $\emptyset_m$ = 1/(4.44 f T_e)

$$= 1/(4.44X50X2) \text{ wb}$$

$$= 2.23 \text{ mwb}$$

The maximum flux density, B_m in the core is assumed as 1 Wb/m^2 .

∴ Net area of the core,

A_i = (2.23X10^{-3}/1) m^2 = 22.3 cm^2

Assuming stacking factor to be 0.9, gross area

of the core, A_c = 22.3/0.9 $\simeq$ 25.0 cm^2

Taking a square cross-section for the central limb, width of the central limb,

$A = \sqrt{25.0}$ = 5.0 cm

Winding

Number of turns, $T = V \times T_e$

$= 250 \times 2 = 500$

Taking a current density of 1.5 Amp/mm^2 for the winding, area of conductor required,

$a = 2.5/1.5 \simeq 1.67$ mm^2

Diameter of bare conductor (round),

$d = \left[(4/\pi) \times 1.67 \right]^{1/2} \simeq 1.46$ mm

Referring to the table of available standard synthetic enamelled copper conductors, the nearest standard conductor has :

bare diameter , d = 1.5 mm

Diameter with medium covering, d_1 = 1.605 mm

$\therefore$ Area of conductor provided,

$a = (\pi/4) \times (1.5)^2 = 1.77$ mm^2

Space factor, $S_f = 0.8 (d/d_1)^2$

$= 0.8 (1.5/1.605)^2 = 0.699$

Window area required, $A_w = 1.2 \, T \, a/S_f$

$$= 1.2 \times 500 \times 1.77/0.699 \text{ mm}^2$$

$$= 15.2 \text{ cm}^2$$

Stampings

Referring to the table of available E - I stampings, stamping No.43 has the desired dimensions (see Fig. A1) as follows.

A = 2"

B = 6"

C = 5"

D = 1"

E = 1"
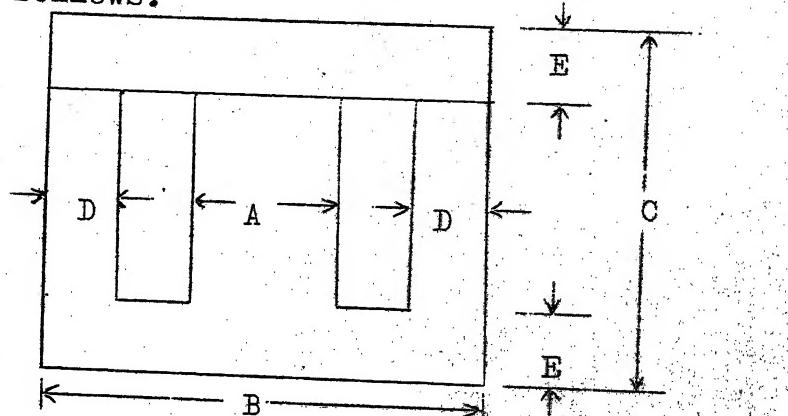
Fig. A1. Stamping Dimensions.

Width of the window,

$$W_w = (B - A - 2D)/2 = 1"$$

Height of the window, $H_w = C - 2E = 3"$

∴ Area of window provided, $A_w = 3 \times 1 \text{ inch}^2 = 19.35 \text{ cm}^2$

Air-gap

From the B - H curve corresponding grade H10 stampings, mmf per metre at a flux density of 1 Wb/m^2 is

$$at_i = 69 \text{ AT/m}$$

Length of flux path in iron,

$$l_i = 2(C - E) + A + D + W_W = 12" \simeq 0.3 \text{ m}$$

Mmf per metre required for air-gap,

$$at_g = 800000 \, B_m/\sqrt{2} = 565000 \text{ AT/m}$$

Number of air-gaps in flux-path, $n_g = 2$

Therefore, impedance of inductor,

$$Z = T^2 / \left[(at_i l_i + n_g at_g l_g) \, T_e \right]$$

Also,

$$Z = 250/2.5 = 100$$

Hence,

$$100 = \frac{500^2}{(69 \times 0.3 + 2 \times 565000 l_g) \times 2}$$

which gives

length of air-gap, $l_g = 1.1$ mm

Inductance, $L = Z/(2\pi f) = 100/(100\pi) = 0.318$ H